YGS Bulletin 18

Surficial geology and Quaternary history of Stevenson Ridge and northern parts of Kluane Lake map areas, Yukon (115K and 115F)

Panya S. Lipovsky and Jeffrey D. Bond

Yukon

Published under the authority of the Department of Energy, Mines and Resources, Government of Yukon yukon.ca.

Printed in Whitehorse, Yukon, 2022.

Publié avec l'autorisation du Ministères de l'Énergie, des Mines et des Ressources du gouvernement du Yukon, yukon.ca.

Imprimé à Whitehorse (Yukon) en 2022.

This, and other Yukon Geological Survey publications, may be obtained from:
Yukon Geological Survey
102-300 Main Street
Box 2703 (K-102)
Whitehorse, Yukon, Canada Y1A 2C6
email geology@gov.yk.ca

Yukon Geological Survey website https://yukon.ca/en/science-and-natural-resources/geology.

In referring to this publication, please use the following citation:

Lipovsky, P.S. and Bond, J.D., 2022. Surficial geology and Quaternary history of Stevenson Ridge and northern parts of Kluane Lake map areas, Yukon (115K and 115F). Yukon Geological Survey, Bulletin 18, 84 p. plus appendices.

Cover photo: A view of the tors outcropping on Britton Ridge, located between the Klotassin and Nisling rivers. Photo credit: Lesley Dampier.

Yukon

Bulletin 18

Surficial geology and Quaternary history of Stevenson Ridge and northern parts of Kluane Lake map areas, Yukon (115K and 115F)

by
Panya S. Lipovsky and Jeffrey D. Bond

Published under the authority of the Department of Energy, Mines and Resources, Government of Yukon, https://yukon.ca.

Printed in Whitehorse, Yukon, 2022.

Publié avec l'autorisation du Ministères de l'Énergie, des Mines et des Ressources du gouvernement du Yukon, https://yukon.ca.

Imprimé à Whitehorse (Yukon) en 2022.

This, and other Yukon Geological Survey publications, may be obtained from:

Yukon Geological Survey

102-300 Main Street

Box 2703 (K-102)

Whitehorse, Yukon, Canada Y1A 2C6

email geology@gov.yk.ca

Yukon Geological Survey website https://yukon.ca/en/science-and-natural-resources/geology.

In referring to this publication, please use the following citation:

Lipovsky, P.S. and Bond, J.D., 2022. Surficial geology and Quaternary history of Stevenson Ridge and northern parts of Kluane Lake map areas, Yukon (115K and 115F). Yukon Geological Survey, Bulletin 18, 84 p. plus appendices.

Cover photo: A view of the tors outcropping on Britton Ridge, located between the Klotassin and Nisling rivers. Photo credit: Lesley Dampier.

Preface

This bulletin describes the surficial geology and Quaternary history of the Stevenson Ridge and northern Kluane Lake map sheets, an area covering more than 12 000 square kilometres of southwestern Yukon. The map area straddles the Pleistocene glacial limits that formed the eastern margin of Beringia during glacial periods. As a result, the landforms of this region are diverse and reflect the contrasting geomorphology characteristic of glaciated versus unglaciated terrain. Importantly, work in this region filled a significant gap in our knowledge of central Yukon glacial limits and how adjacent landscapes were impacted by the Cordilleran Ice Sheet.

Our goal was to produce an in depth description of the region's surficial geology that is applicable for a wide range of purposes. While this region is remote, there is growing interest in its mineral endowment, specifically in the Dawson Range, east of the White River, and in the Ruby Range. Knowledge of the surficial geology can be employed in exploration geochemistry programs to improve sampling and can assist in placer exploration. Future development in the region will also benefit from this work by providing a framework on terrain hazards, such as permafrost and landslides, and construction materials like aggregate. From a land use planning perspective, the surficial sediments and associated soils are an important control on the region's biogeography and therefore, habitat. Hundreds of soil pits were hand excavated during this program and this work is reflected in the detailed descriptions within the bulletin and on the maps.

Fieldwork for this project began in 2007 and continued in 2008 and 2010. A total of seventeen 1:50,000-scale surficial geology maps were produced between 2009 and 2015, along with two papers in Yukon Exploration and Geology, and a PhD thesis by Dr. Derek Turner. Many valuable contributions were made by student assistants, academic researchers, camp and transportation personnel, industry partners and volunteers. Without their help our understanding of this unique and complex area of Yukon would not be nearly as complete.

The information contained in this bulletin and associated maps represents a beginning. There are many details to the Quaternary history and the evolution of the landscape that we have not told and will be a job for the next generation. Hopefully this work provides context and aids in many future discoveries.

Jeffrey Bond

Jeffrey D. Bond
Head, Surficial Geology
Yukon Geological Survey

Acknowledgements

The authors would like to thank Northern Affairs Canada and Natural Resources Canada (Geoscience for Energy and Minerals program) for their financial assistance and logistical collaboration. Camp logistics were provided by the White River RV park and Aurora Geoscience in 2007, Larry Nagy and José Janssen at Tincup Lodge in 2008 and by Western Copper and Gold Corporation (Scott Casselman) in 2010; without their hard work and cooperation, the fieldwork would not have run as smoothly as it did. A sincere thank you goes out to all the field assistants who contributed to this project: Catherine Welsh, Amaris Page, Sydney van Loon, Leslie Dampier, Logan Cohrs, Riley Gibson, Victor Bond and Peter Von Gaza. Additional thanks go to the bedrock mapping team led by Don Murphy, for always keeping an eye open to high elevation Quaternary features. Trans North, Kluane Helicopters and HeliDynamics provided safe and reliable helicopter transportation. Many thanks also to: Derek Turner, Brent Ward, Britta Jensen, Alice Telka, Grant Zazula, Nancy Bigelow and Duane Froese for their contributions toward increasing our understanding of the stratigraphy and paleoenvironments of the White River area. John Gosse at Dalhousie University completed cosmogenic dating laboratory analyses, which enabled us to constrain the timing of deglaciation. Lionel Jackson, who has mapped in the neighboring map sheets, graciously undertook the technical review of this bulletin. His contribution is very much appreciated. Editing and layout was completed by Karen MacFarlane, and we greatly appreciate all her efforts.

Table of Contents

Appendices

The appendices are only available as digital files. They are included in a .zip file that accompanies this document, and are available from https://data.geology.gov.yk.ca.

Appendix 1 – Detailed heavy mineral sampling results.

Appendix 2 – Stevenson Ridge Open File maps; there are 17 maps in total.

A digital surficial compilation for Yukon can be found at https://data.geology.gov.yk.ca/Compilations/33#InfoTab.

Chapter 1
Introduction

The Yukon Geological Survey (YGS) conducted a three-year surficial geology field mapping program for the Stevenson Ridge (NTS 115J/1–13) and northern Kluane Lake (NTS 115G/9, 14, 15, 16) map areas during the 2007, 2008 and 2010 field seasons (Fig. 1-1). This area was previously unmapped and represented a large gap in the territorial surficial geology mapping coverage. It was also of particular interest as it spans the full range of Yukon glacial limits and includes a large proportion of unglaciated terrain. The project provides baseline surficial geology information that serves as a foundation for mineral exploration and development, infrastructure development and ecological studies. It was particularly valuable for supporting the Dawson Range exploration surge following the discovery of the White Gold deposit in 2008–2009.

The primary objective of the project was to produce 1:50 000 scale surficial geology maps for the region using air photo interpretation and field investigations of surficial geological features including surficial materials, stratigraphic exposures, landforms, permafrost characteristics, terrain hazards, ice-flow indicators and glacial limits. Interpretation of compiled results in combination with previous research then facilitated further analysis of local Quaternary history, stratigraphy and regional placer potential.

Seventeen 1:50 000 scale open file maps covering the study area were released between 2009 and 2015 (Bond and Lipovsky, 2009a–d; Bond and Lipovsky, 2012a,b; Lipovsky and Bond, 2012a–c; Lipovsky and Bond, 2013a–f; Bond and Lipovsky, 2015a,b). These maps should be referred to in locating specific site numbers and local landmarks discussed in this bulletin. Mapping was based on interpretation of high resolution digital stereo air photo and satellite imagery viewed with PurVIEW software in an ESRI ArcGIS environment.

The study area is remote with no road access. Fieldwork was helicopter-supported and largely conducted by two 2-person crews each day. The first season of fieldwork focused on the Wellesley Basin and western Nisling Range, with a camp based at White River Lodge from June 19 to July 16, 2007. The second season of fieldwork was staged out of Tincup Lake from July 2–29, 2008 and concentrated on the eastern Nisling Range and southern Dawson Range. The final field season targeted the northern Dawson Range and was based out of Western Copper and Gold Corporation's Casino camp from July 7–25, 2010. More than 400 field stations were documented during the three seasons of fieldwork.

Previous and related work

No surficial geology maps previously existed for the study area prior to this project. Adjacent areas were mapped at: 1:50 000 scale to the north by Jackson *et al.* (2009), Jackson (2005) and Huscroft (2002a,b,c); and at 1:100 000 scale to the south (Rampton, 1979c,d), west (Rampton, 1979a,b) and east (Jackson, 2000; Jackson, 1997a,b; Hughes, 1989a,b). Duk-Rodkin (2001a,b) previously mapped glacial limits for the region using air photo interpretation. These collective works provide an excellent regional context for the study area and greatly helped guide our investigations.

This project involved partial support of a doctoral thesis that examined Pleistocene stratigraphy, glacial limits and interglacial environments along the White River, near its confluence with the Donjek River (Turner *et al.*, 2013; Turner, 2014). A summary of this work is provided in Chapter 5.

Interim results from this project also supported the development of guidelines for property-scale surficial geology classification in the unglaciated Klondike Plateau region, specifically targeting soil geochemical sampling as an exploration tool (McKillop *et al.*, 2013).

In tandem with this project, and working out of shared camps, bedrock mapping was completed by the YGS between 2007 and 2009 (Murphy, 2007; Murphy *et al.*, 2007, 2008). The Geological Survey of Canada also led a bedrock geology mapping campaign (Ryan *et al.*, 2014b) in the northern Stevenson Ridge area in 2010 and 2011.

Following completion of fieldwork for this project, D. Cronmiller completed a Masters thesis investigating surficial geology, stratigraphy and placer deposits in the Gladstone Creek and Ruby Range areas east of Kluane Lake's Talbot Arm (115G/7 and 8; Cronmiller, 2019; Cronmiller *et al.*, 2018, 2019)

***Figure 1-1**. Study area location and major physiographic features.*

Chapter 2
Setting

Location and access

The approximate location of the study area is between Yukon River to the north and Kluane Lake to the south, bounded by the White River to the west (Fig. 1-1). While there is no public road access to the area, a handful of resource roads and historical trails exist throughout the region, extending to the Casino property, in Dip Creek drainage, upper Nisling River valley and east of Mount Cockfield. The communities of Carmacks, Pelly Crossing, Beaver Creek, Burwash Landing and Destruction Bay are all located within 90 km of the study area boundary.

Physiography and drainage

The study area lies primarily within the Yukon Plateau physiographic region, which is divided into the Nisling and Ruby ranges (Kluane Plateau) south of the Nisling River, and the Dawson Range (Klondike Plateau) to the north. These mountain ranges trend in a northwesterly direction, reflecting the tectonic history of terranes accreted to the margin of ancient North America. The area between the White and Donjek rivers is part of the Wellesley Basin lowland physiographic region; low hills extending up to approximately 1200 m surround Wellesley Lake, which lies at approximately 550 m above sea level (asl).

The Dawson Range lies north of Nisling River and is primarily unglaciated with broad, rounded ridges and convex slopes dissected by narrow v-shaped valleys. Higher peaks such as Mount Cockfield (1905 m) and Apex Mountain (2022 m) supported isolated alpine glaciers during the Pleistocene.

The Nisling Range lies to the east of Wellesley Basin and south of Nisling River and was partially glaciated during the Pleistocene; elevations extend up to approximately 1900 m.

A small portion of the Ruby Range is found within the study area, south of Talbot Creek, which drains into Kluane Lake (elevation of approximately 780 m asl). The Ruby Range contains the highest peaks in the study area, with elevations up to 2200 m.

The entire study area is located within the Yukon River drainage basin and most of the drainages within the study area are within the Donjek River sub-basin. The Donjek River flows into the White River approximately 100 km upstream of its confluence with Yukon River. Both the White and Donjek rivers flow northerly from their headwaters in the St. Elias Mountains, draining large valley glaciers and transporting heavily sediment-laden glacial meltwater within wide braided floodplains.

Tempelman-Kluit (1980) and others (Duk-Rodkin *et al.,* 2001; Jackson *et al.*, 2009; Ryan *et al.*, 2017) have described how, in the mid-Cenozoic, Yukon River drained south to the Pacific Ocean. Uplift of the St. Elias Mountains, and onset of glaciation during the Plio-Pleistocene transition then forced a reversal in drainage direction to the north. This produced a significant drop in the base level of Yukon River, resulting in deep incision of tributaries draining the north side of the Dawson Range, such as Independence and Carlisle creeks. In contrast, streams flowing into the Donjek and White rivers on the south side of the Dawson Range did not undergo a significant change in base level due to the effects of glaciation in the Wellesley Lake area. These streams therefore have wider, lower-gradient floodplains. Drainage history is discussed further in Chapter 3.

Bedrock geology

The northern Stevenson Ridge area is underlain by metasedimentary and volcanic rocks of the Paleozoic Yukon-Tanana terrane (Fig. 2-1), which accreted to the North American margin. These rocks have been subsequently faulted and intruded by Cretaceous to Paleocene plutons and

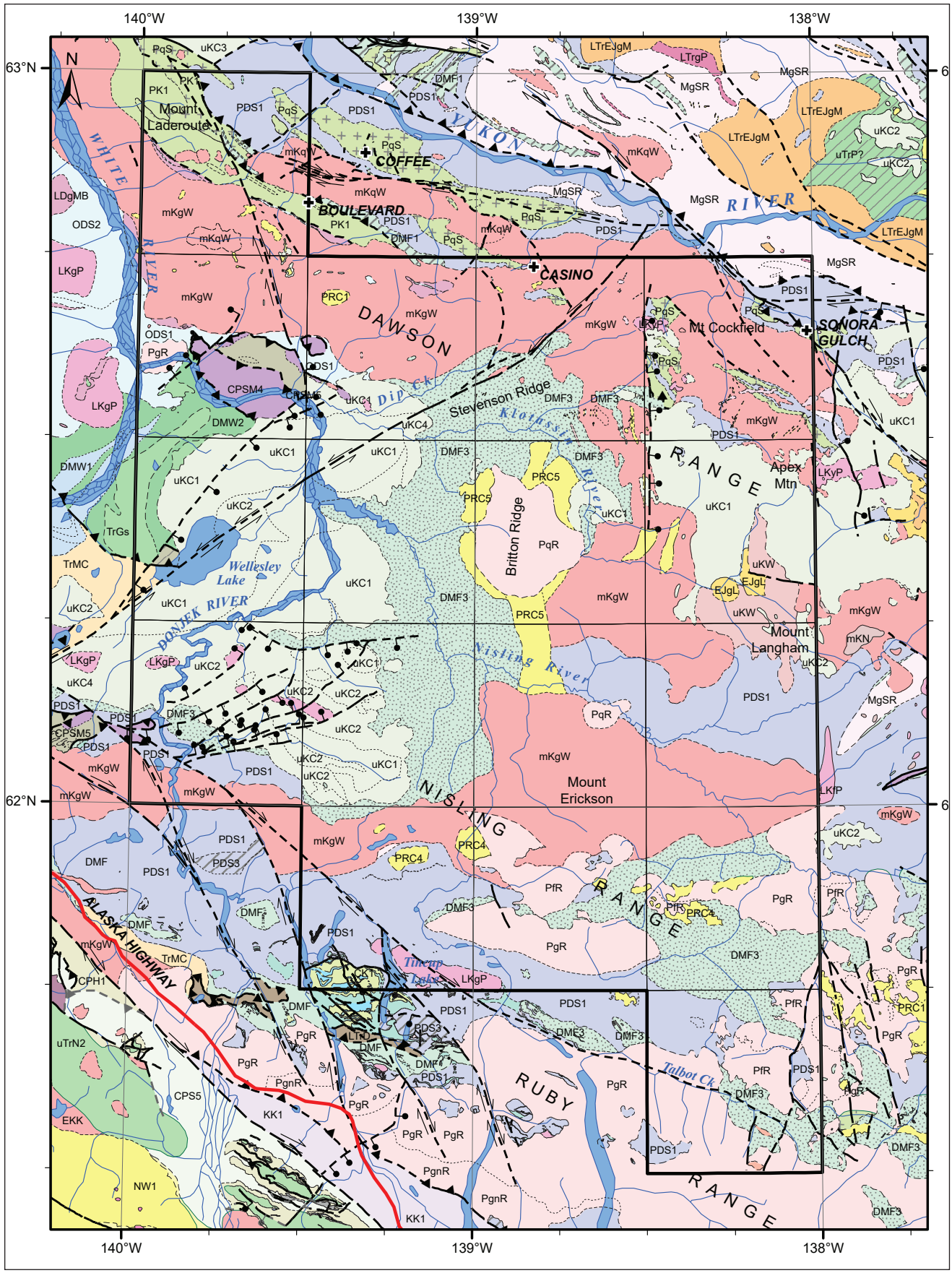

Figure 2-1. *Bedrock geology of the study area and selected mineral properties (after Yukon Geological Survey, 2022). Legend on following page.*

Figure 2-1. *Bedrock geology legend.*

batholiths (Ryan *et al.*, 2014b). A concentration of mineralization can be found in the Dawson Range including the Casino and Coffee deposits, Sonora Gulch and Boulevard occurrences (Fig. 1-1). Farther south, intrusion-related gold mineralization has been discovered west of Wellesley Lake in White River formation (DMW) rocks.

The middle Cretaceous Whitehorse plutonic suite (mKW) is spatially the most extensive intrusive suite. Yukon-Tanana terrane rocks include the pre-Devonian Snowcap assemblage (PDS), Mississippian Simpson Range suite (MSR) and Finlayson assemblage (DMF), and the Permian Klondike assemblage (PK). Ryan *et al.* (2014b), proposed five structural panels, consisting of distinct tectonostratigraphic units and geological histories, to explain the geographic distribution and origin of crustal blocks in the Dawson Range and northern Stevenson Ridge area. The panels are bound by faults with post-Triassic to pre-mid-Cretaceous movement, and Ryan *et al.* (2014b) indicate that emplacement of the mid-Cretaceous Dawson Range batholith occurs along a crustal-scale structure. Mineralization in the Dawson Range, including the Coffee and Boulevard occurrences, appears controlled by this structure and is spatially coincident with rocks of the Klondike assemblage, which may contain metal enrichment or provide structural and chemical traps.

The White River (DMW) and Mirror Creek (TrMC) assemblages lie immediately south of the Dawson Range, near the White River (Murphy *et al.*, 2008, 2009). These assemblages consist of middle Triassic or older schist, phyllite and gabbro bodies. Near the mouth of the Donjek River, these assemblages are in structural contact with the Harzburgite Peak ophiolite complex. Upper Cretaceous dacite, basalt and rhyolite volcanic rocks (uKC1,2) that extend south into the Nisling Range underlie the central portion of the Stevenson Ridge map area (Murphy *et al.*, 2008). Along the eastern margin of the Stevenson Ridge map area, rocks consist of Yukon-Tanana terrane carbonaceous phyllite or schist, quartzite and minor felsic metavolcanic rocks in the vicinity of the Nisling River.

The Nisling Range and parts of the Ruby Range underlie the southern margin of the study area. Rocks in the Nisling Range consist of Yukon-Tanana terrane polydeformed, metavolcanic, pelite, quartzite psammite and quartz-muscovite schist of the Finlayson (DMF) and Snowcap (PDS) assemblages (Israel *et al.*, 2011). The Paleocene Ruby Range (PR) batholith and volcanic and intrusive rocks of the Rhyolite Creek (PRC) complex intrude these rocks. Similar rocks are found within the Ruby Range; however, the Ruby Range batholith is much more pervasive.

White River ash

Two of the largest pyroclastic eruptions in North America in the past 2000 years occurred on the Mt. Bona-Churchill massif in Alaska, which is located southwest of the study area 35 km west of the Yukon-Alaska border. Radiocarbon dating indicates the first and smaller eruption occurred circa 1625 yr B.P. (Lerbekmo *et al.*, 1975; Reuther, *et al.*, 2020) depositing what is known as the north lobe White River ash, which straddles the Yukon-Alaska border and extends north of Dawson City. A second, larger, eruption occurred in A.D. 833–850 (Jensen *et al.*, 2014) and deposited the east lobe White River ash, which covered much of southern Yukon and extended into the Northwest Territories (Clague *et al.*, 1995; Lerbekmo, 2008; Lerbekmo and Campbell, 1969; Preece *et al.*, 2014; Richter *et al.*, 1995; Robinson, 2001). Primary east lobe ash thickness declines exponentially with distance from the eruption source, with a maximum thickness of approximately 30 cm in the study area, and the thickest and coarsest deposits occur directly beneath the northeast-trending ash plume fall axis (Lerbekmo, 2008; Lerbekmo *et al.*, 1975). In some places within the study area, the ash becomes over-thickened due to reworking processes. Where this has occurred, ash thickness may exceed 2 m and occurs as sand-size tephra particles (*see* Chapter 4 for more details). The coarser grained and thicker east lobe deposit is a very prominent and useful stratigraphic marker within the study area. It is also associated with active-layer detachment slides in the area (*see* Chapter 6).

Climate

The study area has a semi-arid subarctic continental climate characterized by very cold, long winters and short, mild summers. Table 1 summarizes the 1981 to 2010 climate normal for the three closest

Table 1. *Canadian climate normals for 1981 to 2010.*

Station	elevation (m)	daily mean temperature (°C)			mean precipitation (mm)		
		January	July	Annual	January	July	Annual
Beaver Creek	649	-25.2	14.1	-4.9	13.9	101.3	417.3
Burwash A	806	-20.5	13.1	-3.2	8.4	67.9	274.7
Pelly Ranch	445	-24.9	15.8	-3.1	19.7	58.0	320.5

Accessed from http://climate.weather.gc.ca/climate_normals/index_e.html (13 July 2017)

Environment Canada weather stations: Beaver Creek, Burwash Landing and Pelly Ranch. Mean annual temperatures at these stations range from approximately -3 to -5°C. Daily mean temperatures in January range from -20.5°C at Burwash Landing to -25.2°C at Beaver Creek. The coldest temperature in North America, -62.8°C, was recorded at Snag, immediately west of Wellesley Lake, on February 3, 1947. Approximate daily mean temperatures in July range from 13 to 16°C at the same stations, although higher elevation sites are cooler in summer. Semi-arid conditions prevail in the region due to the rain shadow effect of the St. Elias Mountains and most summer precipitation is generated from convective and thunderstorm activity (Smith *et al.*, 2004). Total annual precipitation ranges from 275 mm at Burwash Landing to 417 mm at Beaver Creek.

Vegetation

Boreal forest is found below treeline (approximately 1000–1200 m) on lower slopes and valley bottoms, while alpine tundra occurs on upper slopes and ridge crests above 1400 m; willow, subalpine fir and birch shrubs dominate the subalpine zone (Smith *et al.*, 2004). Vegetation commonly reflects the distribution of surficial materials and near-surface permafrost. Below treeline, stunted black spruce forests grow in areas of shallow permafrost that occupy north-facing slopes and ice-rich colluvial aprons flanking floodplains. Thick sphagnum moss is commonly associated with black spruce forests and helps sustain very shallow permafrost tables by insulating the ground from warm summer temperatures. Well-drained surfaces such as glaciofluvial terraces support white spruce forest. Mixed forests, dominated by trembling aspen, birch, balsam poplar, white spruce and willow, grow on warmer sites lacking permafrost such as south-facing slopes.

Soils

Subarctic continental climate, elevation, slope aspect and surficial material strongly control soil development within the study area. Physical weathering processes, particularly in periglacial environments, play an important role in the structure of soils in the study area, whereas chemical weathering, including the alteration of primary minerals, is generally limited (Dampier *et al.*, 2009).

On relatively level upland environments underlain by weathered bedrock, the soil moisture content is variable and this affects the presence or absence of cryoturbation. Relatively dry and well-drained sites contain B-horizon oxidation and are classified as Brunisols. Sites with moderate to high moisture content are cryoturbated, have sorted stone circles and are classified as Orthic Turbic Cryosols. Jackson *et al.* (2009, p. 35) note that very deep weathering and oxidation of bedrock occurred to depths of tens of metres in the Stewart River map area during the Tertiary Period. Comparable depths of weathering were not directly observed within similar materials in the Stevenson Ridge study area, but would be expected in unglaciated terrain.

On sloping terrain, soil characteristics are determined by aspect and surficial material (Bond and Sanborn, 2006). On well-drained, warm aspect sites, soils typically have a Dystric Brunisol characteristic with noticeable B-horizon and relatively thin A-horizon. The organic horizons and A-horizon (incorporated decomposed organic matter) are between 4 and 10 cm thick. The B-horizon is emphasized by a zone of iron oxidation that typically extends to approximately 25 cm depth. The oxidation commonly occurs within a loess veneer, although may extend into the underlying weathered bedrock colluvium. Silt caps are present on the tops of clasts, which build gradually as silt is transported downward in

suspension in wet soils. These soils are classified as Brunisols based on the absence of permafrost, limited accumulation of organic matter, and strong oxidized colours.

On poorly drained warm-aspect sites, particularly on lower slope positions, organic cover generally increases and insulates the soil from chemical weathering. Cryosols are common in these environments. On cold-aspect sites, permafrost processes are widespread and Turbic Cryosols are found spanning a broader range of slope positions. Cryoturbation may extend to 75 cm depth and will combine both the loess and weathered bedrock or glacigenic parent materials (Smith *et al.*, 2009). The thick organic accumulations on cold-aspect sites reflects the reduced rate of organic matter decomposition. As a result, evidence of B-horizon weathering is limited to 0–10 cm depth. Regosols characterized by poorly developed soils composed of gravel parent material (Smith *et al.*, 2004) form in active floodplain environments in the study area.

Permafrost – general

Permafrost is widespread but discontinuous in the study area. Permafrost distribution and character (depth, thickness and ice-content) varies widely with local scale variations in both macro and micro-topography (slope, aspect and position), vegetation cover, soil texture and soil moisture. Soil texture and organic content strongly control soil moisture and therefore ice-content in permafrost regions (*i.e.*, organic-rich and/or finer textured soils generally have higher ice contents; French and Heginbottom, 1983). Permafrost is most prevalent on north-facing slopes and in valley bottoms within thick fine-grained sediments, while it is generally absent on steep, well-drained south-facing slopes and within coarse-grained sediments adjacent to recently active floodplains. At a coarse regional scale, the entire study area is classified within the extensive discontinuous permafrost zone, in which 50–90% of the land surface is underlain by permafrost with low to medium ground ice content (up to 20% visible ice) in the top 10–20 m (Heginbottom, 1995).

South and west of the study area, more detailed regional-scale mapping indicates that permafrost underlies most of the nearby landscape, particularly within alluvial fans, plains and terraces, and till and colluvial blankets (Heginbottom and Radburn, 1992). These landforms have low to moderate ice contents with ground ice in the form of lenses and reticulate veins. Permafrost is also considered continuous in glaciolacustrine plains, but higher ice contents can be found within these materials (Heginbottom and Radburn, 1992). In contrast, active floodplains of the Donjek and White rivers and glaciofluvial sediments south and west of the study area support only discontinuous or isolated patches of permafrost with low ice content (Heginbottom and Radburn, 1992).

Rampton *et al.* (1983) used geotechnical drillhole data to characterize the distribution and ice content of permafrost along the proposed Alaska Highway gas pipeline route. Results from this study found that more than 80% of the terrain traversed by the right-of-way north of Kluane Lake (roughly paralleling the Alaska Highway) is underlain by permafrost (Rampton *et al.*, 1983). Permafrost thickness in southwestern Yukon is reported to be up to 15 m near Beaver Creek, 18 m at Burwash Landing, and up to 27 m near Aishihik Lake (115H; Smith *et al.*, 2004). The thickness of the active layer, or the surface layer that seasonally thaws and refreezes, is generally between 0.3 and 2.2 m in the same region (Smith *et al.*, 2004).

Rampton *et al.* (1983) also highlighted specific sedimentary conditions that are commonly associated with shallow ground ice in the Alaska Highway corridor, all of which relate to the presence of fine-grained sediments and ample groundwater supply. These areas include locations where fine-grained material overlies, truncates, or is interstratified with more permeable coarse-textured material, poorly drained areas adjacent to wetlands and streams, and sites adjacent to bedrock valley walls (Rampton *et al.*, 1983).

A detailed (30 m grid) permafrost probability model (Bonnaventure *et al.*, 2012) classifies permafrost in the study area as primarily extensive discontinuous with lowest probabilities of permafrost on south-facing slopes. Patches of continuous permafrost are modeled on north-facing slopes and in alpine areas (Fig. 2-2).

Field observations and interpretive mapping completed for this study suggest that the study area is underlain by nearly continuous permafrost.

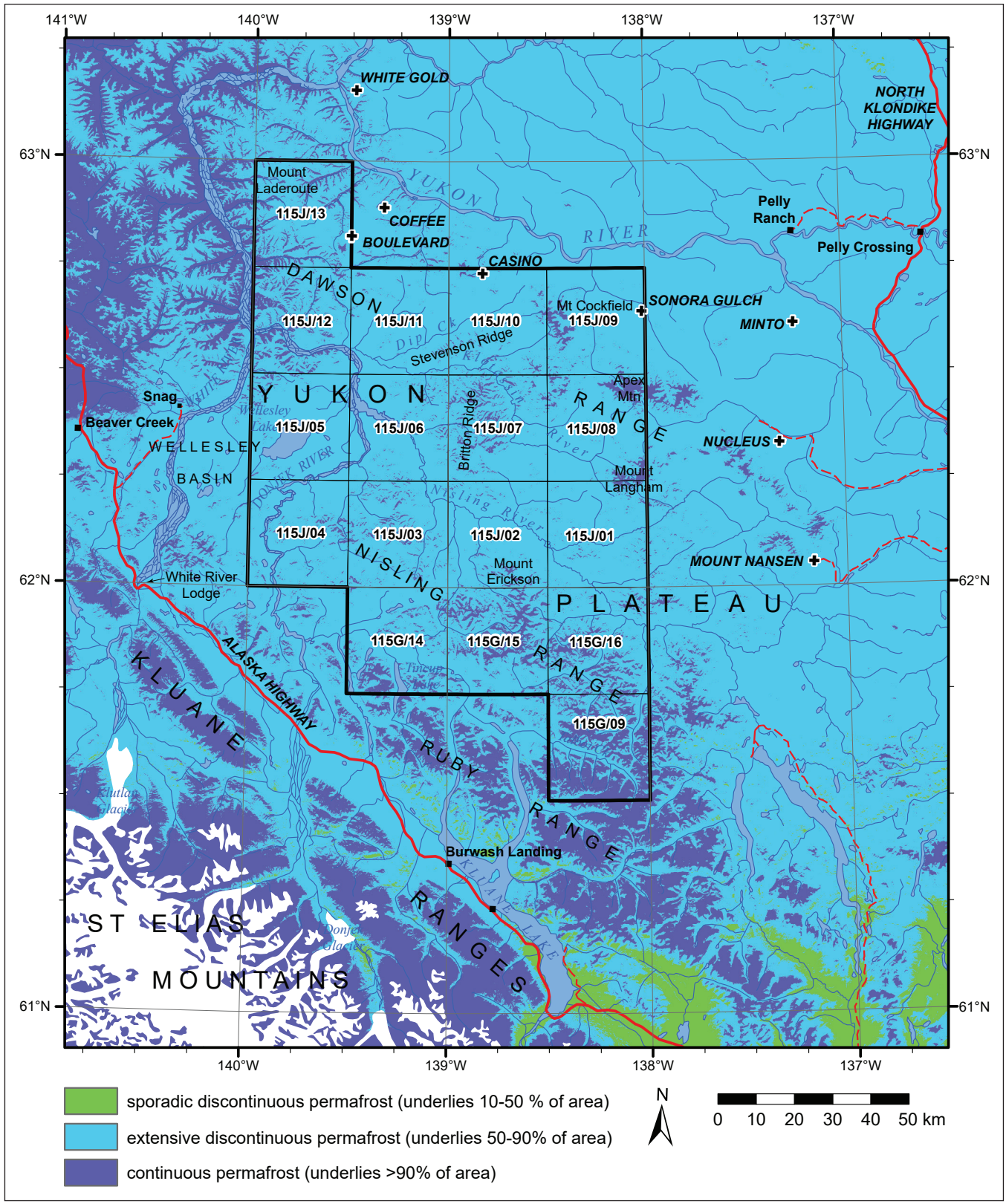

Figure 2-2. *Permafrost classification of the study area, derived from permafrost probability modeling completed by Bonnaventure et al., 2012.*

Permafrost-related landforms such as thermokarst thaw ponds, ice-wedge polygons, rock glaciers, active-layer detachment slides, cryoplanation terraces and open-system pingos are widespread (*see* Chapter 6 for further details). Ice-rich permafrost in the area is generally associated with fine-grained alluvial and glaciolacustrine sediments in valley bottoms, although massive ice is found in coarse-grained glaciofluvial materials in the region. The frost table is generally very shallow (<1 m), resulting in poor drainage and saturated surface soils. Permafrost thicknesses up to 12 m were observed in the field.

Chapter 3
Quaternary history

Pre-glacial drainage and reversal of the Yukon River

Reconstruction of the pre-glacial drainage in the study area is based on previous modeling, identifying drainage anomalies such as under-fit valleys, and analyzing the effect glaciation and displacement along the Tintina fault had on drainage reorganization. Throughout the late Cretaceous and Cenozoic, much of central Yukon drainage, including the paleo-Yukon River, was thought to drain south through the White River valley and then northwestward into Alaska and the Tanana River system (Fig. 3-1; Ryan *et al.*, 2017). This network would have included drainage from much of the Dawson and Nisling ranges. The Nisling River, Klotassin River and Dip Creek would have converged and likely drained to the southwest through the Wellesley Basin and into the paleo-Yukon River (Fig. 3-1). Grayling Creek was likely westerly flowing and also joined the paleo-Yukon River in the Wellesley Basin. Pre-glacial drainage configurations for the Ruby Range, at the south-end of the study area, are less certain, being close to a regional drainage divide between the Yukon and Alsek river systems. The paleo-Donjek River was likely confined to the Shakwak Trench and either flowed northwest or southeast within this fault-controlled topographic lineament.

With the onset of Quaternary glaciations, the Yukon River was diverted northward, including drainage from the study area (Tempelman-Kluit, 1980; Duk-Rodkin *et al.*, 2001). The reversal of the drainage occurred with the first continental glaciation and buildup of ice in the St. Elias Mountains. As glaciers advanced to the mountain front, glaciofluvial sedimentation would have increased into the Yukon River valley in the area between Snag and Northway Junction in Alaska (Fig. 3-2). The aggradation of proglacial glaciofluvial sand and gravel would have raised base level significantly, forcing the Yukon River to backup. A modern analogue for this process has been documented for the Slims River and Kluane Lake during the Little Ice Age when the Slims River reversed from a south-flowing to a north-flowing drainage due to glaciofluvial sedimentation and eventual ice damming (Bostock, 1969; Clague. *et al.*, 2006). A comparison of elevations between the modern glaciofluvial fan surface at Snag along the White River (580 m elevation) and Pliocene terraces at the mouth of the Fortymile River (550 m elevation) near the paleo-Yukon River headwater, indicate a topographic difference of 30 m. At the onset of Quaternary glaciation, the fan surface near Snag would have been lower than 550 m, but glaciofluvial sedimentation into the Yukon River valley could easily raise the base level above 550 m and deflect the Yukon River to the north. Ice blockage may have also contributed to this deflection; however, the limit of Plio-Pleistocene advances from the St. Elias Mountains is uncertain because late Quaternary advances overrode them. Additional support for Plio-Pleistocene floodplain aggradation within the lower White River valley is provided by the absence of Pliocene terraces, suggesting aggradation in the drainage out-competed erosion caused by the Yukon River reversal. Future work such as geophysics and sonic drilling is required to find the former Yukon River channel between Snag and Northway Junction.

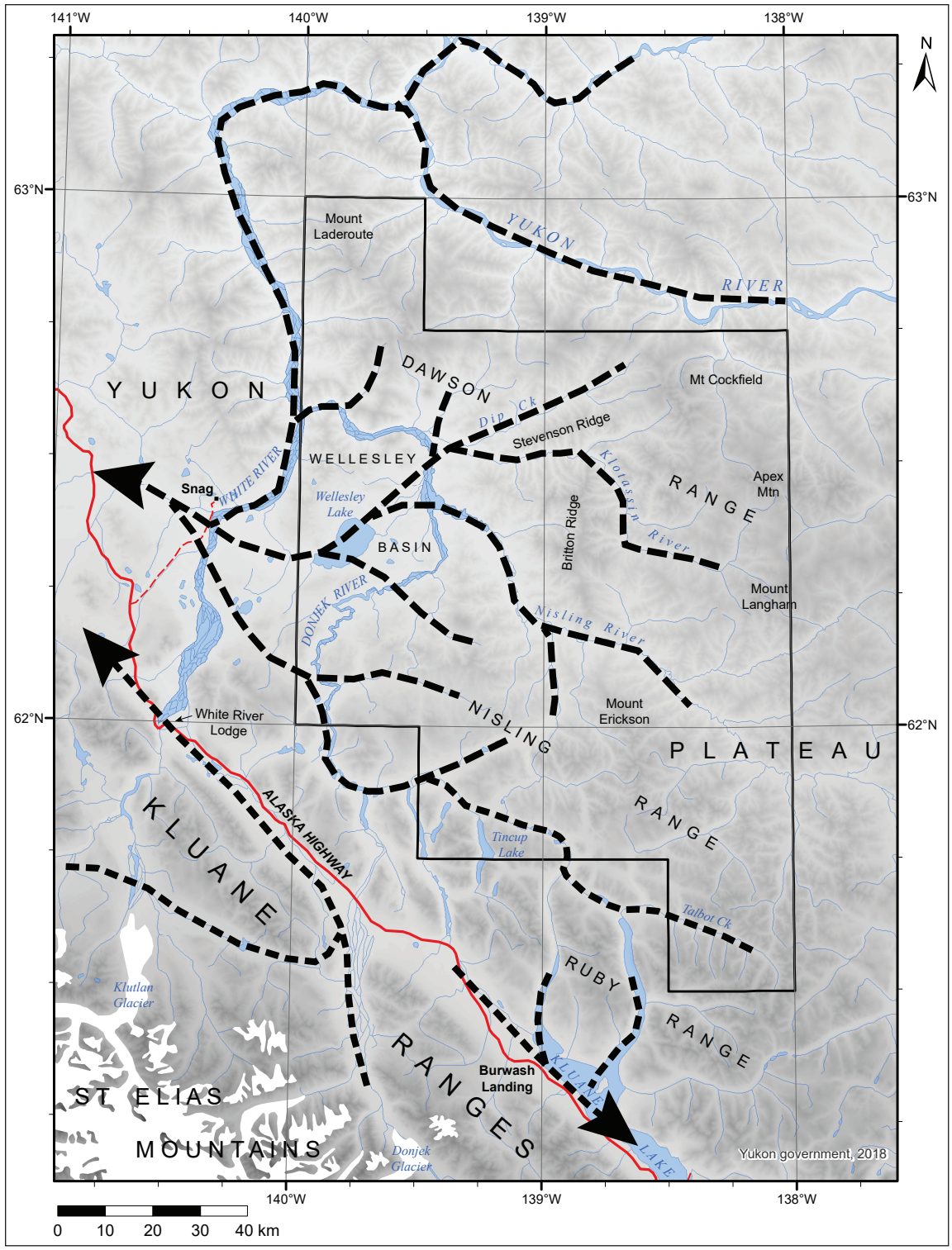

Figure 3-1. *Pre-glacial drainage of the study area. It is proposed that most of the local drainages fed a westerly draining Yukon River system that flowed into eastern Alaska.*

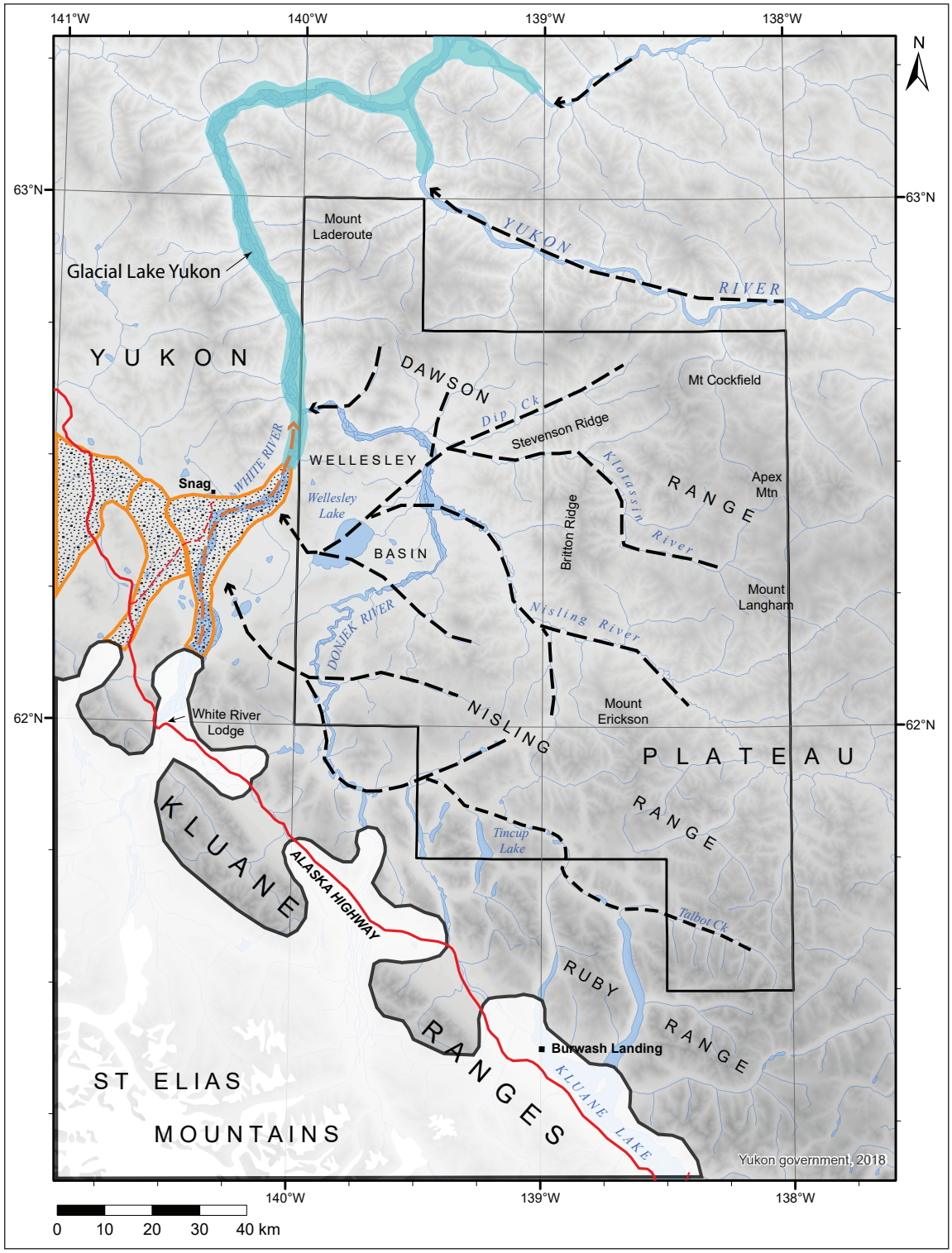

Figure 3-2. *Reversal of the Yukon River drainage to the north during the first Quaternary glaciation occurred with the advance of glaciers from the St. Elias Mountains. Glaciofluvial sedimentation (orange outlined area), together with potentially physical ice blockage, was responsible for redirecting the drainage. Glacial Lake Yukon would have formed during this time until the new outlet was established northwest of Dawson City.*

Glaciation

The Stevenson Ridge map area straddles the limits of at least three Pleistocene ice sheets. They were associated with the Reid Glaciation (Illinoian; marine isotope stage - MIS 6; *ca.* 191–130 ka BP), the Gladstone Glaciation (early Wisconsin; MIS 4; *ca.* 75–55 ka), and the McConnell Glaciation (late Wisconsin; MIS 2; *ca.* 22–11.7 ka BP). During each glaciation, ice advanced northward out of the St. Elias Mountains in what is referred to as the St. Elias lobe of the Cordilleran Ice Sheet (CIS). The St. Elias lobe flowed northward across Shakwak Valley and entered the study area through the White, Donjek and Kluane river valleys, as well as the Brooks and Talbot arms of Kluane Lake. An additional lobe of ice also flowed northwestward out of the Coast Mountains from the Aishihik Lake region and down the upper Nisling River valley (Duk-Rodkin, 1999). These ice lobes penetrated into smaller tributaries and formed a network of coalescing valley glaciers within the Ruby and Nisling ranges. Small, isolated, alpine glaciers also formed on uplands and extended down local drainages. The portion of the Dawson Range in the study area remained largely unglaciated during each successive glacial period, with the exception of alpine glaciation on Mount Cockfield and Apex Mountain.

Most of the glacial deposits preserved at the surface within the study area are attributed to the most recent McConnell Glaciation (Fig. 3-3; Ward *et al.,* 2007a,b; Menounos *et al.*, 2017). McConnell deglaciation was initiated about 17 000 years BP, based on terrestrial cosmogenic nuclide (TCN) ^{10}Be surface exposure dating of samples from erratics located southeast of the map area (*see* discussion below). Radiocarbon dating of a sample collected from a Donjek River cutbank (07JB010) indicates that the McConnell ice had retreated past the site by 12 383 ± 169 calibrated years before present (cal BP; Beta 240021; *see* Chapter 5 for further discussion).

The penultimate Gladstone Glaciation began to retreat by 55 000 BP (Ward *et al.*, 2007b). Deposits from this glaciation are preserved above and beyond the McConnell limit and its outwash trains and near, or slightly below, the limit of the Reid Glaciation. Evidence of the Gladstone Glaciation consists of morainal deposits, outwash terraces and ice proximal features such as meltwater channels.

Based on stratigraphic studies completed at White River (Turner *et al.*, 2013), the oldest and most extensive glacial advance in the study area predates Old Crow tephra (*ca.* 124 ka), which overlies a pre-Gladstone sequence of glacial deposits (*see* Chapter 5 for further discussion). These deposits are assumed to correlate with the Reid Glaciation documented for the Selwyn lobe in central Yukon (Ward *et al.*, 2008). During the Reid Glaciation, the St. Elias lobe extended northward down the White River as far as its confluence with the Donjek River. It also extended across the Wellesley Basin and down the Donjek River nearly to the mouth of the Nisling River, and advanced up several adjacent tributaries such as MacKinnon and Grayling creeks. Smaller Reid valley glaciers that formed the leading edge of the Cordilleran Ice Sheet also extended northward down Onion, Rhyolite, Dwarf Birch and Tyrrell creeks to their confluences with Nisling River (Fig. 3-3).

An earlier group of at least five less extensive “pre-Reid” glaciations also likely affected the study area from the Late Pliocene (about 2.7 million years ago) to the middle Pleistocene (Jackson *et al.,* 1996, 1999; Froese *et al.*, 2000; Duk-Rodkin *et al.*, 2001; Westgate *et al.*, 2001; Barendregt and Duk-Rodkin, 2004). This set of glaciations was previously mapped as the most extensive in the region (Duk-Rodkin, 1999), although no evidence of pre-Reid glaciations was found either at the surface or in section within the study area. The distribution of pre-Reid ice sheets therefore remains uncertain, but they must have been less extensive than the Reid glaciation. Based on relative morphological characteristics, weathered cirques in the Dawson Range are interpreted to be of pre-Reid age. This suggests that although the St. Elias lobe of the Cordilleran Ice Sheet may have been precipitation limited during the early Pleistocene, the equilibrium line was sufficiently low enough north of the St. Elias Mountains to permit alpine glaciers to form at lower elevation than during the late Pleistocene.

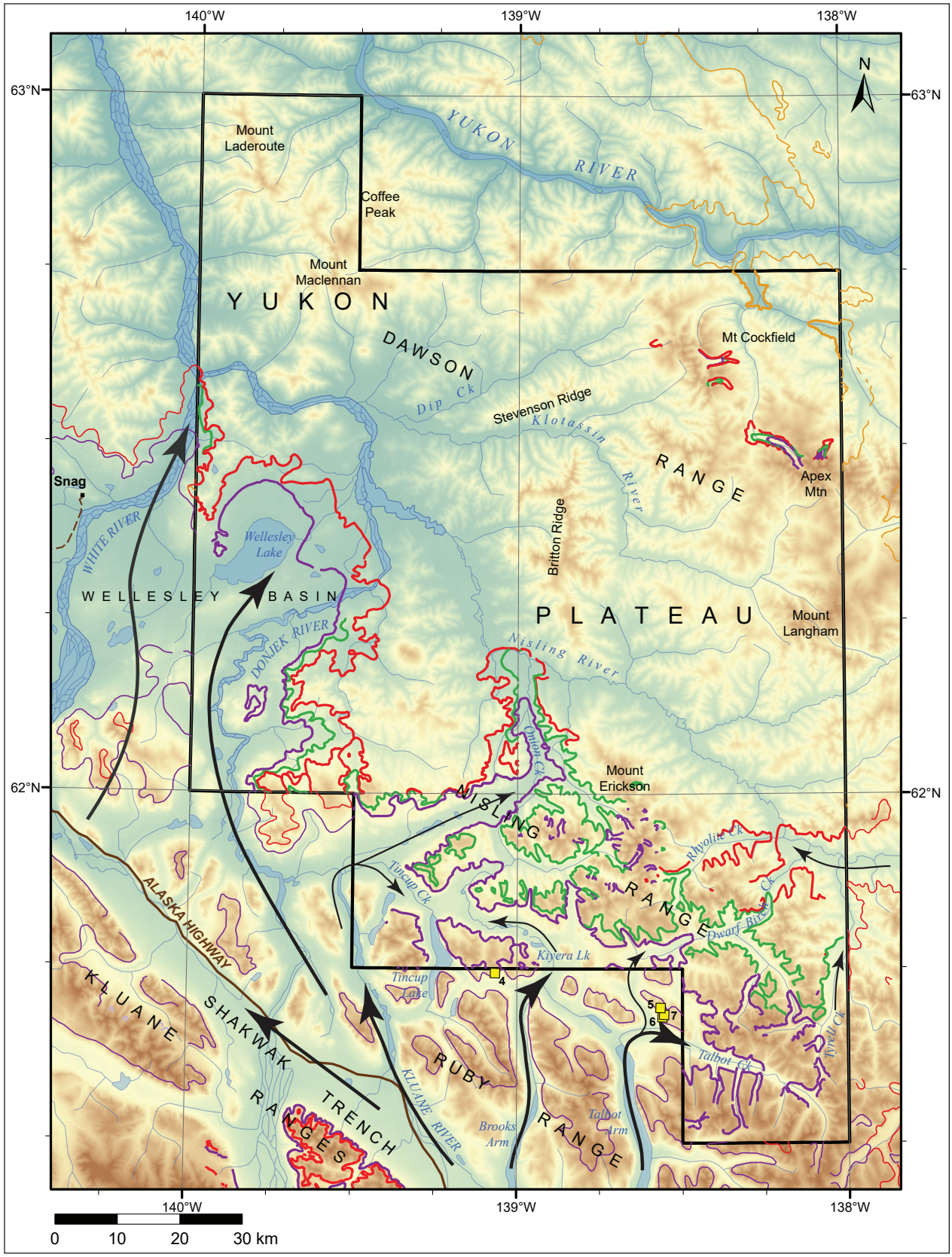

Figure 3-3. Pleistocene glacial limits map of the study area. Up to four glacial limits are evident: McConnell (MIS 2; purple), Gladstone (MIS 4; green), Reid (MIS 6; red) and Pre-Reid (orange). Thicker limits were mapped as part of this study and by Kennedy and Ellis (2020) for the Kluane Ranges; thinner limits outside the study area are from Duk-Rodkin (1999). Arrows show major ice flow directions of the St. Elias lobe of the Cordilleran Ice Sheet. Yellow squares show locations of erratic boulders sampled for terrestrial cosmogenic nuclide dating.

Glacial limits

A major focus of this study was to confirm the maximum limit of the Pleistocene glaciations in the area based on field mapping. Mapping of glacial limits involves air photo landform interpretation (particularly for moraines and meltwater channels), ideally in combination with field-based identification of erratics and confirmation of glacial sediments. Mapping the limits of pre-McConnell glaciations is particularly challenging. Older depositional landforms are either completely obscured, have been eroded by the younger McConnell Glaciation, or are significantly modified by widespread and prolonged permafrost and colluvial activity. This is especially common in mountainous terrain. The most reliable and identifiable pre-McConnell glacial landforms are glacial erratics and meltwater channels cut into bedrock. Moraines from the Gladstone or Reid glaciations are identifiable, but they are typically discontinuous and preserved only where moraine accumulations are relatively thick and unmodified by colluvial and periglacial processes. In alpine settings, the relative degree of surface weathering observed in cirques and their corresponding geomorphological sharpness may be used to interpret a history of glaciation (Nelson and Jackson, 2003).

Prior to this study, field-confirmed glacial limit mapping had never been completed for the Stevenson Ridge and northern Kluane Lake map areas. Field-supported mapping for surrounding areas had been completed to the south and west by Rampton (1979a–e), to the east by Hughes (1989a,b) and Jackson (2000), and to the north by Huscroft (2002a–c) and Jackson (2005). Muller (1967) also mapped regional glacial limits within the study area. Duk-Rodkin (1999) produced a Yukon-wide glacial-limits map, which included the Stevenson Ridge map area, based on a compilation of previous work, complemented by air photo interpretation.

As part of this study, field traverses were completed beyond the limit of the Reid Glaciation to map the potential pre-Reid limit that Duk-Rodkin had mapped. Traverses were on flat alpine plateau summits where organic cover was minimal and frost-boils were abundant. In every location checked, no erratics were present beyond the limit of the Reid Glaciation. Similarly, a road traverse along the Alaska Highway in the adjacent Snag (115K) map area also revealed no erratics beyond the limit of the Reid Glaciation.

In the White River area, south of Donjek River, Turner (2014) mapped the Reid glacial limit as the most extensive Pleistocene glaciation. The penultimate Gladstone limit is slightly less extensive at this location, approximately 1–3 km inside the Reid limit. Reid and Gladstone glacial limits, where distinguishable, were within similar close proximity to each other elsewhere within the glaciated parts of the study area (Fig. 3-3).

While Duk-Rodkin's glacial limits map (1999) has traditionally been the primary reference for Yukon glacial limits, several bodies of work suggest that it needs updating for certain areas. Within the study area, the 1999 map illustrates the pre-Reid glacial limit extending north of Wellesley Lake, down the White River valley past the confluence of the White and Donjek rivers, and down the Donjek River past the mouth of Doyle Creek. No evidence supporting the presence of pre-Reid ice beyond the Reid glacial limit in these areas was found during our field or air photo mapping. To the west, in the adjoining Snag map area (115K), Duk-Rodkin (1999) mapped the pre-Reid glacial limit extending north up Scottie Creek, whereas Rampton (1979a) mapped Scottie Creek as unglaciated. In the McQuesten (Bond and Lipovsky, 2010) and Stewart River (Jackson *et al.*, 2001) areas in central Yukon, pre-Reid glacial limits were also found to be less extensive than previously mapped by Duk-Rodkin in 1999, but generally consistent with Bostock's (1966) mapping. Similarly, recent glacial limit mapping by Kennedy (2018) indicates that unglaciated terrain is more extensive in the northern Kluane Ranges area than previously mapped by Duk-Rodkin (1999).

The absence of previously mapped pre-Reid glaciations beyond the Reid limit in southwestern Yukon has important implications for mineral exploration in the region. Soil and stream-sediment geochemical sampling is one of the primary exploration tools used by the mineral industry for initially locating potential prospects (*see* Chapter 6 for futher discussion). Different approaches are required to determine the potential source of geochemical anomalies when they are located in

glaciated or unglaciated terrain (Bond *et al.*, 2008, Bond and Lipovsky, 2011; McKillop *et al.*, 2013). Recognizing the maximum Pleistocene glacial limit is therefore critical for determining whether bedrock geochemical anomalies have been influenced by glacial erosion and subsequent transport. An understanding of local and regional ice-flow history is also crucial for interpreting soil geochemical anomalies in glaciated terrain.

The revised extents of maximum Pleistocene glaciation also changes our understanding of Cordilleran Ice Sheet history in this region. Investigations into the history of the northern extent of the Cordilleran Ice Sheet by Ward *et al.* (2007a,b) have shown that ice extents in areas of limited annual precipitation may not correspond with global glacier extent patterns, both temporally and volumetrically. In addition, the maximum ice extent of different lobes that comprised the northern limit of the Cordilleran Ice Sheet may not be synchronous during a single phase of glaciation. The lack of relatively extensive pre-Reid ice in southwestern Yukon contrasts greatly with the much more extensive pre-Reid glacial limits in central Yukon. This example raises important and unresolved questions regarding precipitation controls in northwestern North America during the Pleistocene (Bond *et al.*, 2008).

Within the study area, ice extent differences between late Pleistocene glaciations are more noticeable in the southeast compared with the west, despite having a similar source area in the St. Elias Mountains. At Wellesley Lake and along the Donjek River, separation between the Reid and McConnell limits is approximately 8 km whereas in the Ruby Range, at Tyrrell Creek, the separation is more than 27 km. The reason for this discrepancy may be associated with topographic controls and glaciation duration. In the Wellesley Lake area and in Onion Creek, the CIS could flow relatively freely through low topography to its glacial limit north of the Nisling Range. In contrast, north of Kluane Lake, the McConnell CIS does not breach the hydrological divide, and therefore is unable to achieve down-valley ice flow on the north side of the Nisling Range. Had the McConnell Glaciation persisted longer, the CIS in Talbot Creek may have overtopped the Nisling Range hydrological divide and matched relative ice extents observed in Wellesley Basin.

Pleistocene Cordilleran Ice Sheet flow patterns

Glaciation of the study area by the Cordilleran Ice Sheet was controlled by the buildup of ice in the St. Elias Mountains (St. Elias lobe) and the configuration of valleys controlling drainage into surrounding regions. Ice flow patterns remained consistent between each late Pleistocene glaciation. The largest volume of ice to enter the study area occurred in the Wellesley Basin. Accumulation zones in the Donjek River and White River drainage basins, that lie directly south of the Wellesley Basin, fed the volume of ice. A relatively low topographic high on the north side of the Shakwak Trench facilitated movement of ice into the basin. Farther to the southeast, the topography on the north side of the Shakwak Trench is higher and broader and it appears to constrain the northward movement of ice into the Ruby and Nisling ranges (Fig. 3-3).

The movement of the St. Elias lobe into the southeastern part of the study area is controlled by the location of major valleys such as the Talbot and Brooks arms of Kluane Lake, Gladstone Creek and Kluane River (Cronmiller *et al.*, 2019). Ice in the Talbot Arm of Kluane Lake flowed east up Talbot Creek where it converged with local alpine glaciers. A large McConnell end moraine is preserved in Talbot Creek; glacial lake shorelines are eroded into it from water dammed in upper Talbot Creek (Fig. 3-4). During the Gladstone and Reid glaciations, ice in Talbot Creek advanced farther north into Tyrrell Creek, terminating 12 km upstream from the confluence with Nisling River (Fig. 3-5). The valley glacier in Talbot Arm also flowed northward into the Dwarf Birch Creek valley during each of the glaciations. The McConnell limit is situated in the upper reach of the drainage, whereas the Gladstone and Reid limits are mapped near the mouth of the drainage where they merged with ice in the Nisling River valley.

Figure 3-4. *A view to the west looking down Talbot Creek valley. A large end moraine was constructed in the valley during the McConnell glaciation. The ice and moraine dammed the valley and glaciolacustrine sediments were deposited in the foreground. Wave-cut shorelines are eroded into the moraine surface suggesting the minimum water level reached the crest of the moraine (see arrows). Post-glacial fluvial erosion cut through the moraine and drained the lake*

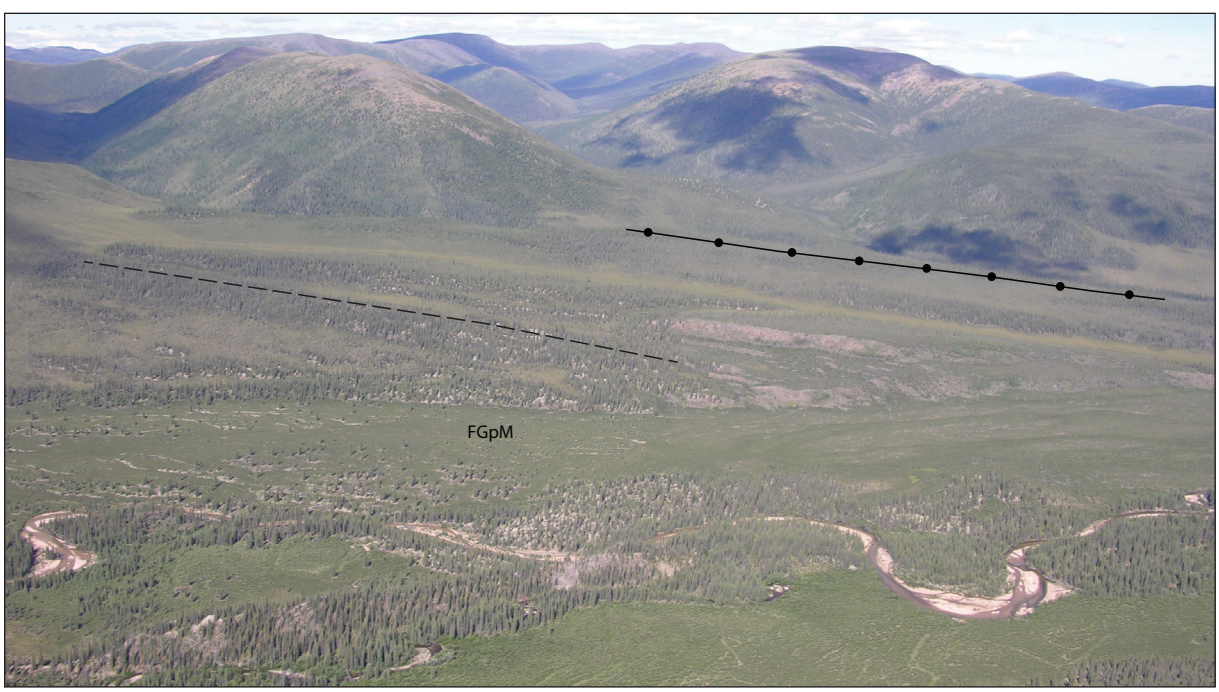

Figure 3-5. *The end moraine (symbolized line) and recessional moraine (dashed line) from the Gladstone glaciation in Tyrrell Creek, Nisling Range. The moraines were deposited by the leading edge of the Cordilleran Ice Sheet that flowed up Talbot Creek and crossed the hydrological divide in the Nisling Range into Tyrrell Creek. Glaciofluvial deposits from the McConnell glaciation (FGpM) are preserved along the margins of the modern floodplain.*

McConnell Cordilleran Ice Sheet deglaciation

Recessional moraines and stagnation terrain near the McConnell glacial limit are present only near Wellesley Lake. Elsewhere in the study area, deglaciation consisted of a period of initial clean frontal retreat, followed by stagnation or a pause in recession. This suggests that frontal retreat was delayed in the Wellesley Basin, likely due to the tendency of glacial ice to flow into the lowland. In the trunk valleys that funneled ice into the study area, thick deposits of ablation moraine, glaciofluvial gravel and glaciolacustrine sediments accumulated during pauses in the deglaciation (Fig. 3-6). A period of clean frontal retreat may have resumed after the ice limit retreated south of the study area. Active ice bedforms, such as drumlinoid ridges, are present in the Shakwak Trench near the Donjek River. These suggest active ice flow persisted through deglaciation and retreat of the ice front into the Kluane Ranges.

Three erratics on the north side of Talbot Creek valley near the McConnell limit were sampled for cosmogenic ^{10}Be surface exposure ages (locations 5, 6 and 7 in Fig. 3-3) following the methods outlined in Ward *et al.* (2007b). Terrestrial cosmogenic nuclide (TCN) dates for these three erratics are 16 394 ± 781 yr BP, 17 445 ± 908 yr BP and 23 967 ± 2,432 yr BP. The two younger dates mark the onset of McConnell deglaciation. The older date may mark an early stage of glacial maximum or may be the product of cosmogenic inheritance.

Ice that advanced northward up the Brooks Arm of Kluane Lake flowed into the Kiyera Lake valley and merged with a valley glacier in Tincup Creek. These glaciers eventually met Kluane River valley ice near Grace Lake that was flowing east into Onion Creek. Multiple glacial limits are preserved in the Onion Creek valley where during both the Reid and Gladstone glaciations, ice reached the Nisling River valley. One cosmogenic ^{10}Be surface exposure date was obtained from an erratic at the McConnell limit east of Tincup Lake that dates the onset of deglaciation at 17 017 ± 833 yr BP (location 4 in Fig. 3-3, and Fig. 3-7).

Figure 3-6. *A view looking north down the Donjek River valley near Wellesley Lake. Stagnation moraine is visible throughout the western side of the valley bottom and suggests that a period of recessional pause occurred during deglaciation.*

Figure 3-7. *A McConnell erratic located east of Tincup Lake that was sampled for cosmogenic surface exposure dating (07JB054) This erratic was deposited 17 017 ± 833 years ago and records the onset of McConnell deglaciation in the study area.*

Pleistocene alpine glaciation

Evidence of Pleistocene alpine glaciation in the Ruby, Nisling and Dawson ranges within the study area includes well-defined moraine ridges, meltwater channels and cirques. The most extensive Pleistocene alpine glaciers accumulated in the Ruby Range on uplands north and south of Talbot Creek (Cronmiller *et al.*, 2018; Fig. 3-8). In the Nisling Range, alpine glaciers were less extensive and developed on uplands east of Onion Creek including Mount Erickson. The most northerly extent of ice accumulation in the study area was mapped in the Dawson Range. Late Pleistocene alpine glaciers developed on Mount Cockfield and on Apex Mountain (Fig. 3-9); multiple glacial limits were mapped in the glaciated valleys emanating from these uplands. Evidence of early Pleistocene alpine glaciation is restricted to weathered cirques and no depositional sediments were observed. These cirques were noted on Mount Langham on the eastern edge of the study area, on Britton Ridge, Mount Maclennan and Coffee Peak.

Figure 3-8. *A McConnell alpine end moraine near the Talbot Creek valley, Ruby Range (08PL007).*

Figure 3-9. *The McConnell alpine end moraine (in foreground) on the east side of Mount Cockfield, Dawson Range.*

Chapter 4

Quaternary deposits and surficial geology map units

Surficial materials are unconsolidated sediments found at the earth's surface, constituting the parent material of most soils. They are produced by a variety of processes, including *in situ* weathering of bedrock, vegetation accumulation, and sediment transport and deposition by wind, rivers, lakes, oceans, volcanos, glaciers, permafrost, periglacial (seasonal freeze/thaw) activity, and gravitational (mass-movement) activity. Surficial materials are relatively young on a geological time scale and they are largely Quaternary in age (up to 2.6 million years old), although some late Tertiary/Pliocene deposits up to 5 million years old do exist north of the study area in the Klondike.

Mapping methodology

For this project, surficial geology units and landforms were mapped using interpretation of stereographic imagery (1987–1989 1:40 000 scale air photos and medium resolution (2.5 m) 2007 stereo satellite imagery; Fig. 4-1) supported by selective ground truthing. Paper air photos were used for field interpretation, whereas high resolution digital stereo imagery was viewed using PurVIEW software to interpret and delineate map units and surface features within an Esri ArcGIS platform in the office. Original air photo negatives were scanned at high resolution (2012 dpi) and could be digitally viewed in stereo at large scales up to 1:10 000. These images were aerial triangulated to 1:50 000 scale CanVec (Natural Resource Canada) topographic base data to produce the PurVIEW models.

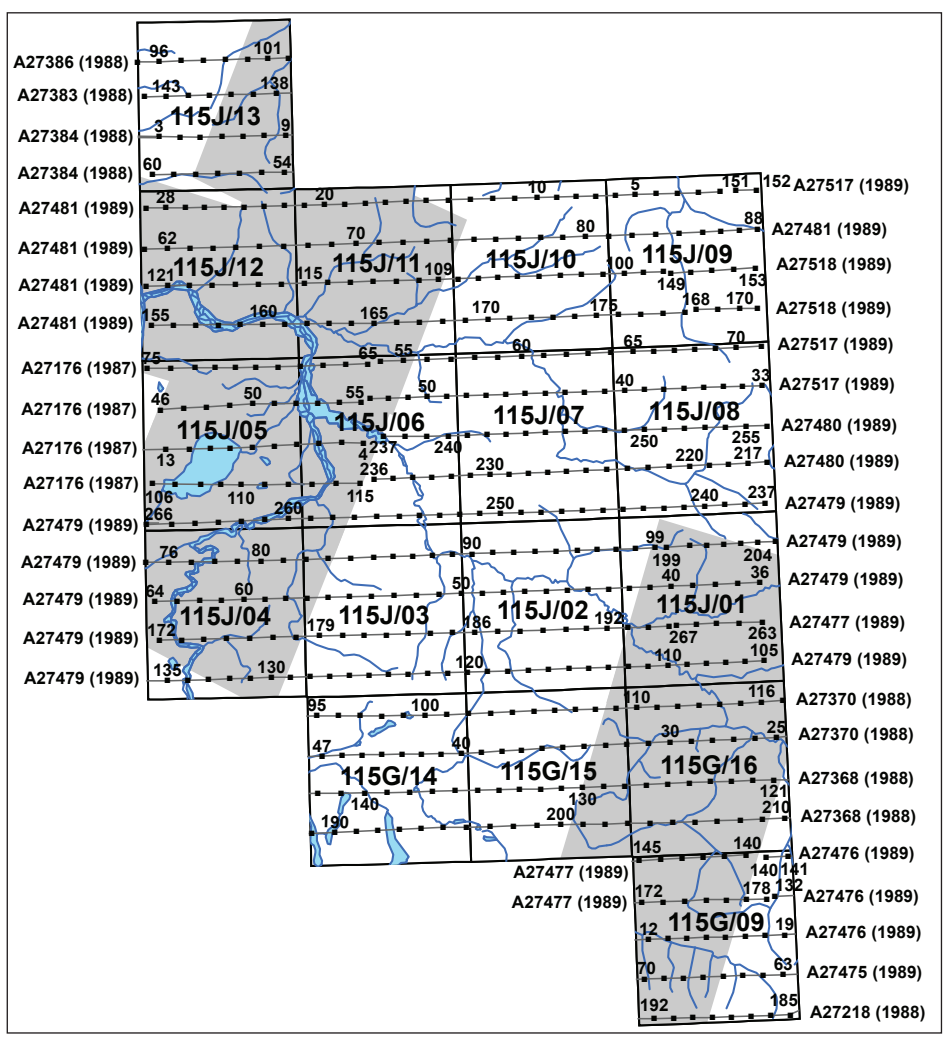

Figure 4-1. *Index map showing coverage of 2.5 m 2007 panchromatic CartoSat-1 satellite imagery (grey swaths) and aerial photos used for map unit interpretation.*

Selected map units were ground truthed in the field by examining riverbank and landslide exposures, and shallow soil pits (generally <1 m) dug in representative locations. Where available, road cuts and drillhole data were also investigated, while many large-scale landforms were verified in helicopter surveys. More than 400 field stations were investigated within the study area. Specific attributes recorded in the field included sediment genesis, texture/grain size, sorting, structure, thickness and general site characteristics (slope, aspect, elevation, topography, and vegetation).

Classification system

Surficial geology map units are classified based on the Terrain Classification System for British Columbia (Howes and Kenk, 1997) with minor modifications to meet Yukon requirements.

As shown in the simplified key to the Yukon Terrain Classification System (Fig. 4-2) and the accompanying surficial geology map legends, surficial or genetic materials form the core of the map unit polygon labels. They are symbolized with the first single upper case letter in the label, with up to 3 textural symbols written in lower case to the left, and up to 3 surface expression symbols written in lower case to the right. The glacial qualifier "G" is added to the surficial materials that were deposited in proglacial lake and river environments, in close proximity to glaciers. Relative age (where known) is indicated by the capital letter listed immediately following the surface expression. Up to 3 geomorphological processes may be specified following a dash. Up to 4 material types may be combined in a complex polygon map label, with individual components separated by delimiters which indicate relative proportions or stratigraphic relationships.

Surficial/genetic materials and associated landforms

Organic deposits

Organic deposits consist of at least 30% organic matter by weight, resulting from the accumulation of vegetative matter primarily in wetlands. They are most commonly found at the surface above mineral soil and comprise partially decomposed fibrous peat with recognizable remains of moss, shrubs, sedges and fine roots. Surface organic veneers (Ov) up to 30 cm thick are so widespread throughout the study area that they are generally unmapped. Thicker surface blankets (Ob; >1 m thick) or plains (Op) are most common in valley bottoms in low-lying, poorly drained wetland areas (*e.g.*, Fig. 4-3), and on gentle to moderate north-facing slopes. Many organic deposits are easily distinguished in valley bottoms by their very sparse or lack of tree cover. Organic material is very effective at insulating the ground in summer, and it is strongly associated with near-surface ice-rich permafrost (*e.g.*, Fig. 4-4), ice wedges and thermokarst collapse. Organic deposits are commonly associated or interstratified with valley-bottom accumulations of reworked loess. The initial silt deposition provides an insulative layer causing permafrost development, which inhibits drainage and promotes wetland vegetation.

The most extensive organic deposits in the map area occur in the Wellesley Basin lowlands and adjacent to the Donjek River near the mouths of Nisling River, Wellesley Creek, Dip Creek and Doyle Creek (*e.g.*, Fig. 4-3). All of these areas are situated near former extensive glaciofluvial plains that were significant source areas for loess.

Buried organic deposits are also common within colluvial deposits, where landslides have buried former surfaces, or in areas affected by periglacial processes such as cryoturbation and solifluction; however, these layers are typically too thin or laterally discontinuous to be mapped.

Simplified Key to Yukon Terrain Classification System & Surficial Geology Map Labels

Based on the Terrain Classification System for British Columbia (Howes & Kenk, 1997).
Yukon custom modifications written in *italicized text* and highlighted by asterisks (∗).

TEXTURE(S) (s = sand, g = gravel)
SURFICIAL MATERIAL (F = fluvial)
QUALIFIER (G = glacial; A = active; or I = inactive)
SURFACE EXPRESSION(S) (p = plain, t = terrace)
AGE (M = McConnell) ∗
GEOMORPHOLOGICAL PROCESS(ES) (X = permafrost)
SUBCLASS(ES) (s = sheetwash)

sgFGptM-Xs

TEXTURE - up to 3 lower case letters in front of surficial material, *in order of decreasing dominance* ∗

a	blocks (>256 mm, angular)
b	boulders (>256 mm, rounded)
k	cobble (64-256 mm, rounded)
p	pebbles (2-64 mm, rounded)
s	sand (0.062 - 2 mm)
z	silt (0.002 - 0.062 mm)
c	clay (<0.002 mm)
m	mud (mix of silt and clay)
d	mixed fragments (>2 mm, rounded and angular)
g	gravel (>2 mm, rounded; mix of b, k, p)
x	angular fragments (>2 mm; mix of r & a)
r	rubble (2-256 mm, angular particles)
y	shells (shells or shell fragments)
e	fibric organic (poorly decomposed)
u	mesic organic (intermediate decomposition)
h	humic organic (highly decomposed)

SURFICIAL MATERIAL - first single upper case letter shown in map unit. (Upper case letter immediately following surficial material is the glacial or activity QUALIFIER.)

A	Anthropogenic
C	Colluvium
D	Weathered Bedrock
E	Eolian
F	Fluvial (FA = Active Fluvial)
FG	Glaciofluvial
I	Ice (Glacier)
L	Lacustrine
LG	Glaciolacustrine
M	Morainal (till)
O	Organic
R	Bedrock
U	Undifferentiated materials *(UG = Glacial Drift)* ∗
V	Volcanic

∗ *H* *Water bodies*
∗ *S* *Snow patches*

SURFACE EXPRESSION - up to 3 lower case letters following surficial material

∗	a	*apron (BC steepness codes "j", "a", "k" and "s" not used)*
	b	blanket (>1 m thick)
	c	cone(s)
	d	depression(s)
	f	fan(s)
	h	hummock(s)
∗	l	*delta*
	m	rolling
	p	plain
	r	ridge(s)
	t	terrace(s)
	u	undulating
	v	veneer (0.1 - 1 m thick)
	w	mantle of variable thickness
	x	thin veneer (2 - 20 cm thick)

COMPONENT DELIMITERS - separators for up to 4 components that may be included in a map unit label. All components are listed before process(es), e.g.

sgFGptM.dsmMbM/xsCv\zcLGpM-XsV

.	components on either side of the "." symbol are of approximately equal proportion
/	the component in front of the "/" symbol is more extensive than the one that follows
//	the component in front of the "//" symbol is considerably more extensive than the one that follows
\	the component(s) in front of the "\" symbol stratigraphically overlies the component(s) that follows

∗ **AGE -** *single upper case letter following surface expression*

H	Holocene
>H	pre-Holocene
N	Neoglacial
<M	Postglacial
M	McConnell (late Wisconsinan)
>M	pre-McConnell
S	Laurentide, Tutsieta (late Wisconsinan)
L	Laurentide, maximum (late Wisconsinan)
G	Gladstone (early Wisconsinan)
>G	pre-Gladstone
R	Reid (Illinoian)
>R	pre-Reid (Pliocene - early Pleistocene)
P	Pleistocene undifferentiated
Q	Quaternary
>Q	pre-Quaternary
T	Tertiary
U	undifferentiated

GEOMORPHOLOGICAL PROCESS - up to 3 upper case letters following dash "-". Lower case letters indicate subclasses.

	-V	Gully erosion
	-B	Braided floodplain
	-I	Irregularly sinuous floodplain
	-J	Anastamosing floodplain
	-M	Meandering floodplain
	-A	Snow avalanches
	-F	Slow landslide (subclasses: g = rock creep)
	-R	Rapid landslide (subclasses: b = rockfall; d = debris flow)
∗	-L	*Undifferentiated landslide* (subclasses: s = slide; u = slump)
	-C	Cryoturbation
	-N	Nivation
	-S	Solifluction
	-Z	General periglacial processes (*subclass: c = cryoplanation*)
∗	-X	Permafrost (*subclasses: s = sheetwash; n = pingo; l = seg. ice*)
	-E	Glacial meltwater channels
	-H	Kettled
∗	-T	*Glacial ice-contact*
∗	-U	Inundation (*subclass: b = beaver damming*)

Figure 4-2. *Terrain classification scheme applied to mapping the study area.*

Figure 4-3. *Thick organic deposits blanket the Doyle Creek valley bottom and are associated with the presence of underlying permafrost. Note thermokarst collapse pond in the background and forested pingo (10PL032) in the foreground.*

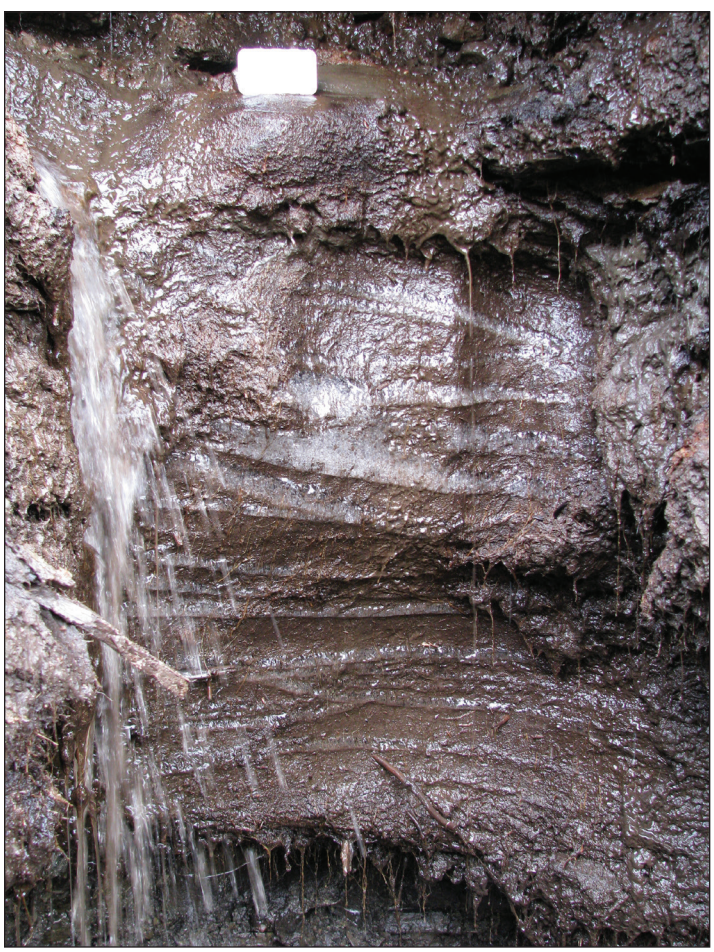

Figure 4-4. *Ice-rich peat exposed in a thaw slump scarp in a tributary valley of upper Dwarf Birch Creek (Nisling Range; 08PL026). Ice lenses are up to 5 cm thick.*

Volcanic (White River ash)

The most prominent volcanic deposit found in the map area is the east lobe of the White River ash, which fell from the A.D. 833–850 eruption (Lerbekmo, 2008; Jensen *et al.*, 2014) on the Mt. Bona-Churchill massif. This tephra is distinctly white to grey or beige in colour with a "salt and pepper" appearance when viewed up close and grain size ranges from fine to coarse sand within the study area. The thickness of the ash is variable and declines gradually to the east and more abruptly to the north (Lerbekmo and Campbell, 1969). Primary (air fall) White River ash is estimated to have had an average thickness of 10–20 cm throughout the Ruby and Nisling ranges, with thicker accumulations on westerly facing slopes (Fig. 4-5; West and Donaldson, 2002). Subsequent reworking by eolian and fluvial activity has resulted in very thin, discontinuous or entirely absent ash deposits on exposed or erosional surfaces such as ridge tops, steep hillslopes and active floodplains. White River ash is very rarely observed in the Dawson Range, but is present in a few valley bottoms or lower slope locations, where it occurs in discontinuous lenses less than 2 cm thick (*e.g.*, 10JB018, 039 and 040; 10PL004 and 045).

Secondary resedimentation has resulted in much thicker accumulations in valley bottom dunes, lake basins, fluvial fans, deltas, and in the floors of some alpine cirque basins. The thickest resedimented White River ash deposits were observed in the broad valley bottoms near Grace Lake (07PL016) and Tincup Lake (07JB015, 08PL069; Fig. 4-6a) where ash dunes 1.5 to 6 m high were noted. At Toshingermann Lakes, White River ash accumulation on a nearby fluvial fan plugged the outlet of the northern lake and caused the lake level to rise by more than 2 m. Subsequent re-incision of the outlet to its former level has exposed more than 3 m of resedimented ash at that location (07JB022; Fig. 4-6b). Resedimented ash, at least 2.4 m thick, was observed within tributary fluvial fan deposits exposed in a lower Klaza River cutbank (08JB081; Fig. 4-6c). An exposure of more than 2 m of resedimented ash is present in a Kluane River cutbank (07PL044; Fig. 4-5). Resedimented and cryoturbated ash is nearly 2 m thick in the floor of a cirque, located approximately 10 km south of Mount Erickson (08JB053).

Immediately south of study area, the White River ash is commonly associated with shallow permafrost and active-layer detachment slides due to its high insulation capacity and its loose, granular consistency (*see* Chapter 6).

Figure 4-5. *Two metres of resedimented White River ash overlies 30 cm of primary ash fall (bright white layer) in a Kluane River cutbank (07PL044).*

Figure 4-6. (a) *Tephra dunes formed by eolian resedimentation of White River ash. Note person standing in background for scale (08PL069).* ***(b)*** *White River ash at the north end of Toshingermann Lakes. The dark grey line within the sequence is composed of detrital mafic tephra mineral particles that were sorted by wave action along a lake shoreline immediately following the eruption. Post-eruption resedimentation from nearby hillside sources subsequently buried the primary ash fall deposit.* ***(c)*** *Resedimented White River ash along the Klaza River. The exposure illustrates the extreme volume of volcanic material that inundated some floodplains in the study area.*

Eolian

Eolian materials are sediments that have been transported and deposited directly by wind. They were primarily deposited during glacial and deglacial periods, and were sourced from areas where an abundance of fine-grained sediment was exposed at the surface. These include glacial meltwater floodplains and drained glacial lakebeds. Slopes blanketed by thick eolian deposits are easily distinguished by the presence of numerous shallow gullies (*e.g.*, Fig. 4-7).

The dominant eolian sediment in the map area is loess, which is silt-sized in texture, with minor fine sand. The Dawson Range was inundated by loess generated largely from the broad, braided floodplains of the Donjek and White Rivers to the south. The Nisling River floodplain was also an important sediment source. A thin veneer (10–20 cm) of loess was deposited over most of the landscape during the last glaciation. Although generally not mapped because it was so widespread, it should be expected to occur at the surface in most areas. On stable drier sites, the loess is intact and commonly massive and oxidized to orange-brown in colour (Fig. 4-8c). Loess also commonly translocates downward through the soil profile, forming silt caps on the top surfaces of clasts. On hillslopes, colluviation and cryoturbation rework loess into the soil profile. Loess veneers have important implications on soil geochemistry as they effectively dilute the geochemical signature of more locally derived surficial materials.

Remnants of a northeast-trending parabolic sand dune near Donjek River (north of its confluence with Wellesley Creek; 10JB043) indicates that the dominant paleo-wind direction in the area was southwesterly, and suggests that the winds originated from the north Pacific Ocean and katabatically drained down the former St. Elias lobe of the Cordilleran Ice Sheet. The northwest-southeast orientation of the Dawson and Nisling ranges acted as a barrier

Figure 4-7. *Near the mouth of Maloney Creek, prominent gullies have developed on slopes blanketed by eolian sand which was blown off the Nisling River floodplain during the last glaciation.*

against these winds, resulting in the thickest loess deposition on the windward, or southwest side, of the northern Dawson Range, particularly along the lower slopes of tributary valleys to the Donjek, White and Nisling rivers. For example, loess accumulations greater than 20 m thick were observed near the mouths of Home Creek (Fig. 4-8a; 10PL050) and Tom Creek (10JB042).

Blankets and dunes of well-sorted eolian sand are present in a few valley bottom and lower slope locations more proximal to the original sediment sources (*e.g.*, near the mouth of Maloney Creek in the Nisling River basin (Figs. 4-7 and 4-8b) and immediately north of the confluence of Wellesley Creek and Donjek River (10PL048)).

Figure 4-8. (a) *Loess benches >20 m thick (see area outlined with dashed line) are found along the south side of Home Creek valley (White River visible in background).* ***(b)*** *Medium to fine-grained eolian sand exposed in a soil pit at 08PL049 near the Nisling River is greater than 150 cm thick.* ***(c)*** *A veneer of loess overlies a glaciofluvial gravel adjacent to the Nisling River. The loess unit was buried by White River ash.*

Colluvium

Colluvium is material that was transported and directly deposited by down-slope, gravity-driven mass movement processes such as creep, landslides and snow avalanches. Due to the extensive mountainous terrain, shallow permafrost and active periglacial processes in the map area, colluvium is one of the most widespread materials found on upland, hillslope and slope toe topographic positions. It is also the most dominant surficial material in unglaciated portions of the map area, such as the northern Dawson Range.

Within the map area, the texture and composition of colluvium varies more than any other material and is very dependent on the parent material, and the mechanism and distance transported. Some colluvial materials deposited by rapid mass movement processes, such as rock falls, debris flows and avalanches, are typically found on steep to moderate slopes. Conversely, slower processes such as solifluction and creep occur on gentle to moderate slopes and are commonly associated with the presence of shallow permafrost.

Colluvium most commonly comprises silt-rich diamicton with crude stratification that parallels the slope. In unglaciated and alpine settings, colluvium is dominantly derived from frost-shattered weathered bedrock fragments with angular clasts of uniform lithology, and a silt-rich matrix resulting from incorporation of loess and minor organics (Fig. 4-9). Conversely, colluvium derived from till strongly resembles *in situ* till, but contains slope parallel resedimentation structures, and subrounded erratic clasts of mixed rock types.

Colluvial veneers and blankets (*i.e.*, Cv and Cb) are the most extensive surficial materials mapped in the study area, particularly in unglaciated terrain. Thinner colluvial veneers are found on steeper upper slopes, while thicker (>1 m) blankets are found on gentler and mid to lower slopes. Both units have very similar composition and commonly occur together (*e.g.*, Cvb; Fig. 4-10).

Colluvial aprons (Ca) are also a very common landform in the map area, particularly in unglaciated valley bottoms. The aprons fringe the toes of permafrost slopes in a nearly continuous low-angle wedge. They comprise a stratified mixture of sheetwash sediment (sand and granules that have been carried downslope by unconcentrated water seeping along the permafrost table) with resedimented loess, and peat or organic material. Incorporation of lenses of coarser sediment may also occur at the base of steeper slopes. Due to their high silt and organic content, these colluvial aprons are very poorly drained deposits that commonly contain extensive ice-rich permafrost (Fig. 4-11). Ice-rich colluvial apron sediments >30 m thick were reported in drill records from Dip Creek valley near the mouth of Casino Creek (Knight Piésold, 2012).

Figure 4-9. *Colluviated weathered bedrock and organic material on a slope in Sonora Gulch.*

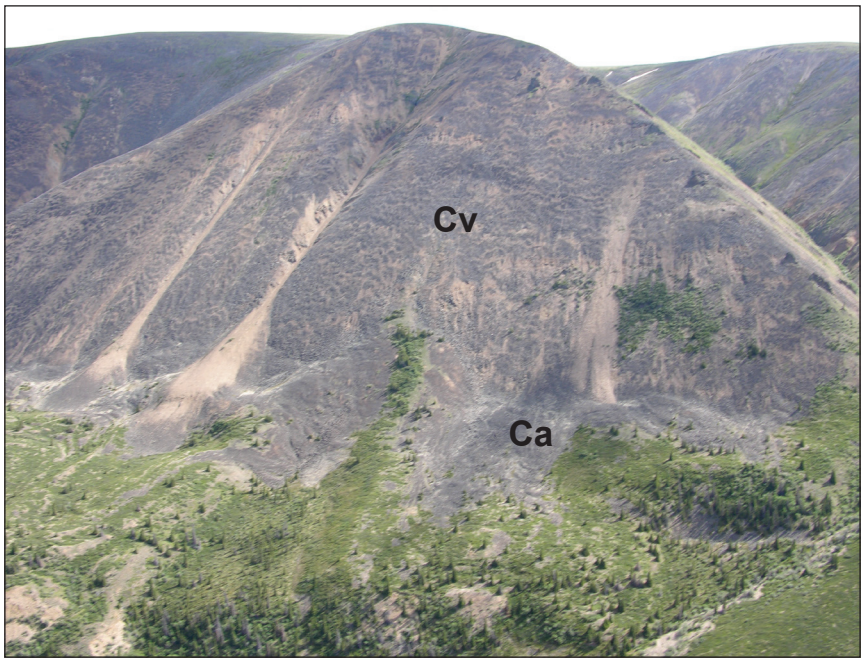

Figure 4-10. *Ridge crests and upper slopes of steep glaciated terrain in the Nisling Range are covered with a veneer of colluviated weathered bedrock that grades into a thicker colluvial blanket on mid to lower slopes. At the base of these slopes colluvial cones and aprons, comprising coarse rubble, commonly develop into rock glaciers.*

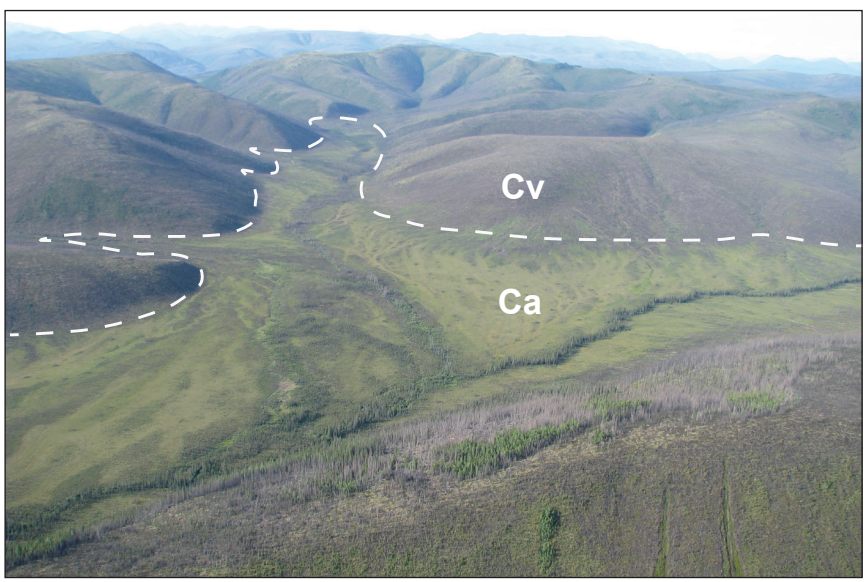

Figure 4-11. *Colluvial aprons form extensive landforms, particularly in the unglaciated portion of the study area on the south slope of the Dawson Range.*

Veneers or blankets of coarse rubbly talus derived from weathered bedrock generally cover steep alpine slopes in the Ruby and Nisling ranges. These slopes are commonly subject to rockfall activity beneath steep rock outcrops, and debris flows in narrow channels or gullies. Rubbly talus cones and aprons commonly form at the base of such slopes. In some locations, rock glaciers form within the talus when interstitial ice grows and deforms in the void spaces between the rock fragments (Fig. 4-10).

Solifluction is a very common periglacial process that modifies colluvial deposits throughout the map area; this is the slow downslope flow of saturated unfrozen earth materials (van Everdingen, 2005). Within the study area, it most commonly occurs on slopes of variable steepness and aspect underlain by shallow permafrost, particularly in alpine settings (*e.g.*, Fig. 6-11). Permafrost is strongly associated with solifluction because it acts as a barrier to drainage, promoting saturated ground conditions above, particularly where the active layer is thin and/or ice-rich at the base. Solifluction lobes investigated north of Mount Pattison primarily comprise coarse bedrock fragments and little matrix, with silt content decreasing with depth. The lobes appeared to move largely as a result of deformation in the basal coarse fragment layer (Fig. 4-12).

Figure 4-12. *A soil pit within a solifluction lobe north of Mount Pattison (10JB054). The lobe contains abundant coarse rock fragments mixed with organics and minor silt.*

Fluvial

Fluvial sediments (or alluvium) are transported and deposited by modern streams and rivers and are found in floodplain, terrace and fan landforms. They typically consist of stratified sand and gravel that is moderately to well-sorted with subrounded to rounded clasts and minor silt and organic deposits (Fig. 4-13a). Due to scale limitations, fluvial deposits in most of the smaller valleys are not mapped.

Fluvial sediments are considered active where subject to periodic reworking and inundation by flooding. Floodplains occur close to modern river levels, while terraces are older floodplain surfaces that have been incised following a base level change, leaving a sharp escarpment along one side. Fluvial fans occur at the mouths of steeper drainages where flows become unconfined upon entering a higher-order or lower-gradient valley bottom. They typically comprise coarser and more poorly sorted material that may be interstratified with colluvial/debris flow deposits. They are also subject to avulsions, when a sudden change occurs in the course of a stream channel (Fig. 4-13b).

Sheetwash (also referred to as slopewash) is a widespread indicator of shallow permafrost (indicated by the geomorphological process symbol “-Xs”). It occurs when water flows in thin sheets, rather than in channels, along a shallow impermeable permafrost table. The process gradually transports fine sediment (sand, silt and clay) down to the foot of slopes through unconcentrated overland flow and percolation through saturated sediment (French, 2017). Evidence of sheetwash is reflected by a distinctive surface expression in which the land surface appears to be flowing when viewed from the air (Fig. 4-13c). Sheetwash is most commonly found on gentle to moderately sloped valley sides that are blanketed by till or colluvium.

Figure 4-13. (a) *The texture of fluvial deposits in the study area can vary widely. Here a coarse, poorly sorted cobble-pebble gravel is exposed near Grayling Creek.* ***(b)*** *An aerial view of the Dwarf Birch Creek floodplain in the Nisling Range. The floodplain (Fp) contains remnant stream channels and is bounded by small fluvial fans (Ff) originating from tributary valleys. The toe of the fluvial fans consist of fine-grained sediment that host near-surface permafrost, whereas the active floodplain is permafrost-free.* ***(c)*** *An aerial view of sheetwash fluvial processes in Dip Creek valley. These deposits are typically fine grained and interstratified with organic material. A portion of the landform may accumulate through colluvial processes. Tree growth is limited on these deposits due to the shallow permafrost table.*

Glaciolacustrine

Glaciolacustrine sediments are deposited in lakes that form on, in, under or beside a glacier. Glaciolacustrine sediments generally consist of fine-grained, laminated sand, silt and clay. Ice-rich permafrost and thermokarst erosion is widespread in these deposits as their poor drainage and high *in situ* moisture content can result in massive ice lenses (Fig. 4-14a,b).

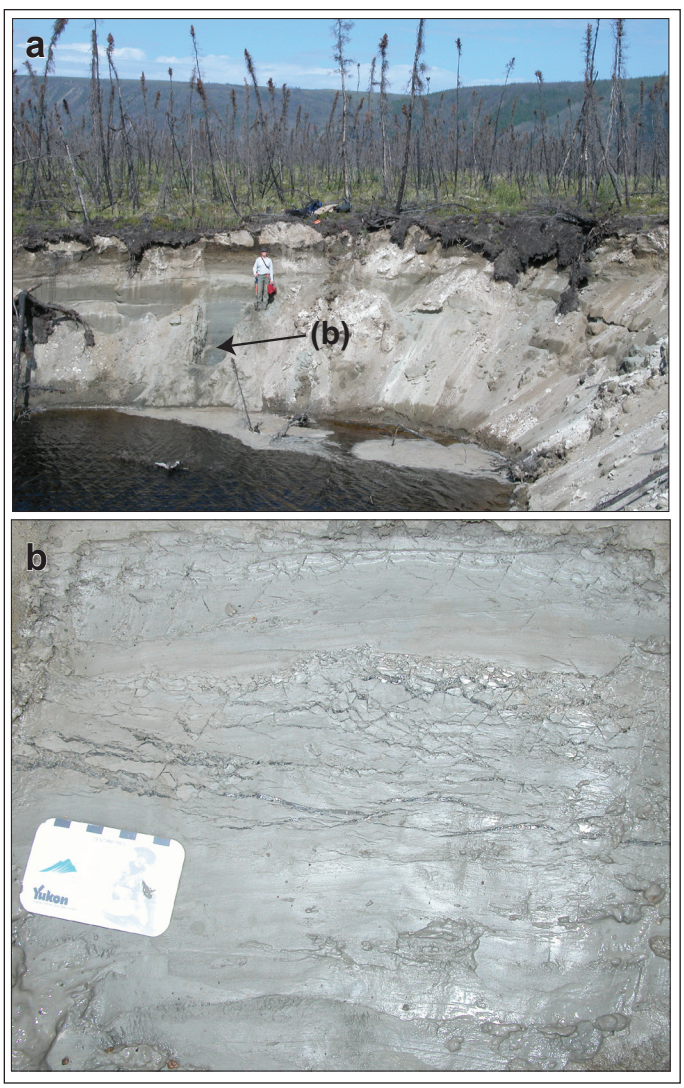

Figure 4-14. (a) *Glaciolacustrine sediments exposed in a thermokarst pond in the Grace Lake valley (07PL010). Permafrost degradation may have been initiated by a recent forest fire.* ***(b)*** *A close-up view of the glaciolacustrine sediments exposed in the Grace Lake valley (07PL010). Up to 15% visible ice is contained within the silty clay unit near the base of the section shown in (a).*

The distribution of glaciolacustrine sediment in the study area was controlled by topographic constraints and interconnected valleys that permitted ice damming by the St. Elias lobe of the Cordilleran Ice Sheet. As the St. Elias lobe flowed northward into the Ruby and Nisling ranges, it flowed against the topographic gradient in many valleys, resulting in the formation of proglacial lakes during both glacial advance and deglaciation. This would have included large glacial lakes in main trunk valleys as well as small ice marginal lakes in first or second order tributary valleys.

The largest McConnell glacial lake in the map area was impounded in the Grace Lake and Tincup Creek valleys by St. Elias valley glaciers flowing down the Donjek and Kluane River valleys and east up Swanson and Tincup creeks. The thickness (>5 m) and extent of glaciolacustrine deposits in the Grace Lake and Tincup Creek valleys suggest that the glacial lake existed for an extensive period of time during McConnell deglaciation (Bond and Lipovsky, 2009a).

Relatively large glacial lakes were also present in the Brooks and Talbot creek valleys that presently drain into Kluane Lake. During deglaciation, St. Elias ice impounded a glacial lake in the Brooks Creek valley, where at least 50 m of fine-grained glaciolacustrine sediment was deposited (Fig. 4-15; 07PL037). From the Talbot Arm, McConnell St. Elias ice advanced up Talbot Creek and overrode “Glacial Lake Talbot”, which eventually drained through an outlet in Tyrrell Creek (Bond and Lipovsky, 2009d).

Figure 4-15. *A 50 m-thick sequence of glaciolacustrine sand and silt exposed in a cutbank on Brooks Creek.*

Pre-McConnell glaciolacustrine sediments are rare and restricted to small tributary valleys above the McConnell limit; morainal, colluvial or glaciofluvial deposits obscure most of these deposits. Small pre-McConnell glaciolacustrine deposits were mapped along the eastern side of the White River near its confluence with the Donjek River.

Glaciofluvial

Glaciofluvial materials are deposited directly by glacial meltwater and form above, in, below, or adjacent to a glacier. Deposition occurs in meltwater channels, eskers, outwash plains, terraces, kames, fans and deltas. Glaciofluvial deposits consist of moderately to well-sorted, stratified sand and gravel, and characteristics may vary locally depending on transport distance. Near surface ground ice is generally absent in glaciofluvial deposits unless there is a poorly drained underlying unit present.

Extensive flat-lying McConnell glaciofluvial outwash plains (FGp) and terraces (FGt) occur north of Tincup Lake, near Grace Lake, and along the broad valleys of Brooks Creek, Onion Creek, Tyrrell Creek (Fig. 4-16a), Nisling River and Donjek River (Fig. 4-16b,c). Glaciofluvial deposits up to 40 m thick are exposed in a large terminal moraine in the Talbot Creek valley.

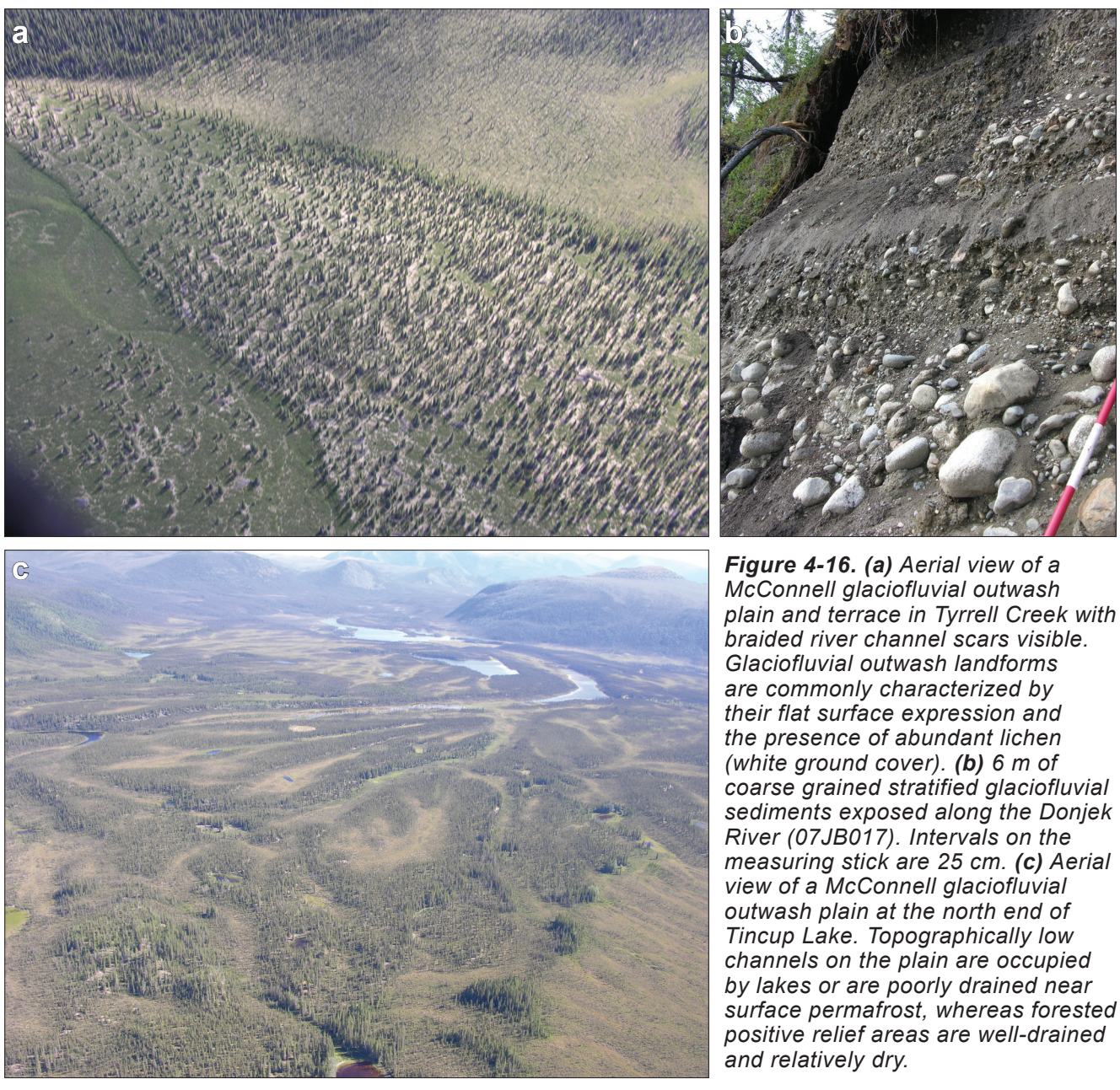

Figure 4-16. (a) *Aerial view of a McConnell glaciofluvial outwash plain and terrace in Tyrrell Creek with braided river channel scars visible. Glaciofluvial outwash landforms are commonly characterized by their flat surface expression and the presence of abundant lichen (white ground cover).* ***(b)*** *6 m of coarse grained stratified glaciofluvial sediments exposed along the Donjek River (07JB017). Intervals on the measuring stick are 25 cm.* ***(c)*** *Aerial view of a McConnell glaciofluvial outwash plain at the north end of Tincup Lake. Topographically low channels on the plain are occupied by lakes or are poorly drained near surface permafrost, whereas forested positive relief areas are well-drained and relatively dry.*

Less extensive remnants of older (Gladstone and Reid) glaciofluvial deposits are scattered along various valleys within the Nisling Range.

A large ice-contact/kame complex (FGhr-HT) occurs along Brooks Creek near Kiyera Lake. Numerous kettle lakes in the area are the result of depressions created when large blocks of glacier ice, buried in the glaciofluvial outwash, melted out. Esker ridges suggest easterly drainage of former subglacial meltwater streams.

Glaciofluvial fan (FGf) and delta (FGl) deposits are rare within the map area and are concentrated within the Talbot Creek valley where McConnell meltwater drained from tributary valleys into Glacial Lake Talbot. In a tributary to Brooks Creek, north of Tincup Lake, 24 m of glaciofluvial fan (FGf) gravel is exposed where ice marginal meltwater drained into the ice-dammed tributary (07JB013; Fig 4-17a).

Glacial meltwater channels are indicated by the geomorphological process symbol "-E". These erosional glaciofluvial landforms are abundant within and proximal to glaciated portions of the map area (*e.g.*, Fig. 4-17b). Where they occur on valley sides, the elevations of the uppermost lateral or ice-marginal meltwater channels are excellent indicators of minimum glacial limits in the local area. Larger-scale subglacial and proglacial meltwater channels also occur in many valley bottoms where they have rerouted or established many contemporary drainage pathways, and currently host underfit streams.

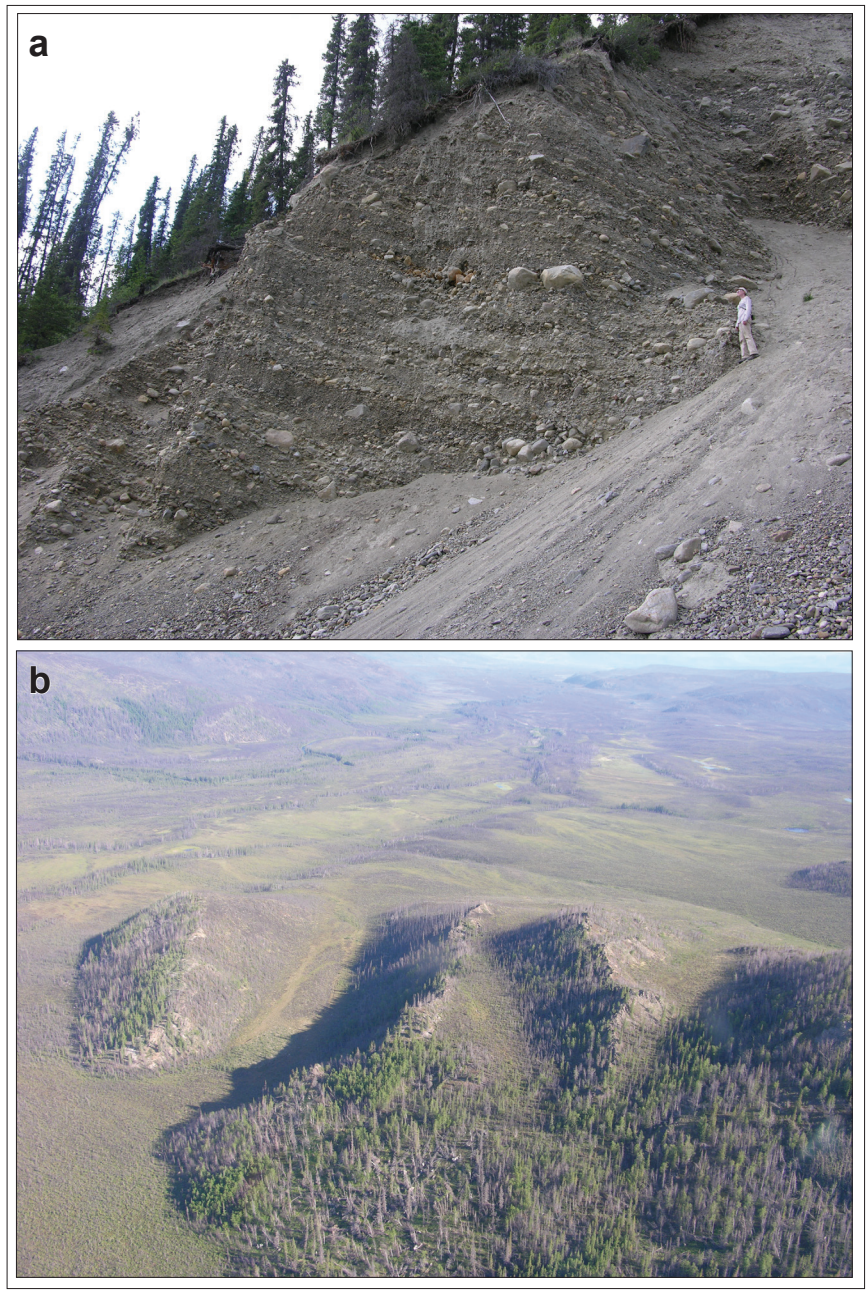

Figure 4-17. (a) *A stream-cut section through a McConnell lateral moraine contains a coarse, advance outwash fan gravel under a lodgement till north of Tincup Lake (07JB013). The coarse gravel was deposited by proglacial meltwater flowing into an ice-dammed, small tributary valley.* ***(b)*** *A series of lateral meltwater channels eroded through a bedrock ridge in the Onion Creek valley. The progressively lower channels record the thinning glacier margin during deglaciation.*

Morainal

Morainal (till) materials are deposited by either primary glacial processes such as lodgement, deformation and ablation (melt-out), or by secondary glacial processes caused by gravity and water (*e.g.*, flow tills). Till generally comprises diamict made up of poorly sorted, subangular to subrounded clasts of mixed rock types with a significant proportion of finer-grained matrix (*i.e.*, texture “dsm”; Fig. 4-18a). In general, morainal deposits from the St. Elias lobe of the Cordilleran Ice Sheet tend to be finer grained than those deposited by smaller alpine valley glaciers (*e.g.*, Upper Tyrrell Creek, 08JB085).

Both lodgement till and ablation till are widespread within the glacial limits. Lodgement (or basal) till typically has an even surface morphology (Mv and Mb; Fig. 4-18b) with a dense silty sand matrix comprising 40–60% of the material. Ablation (or melt-out) till generally has a hummocky (Mh), rolling (Mm), and/or kettled (pitted; M-H; Fig. 4-18c) surface morphology with a looser or sandier matrix comprising 30–40% of the material. Till is commonly modified by colluviation in mountainous areas, as indicated by slope parallel structures within the till. Permafrost is common within morainal deposits, especially within finer-grained lodgement till.

Moraine ridges (Mr) deposited along the flanks or toes of valley glaciers are present in many locations throughout the map area. Prime examples include terminal or end moraines located in the Ruby Range and in Talbot and Tyrrell creeks (Fig. 4-18d), flights of recessional moraines along Tyrrell Creek (*e.g.*, 08JB055) and lateral moraines north of Tincup

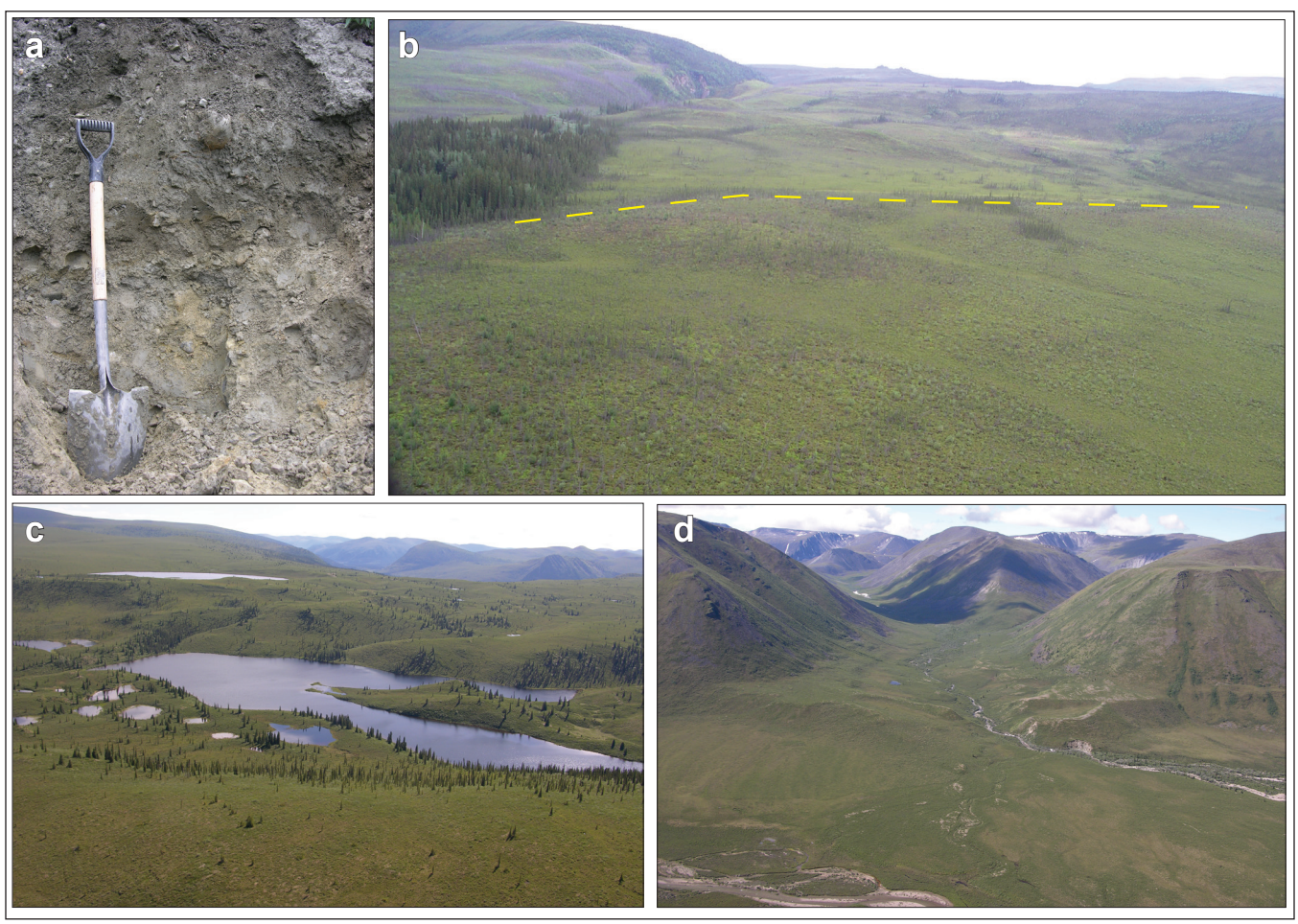

Figure 4-18. (a) *A matrix-supported, compact, McConnell lodgement till exposed in a stream cut section on a tributary to Brooks Creek (07JB014).* ***(b)*** *A McConnell moraine blanket and ridge (dashed yellow line) exposed near Grayling Creek.* ***(c)*** *Hummocky stagnation moraine deposited during the McConnell glaciation at a divide located between Dwarf Birch and Brooks creeks (08JB002).* ***(d)*** *Ruby Range valley glacier end moraine (08PL007), with Talbot Creek in foreground. The ridge is approximately 48 m tall at its highest point above the modern creek. The till comprises approximately 50% silt-rich matrix with clasts dominated by the boulder size fraction.*

Lake (*e.g.*, 07JB013). Some lateral or recessional moraine ridges are heavily modified by slope and periglacial processes and have a distinctive "beaded" appearance. Gladstone and Reid lodgement tills are much less extensive than McConnell tills as they are highly modified by colluviation and periglacial weathering and are only found intact at the surface in a few scattered locations. Similarly, the only place pre-Reid till is mapped at the surface is along Hayes Creek near Sonora Gulch in the northeastern part of the study area.

Weathered bedrock

Weathered bedrock is the most common surficial material in upland parts of the study area (Bond and Lipovsky, 2011). These deposits are typically <1 m thick and are commonly capped by a loess-enriched horizon (10–30 cm thick) on relatively flat sites (*e.g.*, Fig. 4-19). Weathered bedrock varies in texture according to the lithological characteristics of the underlying bedrock, the amount of loess additions to the soil, and the degree of mixing that has occurred of these two material types. Where derived from intrusive rocks, weathered bedrock veneers commonly consist of blocky or angular rubble (texture "x"; Fig. 4-20a) with a coarse-grained sandy (grus) matrix. Under the current climatic conditions, periglacial and mass wasting processes are the primary means by which bedrock is transformed into unconsolidated material. These processes include frost shattering, cryoturbation, solifluction, soil creep and landslides. Weathered bedrock is commonly recognized in alpine environments (stable ridge crest landscape positions) by the presence of patterned ground features, such as stone polygons and mud boils, which have been produced through the action of cryoturbation (Fig. 4-20b).

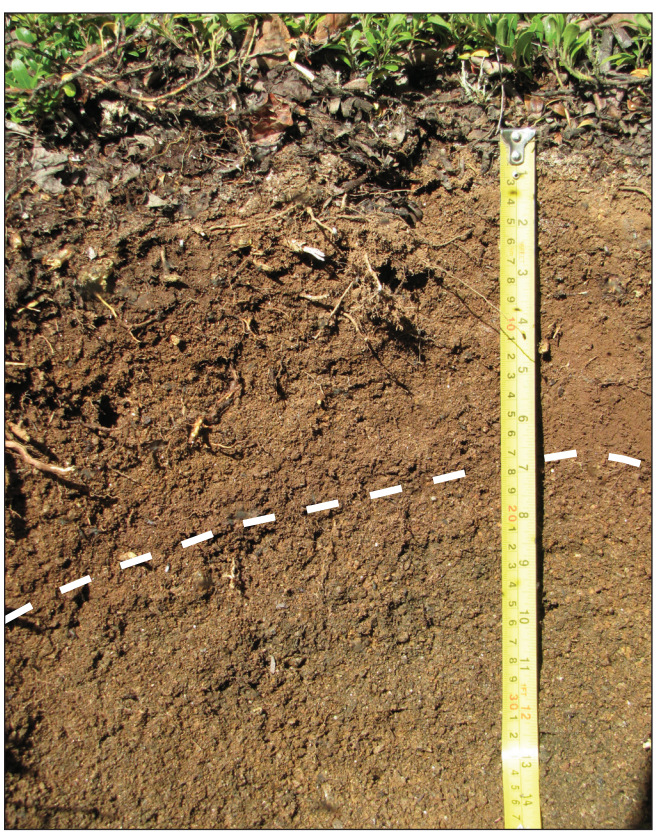

Figure 4-19. *A soil profile from a low ridge-top surface in the Dip Creek valley (10JB019). The loess-rich portion of the soil occurs in the upper 18 cm (above dashed line) and appears oxidized. A weathered intrusive rock forms the lower portion of the profile, which is non-cohesive and has a grus texture.*

Cryoplanation terraces (Dv\Rt) are a distinctive weathered bedrock feature on many ridge crests and summits in the region. These erosional landforms occur as a series of large-scale step-like benches up to several hundred metres wide that are formed by intense periglacial weathering of bedrock (particularly frost wedging) in association with nivation or snowbanks (Fig. 4-20c; van Everdingen, 2005; Reger and Péwé, 1976; and Nelson and Nyland, 2017). They are generally covered by a thin veneer of weathered bedrock or colluvial diamicton and are commonly structurally controlled by weathering concentrated along joints, beds, and/or contacts in the underlying bedrock. Within the study area, the terraces seem to form preferentially on gentle northwest-facing slopes where snow likely persists longest each year. Excellent examples of cryoplanation terraces are found near Mount Laderoute, Mount Langham, and above the headwaters of Onion and Somme creeks. Cryoplanation terraces require extended periods of time to form, and therefore usually indicate very old, unglaciated surfaces.

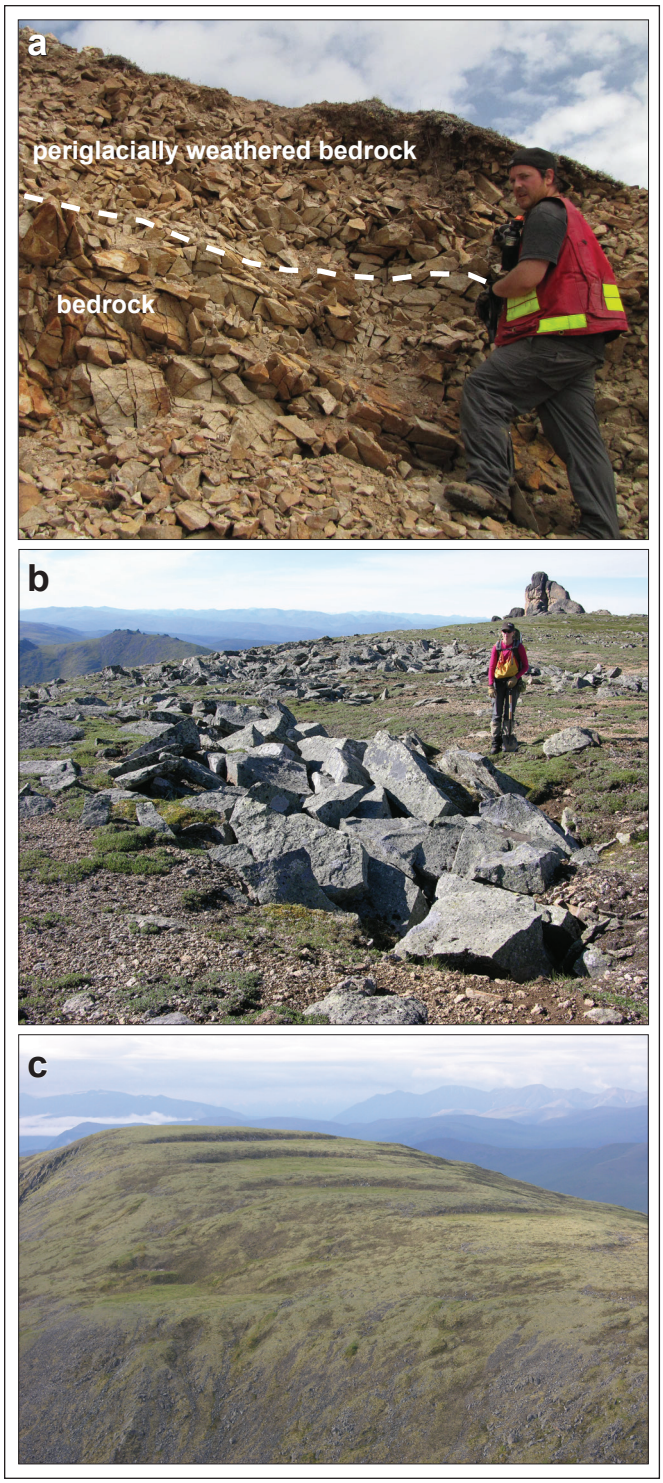

Figure 4-20. (a) *On the uplands bordering Casino Creek in the Dawson Range, a veneer of coarsely weathered bedrock develops from a similarly fractured altered and leached granodiorite.* ***(b)*** *Stone polygons and mud boils are visible on level surfaces of Britton Ridge, located between the Klaza and Nisling rivers. A tor is visible in the background.* ***(c)*** *Cryoplanation terraces on an unnamed mountain near Onion Creek. The terrace scarps are 6 to 8 m high (08JB035).*

Bedrock

Bedrock outcrops are most common in upland areas on summits and ridge tops throughout the map area. Tors are tower-shaped bedrock landforms that are abundant along ridge crests, particularly in unglaciated portions of the map area. They are composed of rocks more resistant than those immediately surrounding them, and form as a result of differential weathering over very long periods (*see* detailed discussion in Hughes, 1990). In the Britton Ridge area, some of the tallest tors in Yukon have developed in intrusive alaskite rocks, which stand up to 25 m high (Fig. 4-21a). Some are also found on lower elevation ridge crests located below tree-line (Fig. 4-21b).

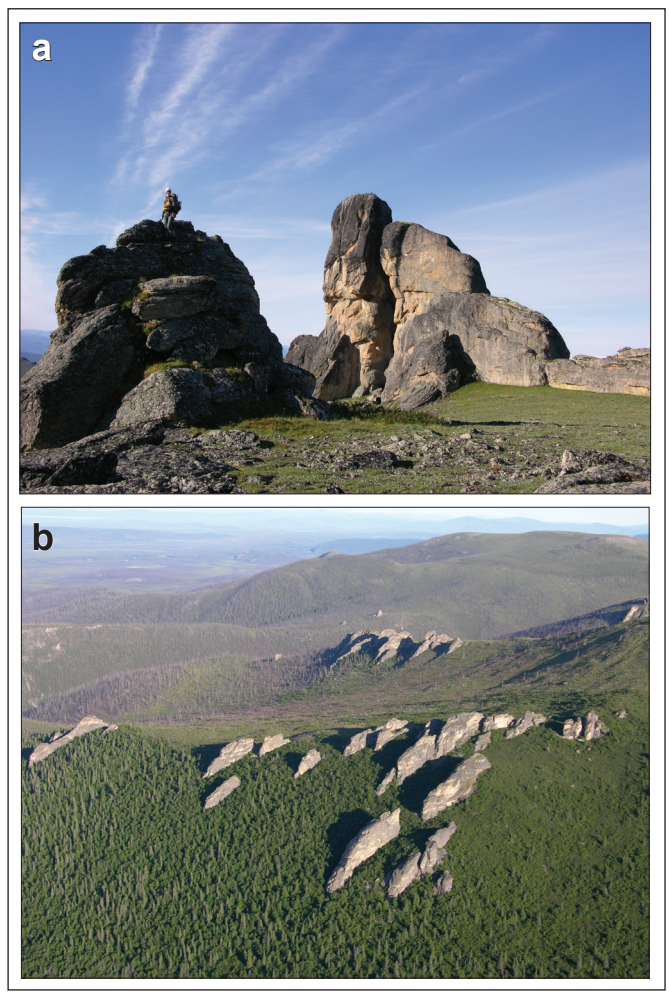

Figure 4-21. (a) *Tors exposed on the summit of Britton Ridge.* ***(b)*** *Tors are found locally at lower elevations in the study area where suitable bedrock occurs. These fin-like tors are found on the flanks of Britton Ridge east of the Nisling River.*

In steep mountainous terrain, bedrock is exposed along mountainsides subjected to intense mass wasting (*e.g.*, rock fall and debris flows) and/or glacial scouring (*e.g.*, the eastern flank of Tincup Lake and rock bluffs exposed on the north side of Brooks Creek). Bedrock is also exposed in several locations where drainages have truncated ridges and spurs or where meltwater has carved channels or diversion canyons (Fig. 4-22).

Figure 4-22. *Glacier drainage diversions have resulted in canyons cut into bedrock. Lower Grayling Creek was diverted through the Mount Forrest uplands by ice in the Donjek River. This has resulted in good exposures of bedrock.*

Chapter 5
Stratigraphy

Detailed stratigraphic sections were logged for 40 field stations. Sections vary in thickness and complexity within the study area. Shallow sections representing near surface and typically 1–2 units of sedimentation were described to better understand surficial geology map unit relationships. Thicker and more complex sedimentary exposures were described to further understand the Quaternary history. In this chapter, only the stratigraphic exposures that contributed to our understanding of the Quaternary history are highlighted. The remaining stratigraphic descriptions are contained within the associated open file maps.

The most significant Quaternary exposures in the study area occur along the White River near its confluence with the Donjek River, at the limit of glaciation. These exposures are the focus of D.G. Turner's PhD thesis, which provides a more in-depth evaluation of the Late Pleistocene stratigraphy and paleo-environmental history (Turner, 2014).

Five key sites, some containing multiple sections, are represented in this chapter. Units were distinguished using field lithofacies descriptions (*e.g.*, texture and structure) and interpreted depositional age and environment.

Pre-McConnell glacial and interglacial sediments

Reid and Gladstone sediments are rarely exposed in section, and are only described for two locations, on the Nisling and White rivers. Pre-Reid deposits were not found exposed in the study area.

Nisling River near the mouth of Dwarf Birch Creek (08JB074)

This section is located at the limit of Pleistocene glaciation along the Nisling River, where end moraine sediments are exposed in a cutbank (Fig. 5-1). The St. Elias lobe of the Cordilleran Ice Sheet flowed through the Nisling Range and terminated at the mouth of Dwarf Birch Creek where it joins the Nisling River (Bond and Lipovsky, 2009c). Six major units were exposed (Figs. 5-1 and 5-2). Unit heights are provided in the descriptions below, and measured in metres above modern river level.

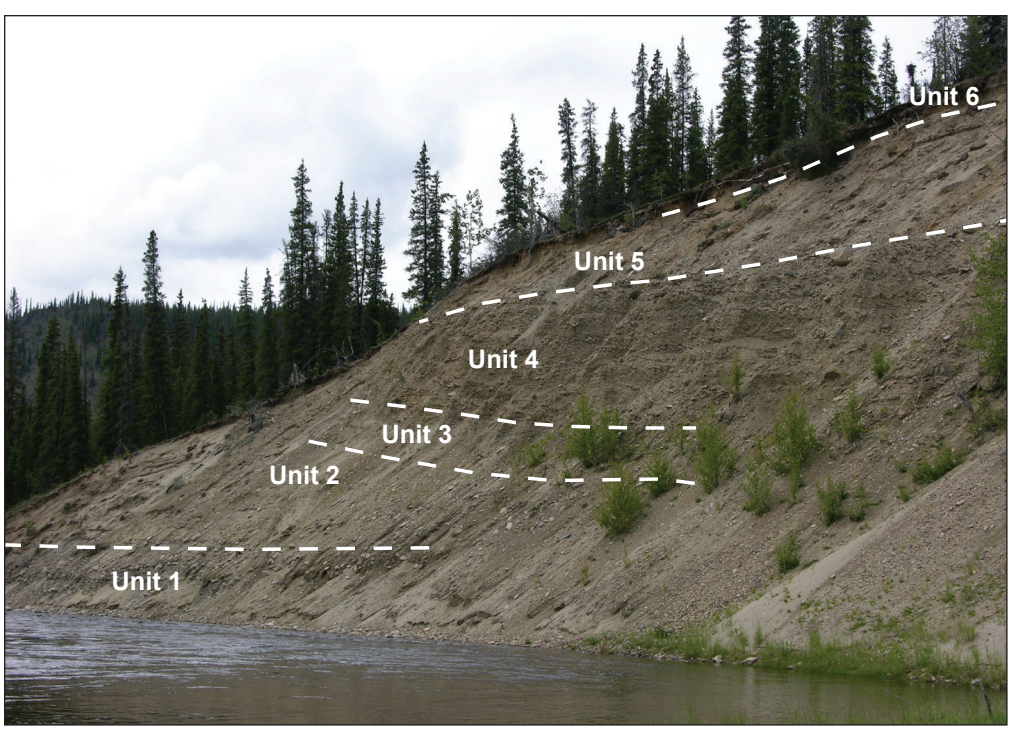

Figure 5-1. *View to the northwest of 08JB074 section, located on the north side of Nisling River. Section is approximately 20 m high.*

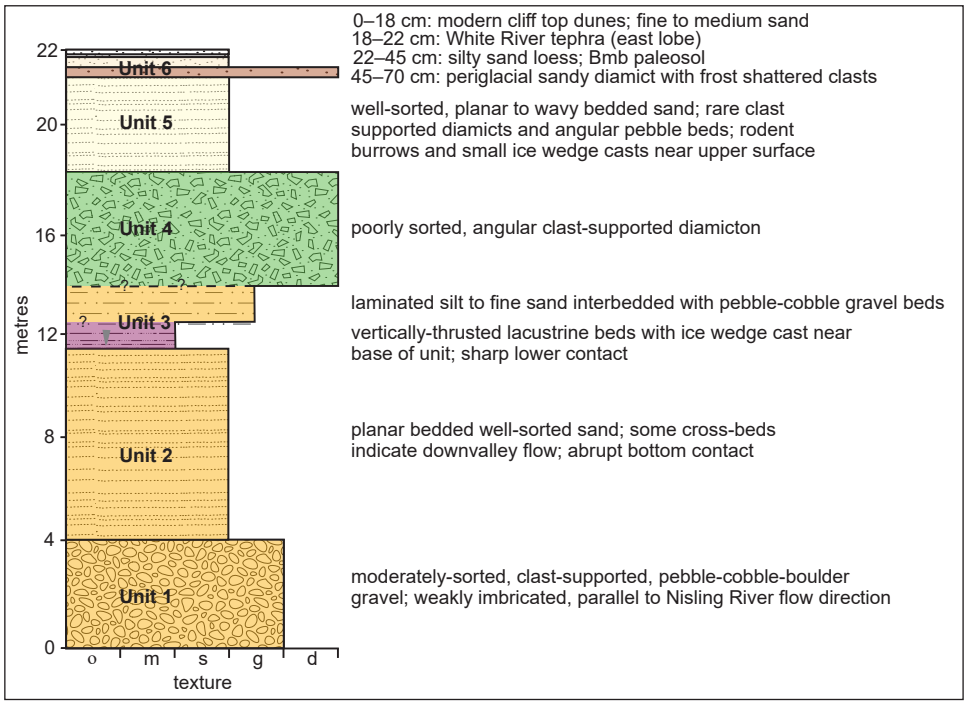

Figure 5-2. *Stratigraphic section for site 08JB074, Nisling River cutbank near the mouth of Dwarf Birch Creek (modified from Bond and Lipovsky, 2009c).*

Unit 1 (0–4 m): moderately sorted, clast-supported, pebble-cobble-boulder gravel. Boulders measure up to 80 cm in length, and clasts have a weak imbrication, indicating flow parallel with the Nisling River. The high-energy gravel deposit is interpreted to be advance Reid glaciofluvial outwash gravel originating from meltwater contributions upstream on the Nisling River.

Unit 2 (4–11 m): planar bedded, well-sorted sand with few pebbly lenses. Minor cross-bedding suggests down-valley flow. This unit is interpreted as proglacial deltaic sedimentation.

Unit 3 (11–13.5 m): coarsening upward unit consisting of laminated silt, fine sand and pebble-cobble beds. Lacustrine beds have been deformed and are thrusted vertically by a compressive source to the south. An ice wedge cast was present near the base of the unit. This unit is interpreted as a proglacial fan overlying glaciolacustrine sediment.

Unit 4 (13.5–17.5 m): poorly sorted, cohesive, clast-supported diamicton. Clasts make up 80% of the unit and consist of pebbles, cobbles and boulders. Rare subrounded boulders, up to 70 cm in length, are present. This unit is interpreted as a Reid glacial diamict or end moraine sediment. The high percentage of clasts may be due to the ice eroding and incorporating proglacial fan sediment from below.

Unit 5 (17.5–21.3 m): well-sorted, bedded sand with angular pebble beds and lenses of angular clast-supported diamict. Sand is planar to wavy bedded and rare ventifacts occur. This unit is interpreted as a periglacial fluvial fan deposit originating from a local valley-side stream. Rodent burrows near upper contact.

Unit 6 (21.3–22 m): silt and fine to medium-grained sand, tephra and discontinuous diamict beds. B-horizon soil oxidation present (Bmb). This unit is interpreted as cliff-top dune sediment with cryoturbated zones producing diamict textures. Holocene soil development is present. Cryoturbation and potential colluviation is primarily located near the lower contact and may reflect periglacial processes associated with the last glaciation.

The units exposed at site 08JB074 record proglacial, glacial and periglacial sedimentation in the Nisling River valley associated with the most extensive Pleistocene glaciation. The glacial sediments are interpreted to be from the Reid Glaciation based on its morpho-stratigraphic position; however, no direct dating was conducted at the site. The stratigraphy records ice blockages in the valley that caused damming and sedimentation of sandy glaciolacustrine beds. These sand deposits were later eroded by katabatic wind and deposited in valleys to the north. Extensive eolian sand deposits were mapped along the north side of the Nisling River valley.

White River near the confluence with Donjek River

A series of gully exposures (Fig. 5-3) were identified during fieldwork on the eastern bank of the White River, a few kilometres upstream of its confluence with Donjek River. The gullies are located less than 15 km beyond the McConnell glacial limit but within the limits of the two previous (Gladstone and Reid) glaciations. These exposures were investigated in detail by Turner *et al. (*2013) and Turner (2014), who used tephra and radiocarbon sampling to date and correlate various units between 18 separate sites. Macrofossil and pollen analysis were also used to interpret paleoecological and depositional environments in the area. The composite section described by Turner (Fig. 5-4) is considered the type section for the study area and provides the primary chronological control and regional context for surficial geology units mapped within the study area. The oldest sediments exposed in the White River sections are Reid in age, and no evidence of pre-Reid glaciations was found.

The oldest units (MIS 6 Reid Glaciation, *ca.* 230 to *ca.* 130 ka) in the composite stratigraphy are units 1, 2 and 3 (Fig. 5-4) which represent Reid till that is at least 15 m thick, overlain by glaciofluvial gravel and glaciolacustrine silt and sand. Following the retreat of Reid ice from the glacial limit a glacial lake formed, possibly behind the terminal moraine. Initial proglacial sedimentation into the lake deposited gravel, and as the ice receded, distal lake sedimentation in the form of silt and sand accumulated in the lake bottom (Fig. 5-5).

Unit 4 marks the transition from the MIS 6 Reid Glaciation to the last interglacial period (MIS 5). It consists of cryoturbated loess that likely formed after draining of the Reid glacial lake. Within the loess bed is the Old Crow tephra (*ca.* 124 ka), which has also been found in Reid deglacial sediments in central Yukon along the Pelly River (Ward *et al.*, 2008).

Units 5 to 12 are interglacial deposits that formed in different landscape positions adjacent to the White River during MIS 5 (*ca.* 124 to *ca.* 82 ka). Incision into the MIS 6 glacial deposits during the last interglacial period (MIS 5) resulted in a gullied terrace landform, similar to today. Loess was deposited on the terrace surface, peat accumulated in localized depressions, pond sediments accumulated on the terrace surface, local tributaries deposited fluvial gravel, and colluviated glacial and interglacial sediment accumulated in gullies. Two well-preserved spruce forest peat deposits were discovered (MIS 5e and 5a)

Figure 5-3. *Gullies cut into an approximately 60 m high terrace above White River provide multiple exposures of pre-McConnell glacial and interglacial sediments.*

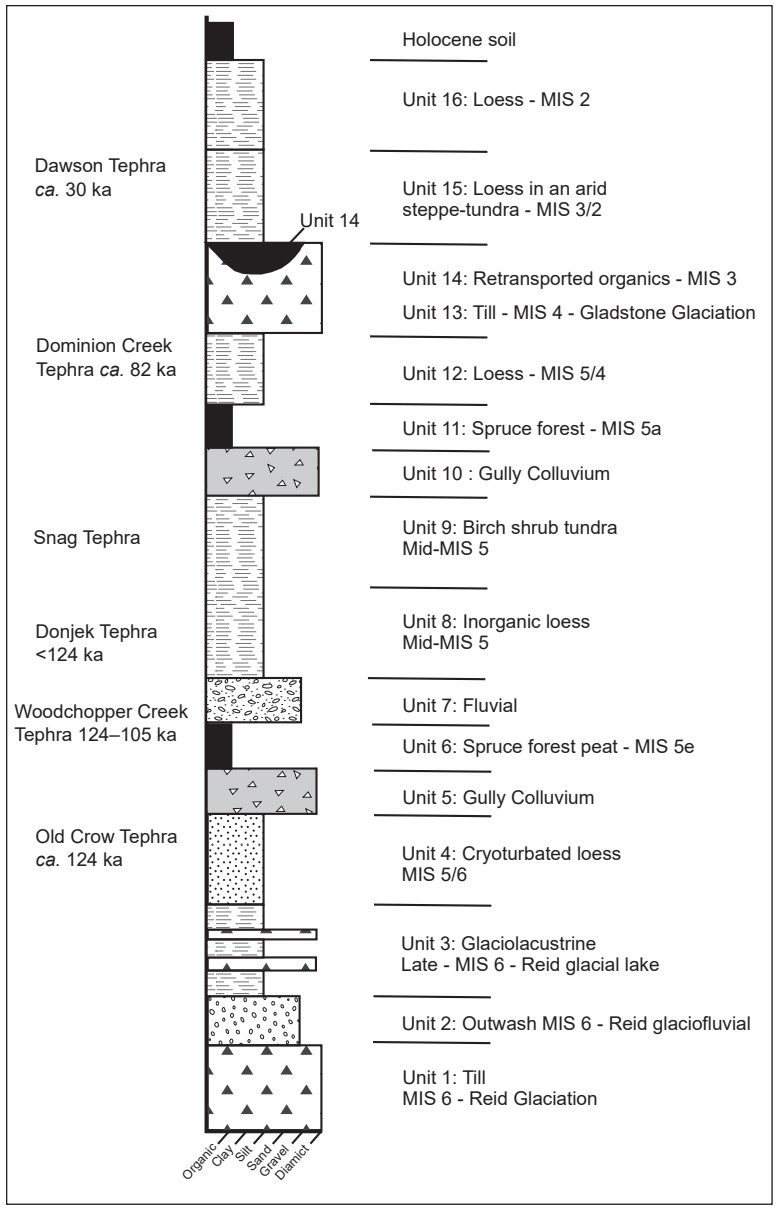

Figure 5-4. *The composite stratigraphy for all the White River exposures described by Turner (2014).*

Figure 5-5. *Reid retreat-phase laminated glaciolacustrine and interbedded colluvial diamict sediments exposed at site 07JB062 (Turner, 2014 site WR95, Unit 3).*

that contain remarkable preservation of needles, cones, logs, seeds, moss, rodent fecal pellets and insect macrofossils (Fig. 5-6a). These two deposits are characteristic of the last interglacial period, which was warm enough to support spruce forests. An intervening treeless, cooler environment, containing pollen and shrub birch tundra macrofossils, was found in the middle of the MIS 5 (units 8 and 9) stratigraphy (Fig. 5-6b). Zazula *et al.* (2011) describe the recovery of a partial phalanx bone from a western camel (*Camelops hesternus*) found in the top of unit 9. This is the oldest reliably dated western camel fossil found in eastern Beringia and provides insights into their range expansion during the last interglacial period. Chronological control on the MIS 5 deposits is provided by numerous tephras including Woodchopper Creek (124–105 ka), Donjek River (<124 ka) and Dominion Creek (*ca.* 82 ka).

Overlying the MIS 5 interglacial sediment is 1.5 to 5 m of till deposited during the MIS 4 Gladstone Glaciation, 3 to 4 m of MIS 3 last interstadial and MIS 2 McConnell Glaciation loess, and the modern Holocene soil. Numerous fossils consisting of mammoth, bison, horse, sheep, caribou and meadow vole were recovered from the upper contact of unit 14 dating from 31 to >48 ka ^{14}C BP (Fig. 5-6c). Plant and insect macrofossils from unit 15 suggest an open, steppe-tundra ecosystem during MIS 3, consistent with the assemblage of fossils recovered. The Dawson tephra (*ca.* 30 ka) was found in unit 15, supporting the ^{14}C ages on the fossils (Fig. 5-6d). The exposures investigated were beyond the limit of the MIS 2 McConnell Glaciation and therefore only loess from this period was recorded in the composite stratigraphy.

The White River exposures provide a detailed record of paleo-environmental change over the last 130 000 years for the study area. Fluctuations between warm, spruce forest-dominated and cool, shrub tundra-dominated environments coincide with the well-established cycles of glaciation and interglacials for North America. The exceptional preservation of last interglacial macrofossils, interbedded with known tephras, make this site an important reference section for eastern Beringian paleo-ecology.

Figure 5-6. (a) *1.5 to 2 m of interglacial spruce forest peat deposited between the Reid and Gladstone glaciations at site 07JB063. The peat contains well-preserved white spruce fragments (needles, cones, logs and seeds), rodent feces and insects (Turner, 2014).* ***(b)*** *Up to 5 m of reworked interglacial loess and organic-rich sediment was constrained to the last interglacial period (MIS 5) based on tephrochronology (site 07JB052; Turner, 2014 site WR99, Units 8 and 9).* ***(c)*** *Pleistocene fossils found in the White River sections (after Turner, 2014): (i) Bison priscus, partial cranium YG 400.1; (ii) Equus sp., metatarsal, YG 308.19; (iii) Camelops hesternus, partial proximal phalanx, YG 400.6; (iv) Castor Canadensis chewed wood; YG 308.14; (v) Mammuthus primigenius, tibia proximal end, YG 308.9.* ***(d)*** *Silty-sand loess deposited during the last interstadial to McConnell time period (site 07JB053; Turner, 2014 site WR95, Unit 15). Discontinuous white lenses are Dawson tephra.*

Donjek River "Big Bend"

A thick sequence of glacial drift and loess is exposed in 3 sections along a large cutbank in the Donjek River, informally named the "Big Bend", about 10 km south of Wellesley Lake (Fig. 5-7). The largest of these sections, site 07JB018, is 35 m high, and contains eight units (Fig. 5-8). This site is located within the McConnell limit and therefore was assumed to contain McConnell glacial sediment, however a radiocarbon date on bone from an upper layer of loess suggests the material predates the McConnell Glaciation. Unit heights are provided in the descriptions below, and measured in metres above modern river level.

A colluvial apron covers the lower 9.5 m of the section.

Unit 1 (9.5–11.5 m): located at the base of the exposed section. Unit 1 consists of an oxidized and cohesive mixture of sand, gravel, and diamict. Organic matter within the diamict yielded a conventional radiocarbon date of 47 060 ± 860 ^{14}C BP (50 670 ± 2110 cal BP; Beta 240022), which is regarded as a non-finite age due to its close proximity to the radiocarbon detection limit.

Unit 2 (11.5–18.1 m): comprises moderately to well-sorted clast-rich, oxidized and cohesive gravel. A 25 cm-thick bed of lacustrine or glaciolacustrine silt is present in the middle of the unit.

Unit 3 (18.1–19.6 m): recessive, unoxidized cobble-pebble gravel (Fig. 5-9a).

Unit 4 (19.6–22.2 m): cohesive, clast-rich diamicton with an abrupt lower contact (Fig. 5-9a).

Unit 5 (22.2–32 m): fining upward sequence of cobble-rich gravel to pebble-rich gravel. Units 3, 4 and 5 are interpreted as having a glacial origin and represent advance outwash, till and retreat outwash deposits, possibly from the Gladstone Glaciation.

Unit 6 (32–33.5 m): consists of loess, which overlies the glacial sediments. Rare organic stringers, lenses of pebbly diamict and cryoturbation features suggest that the unit was probably partially colluviated. A small piece of bone was found near the lower contact and was dated at 35 130 ± 330 ^{14}C BP (38 391 ± 732 cal BP; Beta 240023; Fig. 5-9b). An organic fragment from higher up in the unit yielded a radiocarbon date of 45 330 ± 1020 ^{14}C BP (48 655 ± 1891 cal BP; Beta 240024). While these dates are near the radiocarbon detection limit, it appears the deposit may correspond with MIS 3 interstadial deposition.

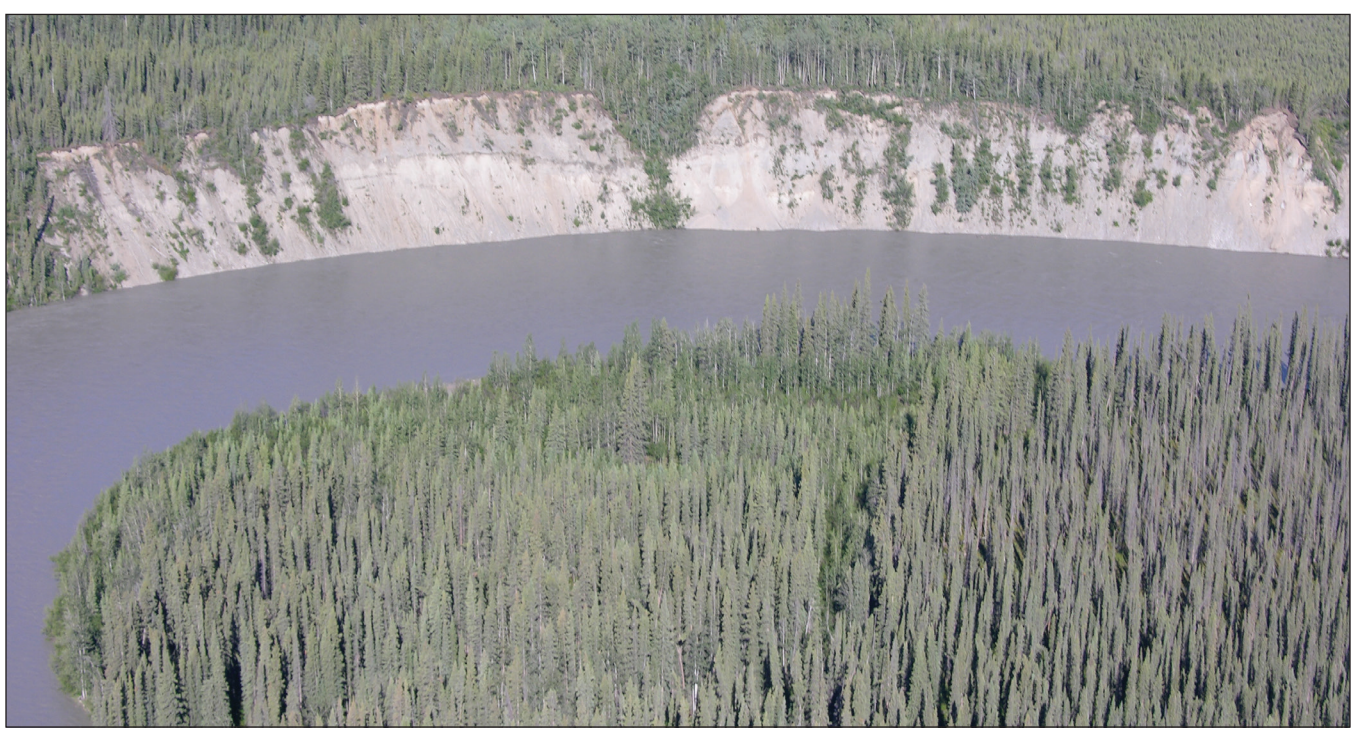

Figure 5-7. *Aerial view of the 35 m high "Big Bend" section on Donjek River (site 07JB018).*

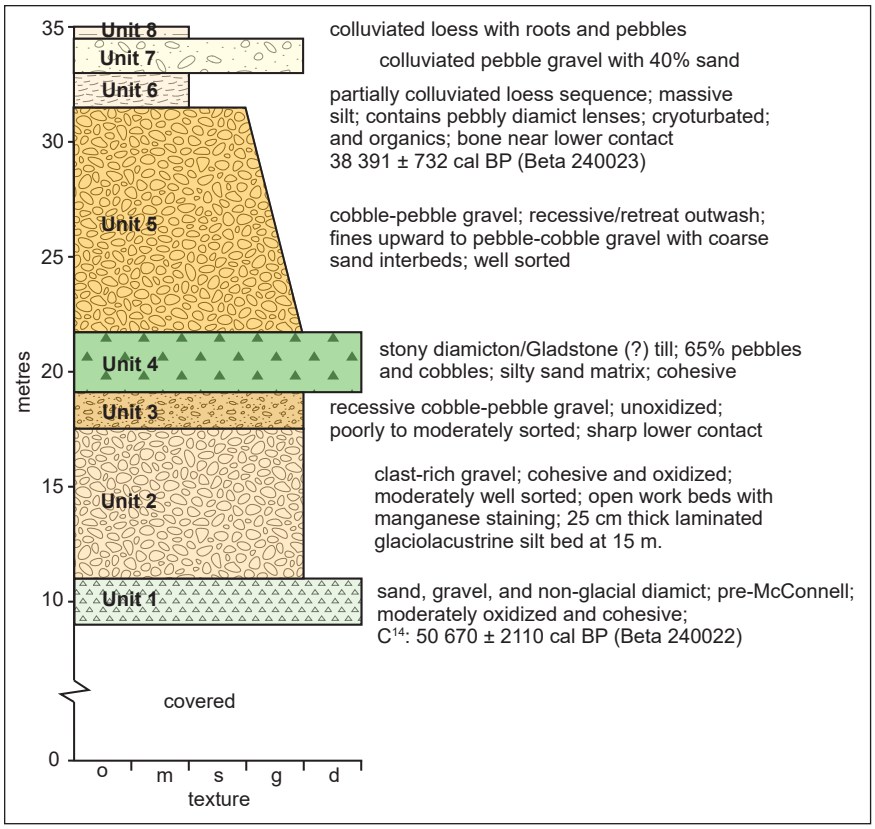

Figure 5-8. *Graphical representation of the "Big Bend" section on Donjek River (site 07JB018; modified from Bond and Lipovsky, 2015a).*

Figure 5-9. (a) *The sharp contact between units 3 and 4 (outwash gravel and till) at the Big Bend section on the Donjek River. Graduations on staff are 25 cm.* ***(b)*** *Colluviated loess (Unit 6) overlying Gladstone retreat outwash (Unit 5). A bone fragment (circled) near the base of Unit 6 yielded a conventional radiocarbon age of 38 391 ± 732 cal BP (Beta 240023). This sediment is interpreted as MIS 3 loess.*

Unit 7 (33.5–35 m): consists of pebble-cobble gravel that may have been deposited by local streams (MIS 1) or by McConnell glaciofluvial outwash (MIS 2).

Unit 8 (35–35.5 m): comprises loess affected by modern soil processes.

The Big Bend section on the Donjek River appears to contain pre-McConnell sediment despite its location within the McConnell limit. The section exposes sediments at the end of a broad valley containing outwash terraces and fluvial deposits that appear inset into McConnell moraine landforms on the valley side. This may indicate that McConnell till has largely been eroded creating an unconformity between units 6 (MIS 3) and 7 (MIS 1). Unit 6 loess, minor organics and bone, have a similar appearance to MIS 3 deposits exposed along the White River, as discussed in Chapter 5. Additional chronological control is needed to clarify the stratigraphy at this site.

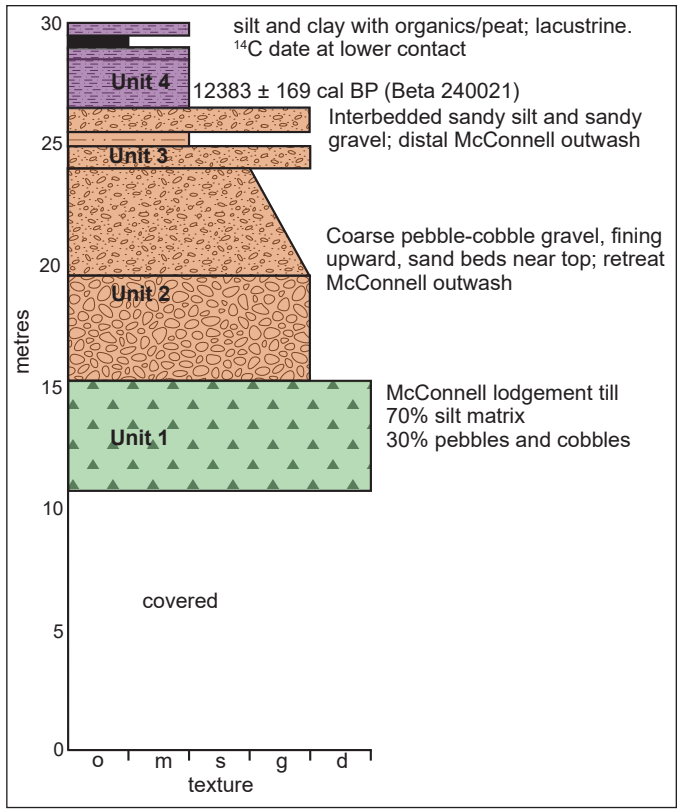

Figure 5-10. *Stratigraphy of the Donjek River cutbank section (07JB010).*

McConnell glacial sediments

Donjek River cutbank, 3 km upstream from the mouth of MacKinnon Creek

A Donjek River cutbank exposure of McConnell glacial and Holocene sediment was described at site 07JB010 (Fig. 5-10), approximately 20 km south of the Big Bend site and 3 km upstream from the mouth of MacKinnon Creek. The section measures 30 m in height and the lower 10 m is covered by colluvium. Unit heights are provided in descriptions below, and measured in metres above modern river level.

Unit 1 (10–14.5 m): fine-grained diamict containing faceted and striated clasts, interpreted as McConnell lodgement till (Fig. 5-11). The lower contact is poorly exposed and the upper contact is sharp.

Unit 2 (14.5–24.5 m): fining upward sequence of coarse cobble-pebble gravel to interbedded silt and sand. The abundance of sand lenses increases from <5% at the base of the unit to 50% in the upper half of the unit. This is consistent with glaciofluvial sedimentation off a retreating ice front and is interpreted as McConnell retreat glacial outwash (Fig. 5-12).

Figure 5-11. *McConnell basal lodgement till (unit 1) exposed on the Donjek River (07JB010).*

Figure 5-12. *McConnell retreat glaciofluvial outwash gravel (unit 2) exposed on the Donjek River (07JB010).*

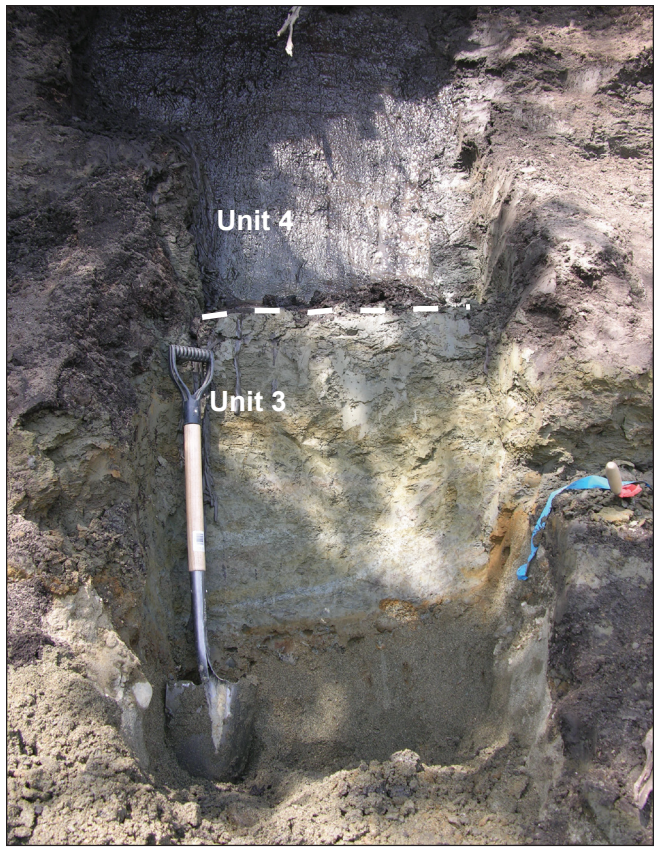

Figure 5-13. *McConnell glaciofluvial sand and silt beds (unit 3) buried by early Holocene organic-rich fluvial overbank or lacustrine sediment (unit 4). The radiocarbon dated organics at the base of unit 4 provide a minimum age for revegetation of the paraglacial environment.*

Unit 3 (24.5–27 m): interbedded silt, sand and gravel that is interpreted as distal glaciofluvial outwash.

Unit 4 (27–30 m): silty lacustrine or fluvial overbank sedimentation that was deposited along the floodplain margin (Fig. 5-13). A layer of organic-rich sediment preserved at the base of unit 4 returned a radiocarbon age of 10 450 ± 40 ^{14}C BP (12 383 ± 169 cal BP; Beta 240021). Additional peat layers are preserved within the lacustrine sediment, higher in the section.

The radiocarbon age near the top of unit 3 is significant because it provides minimum age on McConnell deglaciation of the Donjek River valley, 40 km up-ice from the McConnell glacial limit. Units 2 to 4 also record post-glacial sedimentation and the ^{14}C age suggests there was a shift from deglacial aggradation to interglacial incision about 12 000 years ago. The organic material also provides the earliest evidence of revegetation of the paraglacial environment during the Pleistocene-Holocene transition.

Talbot Creek

As the St. Elias lobe of the Cordilleran Ice Sheet advanced up Talbot Creek valley during the McConnell Glaciation, it dammed a large proglacial lake informally named Glacial Lake Talbot (Bond and Lipovsky, 2009d). The lake was overridden as the ice continued to advance to its maximum extent, which is marked by a large terminal moraine approximately 100 m high (Fig. 5-14). The moraine comprises a range of ice-contact and ice-proximal glaciofluvial, glaciolacustrine and morainal materials.

At 08PL003 (Fig. 5-15a,b), approximately 20 m of fine sandy glaciolacustrine material is exposed at the base of the moraine, overlain by 10 m of till. This is overlain by another 20 m of glaciolacustrine material presumably deposited in a proglacial lake in the early stages of glacial retreat. The section is capped by 40 m of glaciofluvial sediment, which generally

Figure 5-14. *A view looking west down the Talbot Creek valley towards the McConnell end moraine (08PL003). Dashed lines indicate moraine crest.*

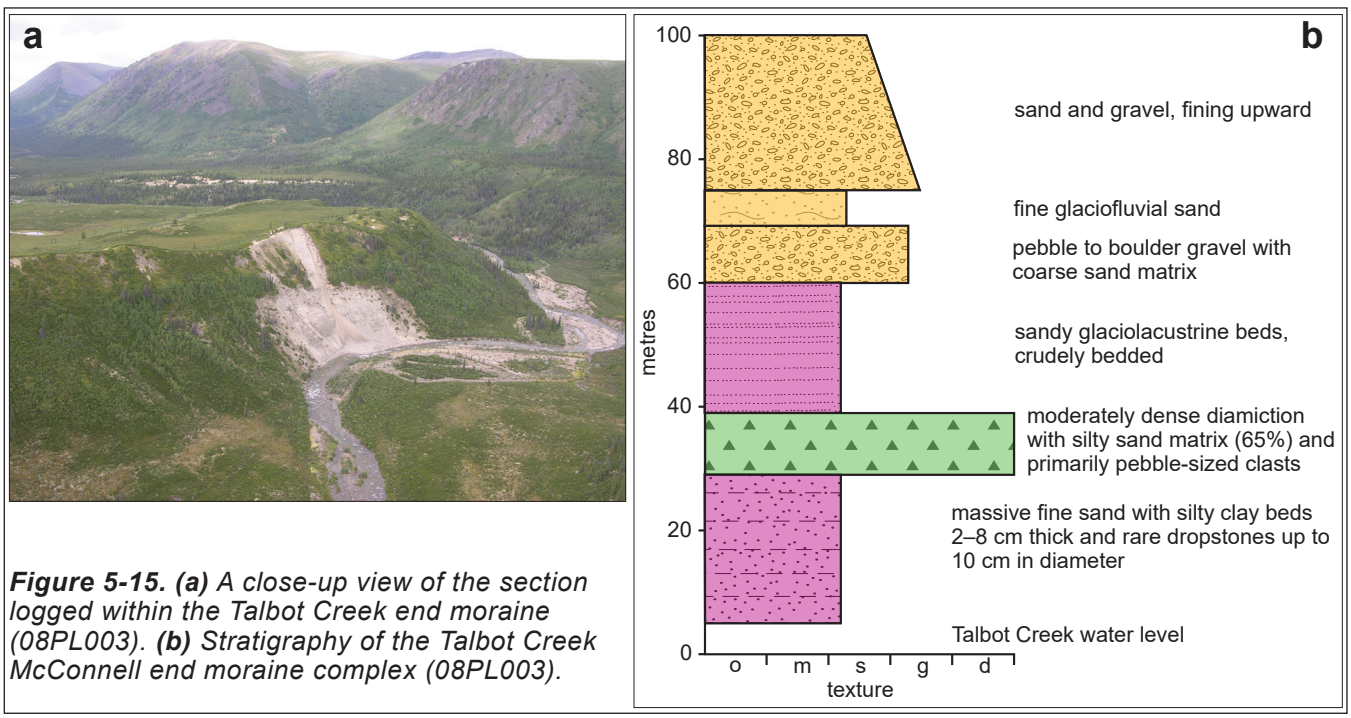

Figure 5-15. (a) *A close-up view of the section logged within the Talbot Creek end moraine (08PL003).* ***(b)*** *Stratigraphy of the Talbot Creek McConnell end moraine complex (08PL003).*

fines upward as sediment was deposited at successively greater distances from the ice front during glacial retreat.

A similar sequence of materials is exposed at 08JB014 (Fig. 5-16), in a 16 m section on the same terminal moraine complex. However, the thicknesses of the units at this location are considerably thinner, and the till is underlain by glaciofluvial gravel rather than glaciolacustrine sediment.

One kilometre upstream at 08JB015, a full sequence of glacial materials is exposed in a Talbot Creek cutbank. Ten metres of advance-phase glaciolacustrine sediment is overlain by 7 m of fining upward glaciofluvial outwash and 5.5 m of retreat-phase, ice-rich glaciolacustrine sediment (Fig. 5-17).

The stratigraphic sections exposed in upper Talbot Creek record the advance of the Cordilleran Ice Sheet into the Ruby Range during the last glaciation. A proglacial lake formed upstream of the up-valley advancing ice front and strandlines are preserved on the end moraine (Fig. 5-18). Glacial Lake Talbot drained north through the Nisling Range via Tyrrell Creek and into the Nisling River drainage.

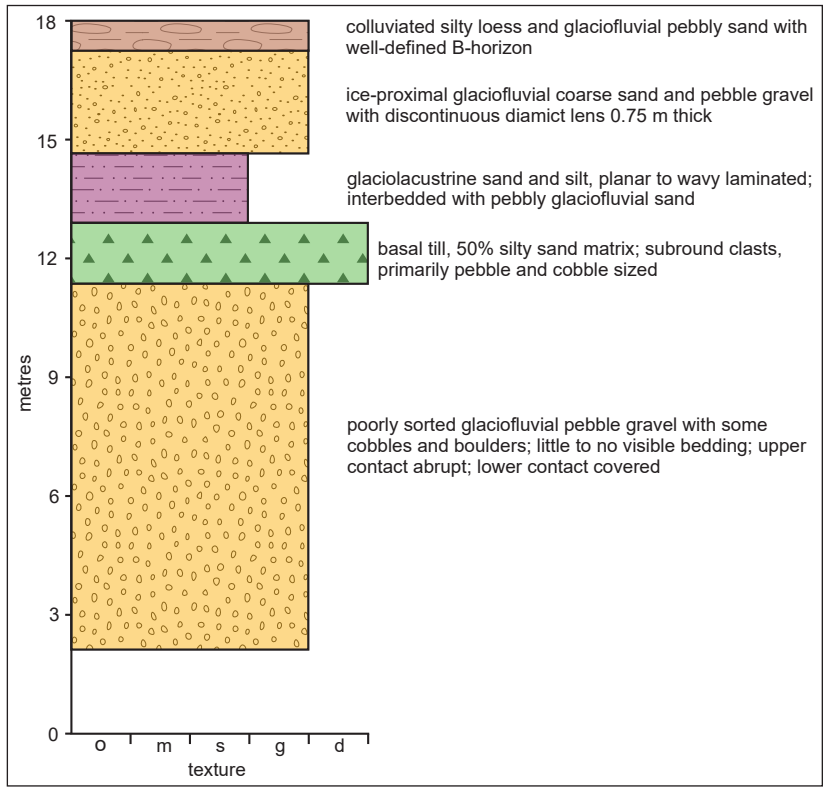

Figure 5-16. *Stratigraphy of the Talbot Creek end moraine complex (08JB014).*

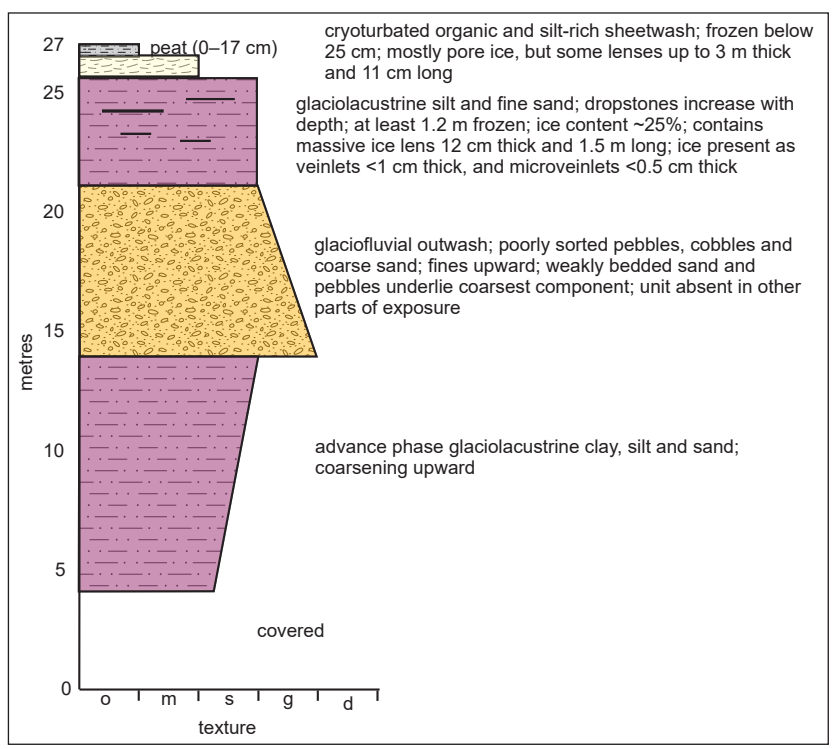

Figure 5-17. *Stratigraphy immediately upstream from the Talbot Creek end moraine (08JB015).*

Figure 5-18. *Shorelines eroded into the leading edge of the Talbot Creek end moraine (see arrows) record the glacial lake history resulting from up-valley ice flow in the valley.*

Chapter 6
Applications

Exploration and Mining

To date, the majority of mineral exploration and mining activity in the study area has focused on gold and copper in the Dawson Range. Significant deposits in or near the study area include the Casino copper-gold and Coffee gold deposits. Other notable properties in the Dawson Range include Sonora Gulch, Rude Creek, Apex Mountain, Canadian Creek and Boulevard. The area is also host to numerous other occurrences and prospects. Placer gold mining in the Dawson Range has occurred on: Canadian Creek, which drains north into the Yukon River from the Casino deposit; Rude Creek, in the Dip Creek drainage; and Sonora Gulch, which drains into Hayes Creek.

South of the Dawson Range, mineral exploration has focused in the Nisling and Ruby ranges, and on uplands west of Wellesley Lake. Limited placer exploration has occurred in Grayling Creek, a tributary to the Donjek River. No placer mining has occurred within the study area south of the Dawson Range.

This section discusses surficial geology applications to mineral exploration and highlights how surficial processes and glacial history may affect various exploration methodologies.

Mineral Exploration

A veneer or blanket of surficial sediment covers much of the study area, largely masking the bedrock. In the southern part of the study area where glaciation facilitated erosion, outcrop is generally limited to upland environments and the higher elevation ranges. Mineral exploration therefore relies heavily on surficial geochemical methodologies, such as soil and stream sediment geochemistry, to target mineralization for further detailed work. These methods are useful in both glaciated and unglaciated terrain; however, surficial processes that may affect the geochemistry need to be considered to obtain optimal results. These processes are discussed below for glaciated and unglaciated terrain.

Glaciated terrain

The effect of glaciation on the landscape and surficial geology is significant in the southern part of the study area. Valleys that were inundated by the Cordilleran Ice Sheet (CIS) are typically broad, have over-steepened valley sides, and contain thick deposits of mixed glacigenic and fluvial sediments in the valley bottom (Fig. 6-1). Upland environments that were glaciated by the CIS have a cover of till, which requires consideration of ice-flow direction when soil sampling. Utilizing the surficial geology maps, and in particular the glacial limits data, is especially important to locate the sharp boundary between glaciated and unglaciated terrain. Where surficial sediment samples collected for geochemistry span the glacial limit, and the terrain is relatively gentle, samples should be divided into two populations for assessing element concentrations. Samples derived from till will be displaced from their source of origin and will contain a broader mix of bedrock fragments. Conversely, samples derived from unglaciated terrain will generally represent more localized bedrock geochemistry (*see* discussion below). Similar considerations should be given in valleys affected by alpine glaciation. Referencing the surficial geology map will inform the user on the local distribution of till and glacial limits for a given area.

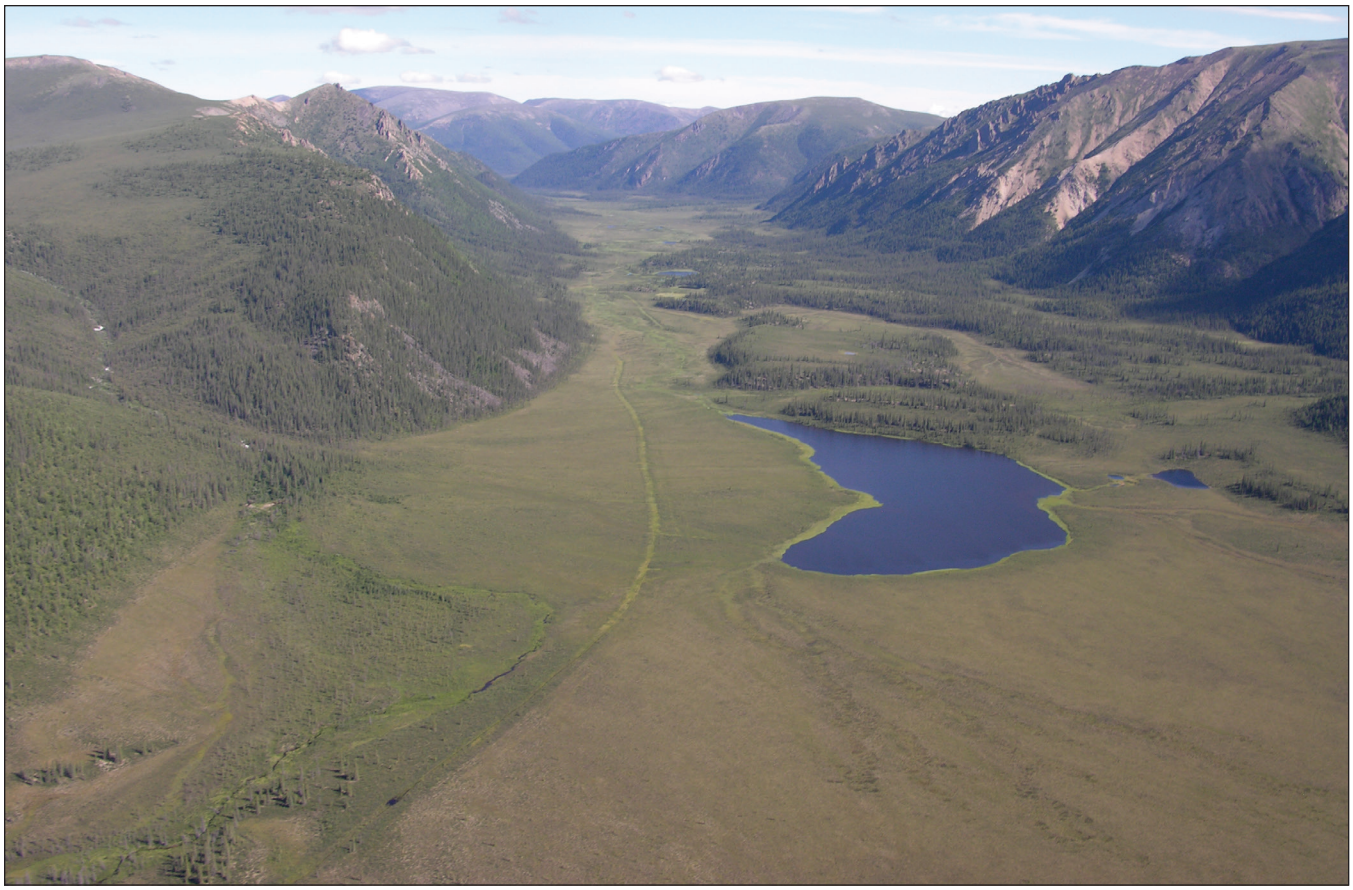

Figure 6-1. *A u-shaped valley located at the headwaters of Onion Creek in the Nisling Range. Thick deposits of glacial and fluvial sediments blanket the valley bottom whereas bedrock is well exposed on the valley slopes.*

Bedrock outcrops are more abundant in glaciated terrain due to the effects of ice erosion. Clusters of cirques in the Ruby and Nisling ranges have good bedrock exposure on headwalls and arêtes. The over-steepened slopes of the u-shaped valleys in these ranges also provide excellent exposure of bedrock or bedrock covered by a thin layer of weathered-bedrock colluvium. Bedrock exposure is very limited in the valley bottoms due to overburden sediment thickness. Finding outcrop in these low areas can be challenging, although meltwater channels or streams affected by ice diversions will commonly contain bedrock canyons on the margins of valley bottoms. Meltwater channels are symbolized on surficial geology maps.

Surficial sediment geochemical sampling in the glaciated valley bottoms should only proceed if widespread basal till is present. Most valley bottoms are blanketed by glaciofluvial, glaciolacustrine or fluvial sediment and should be avoided for soil geochemistry. Valleys glaciated by alpine ice typically have widespread till coverage and geochemical anomalies can be simply traced up-valley. Stream sediment sampling in glaciated terrain can be effective if local bedrock is being incorporated into the fluvial sediment. This is typically evident by the angularity and lithological homogeneity of clasts in the streambed. Where glacial sediment dominates the stream sediment content, the element concentrations should be interpreted with caution.

Unglaciated terrain

Unglaciated terrain covers approximately 75% of the study area. Bedrock outcrop is generally limited; however, the abundance of weathered bedrock colluvium covering the terrain makes it excellent for surficial geochemical exploration. Good summaries of how to approach surficial geochemistry in Yukon's unglaciated terrain are provided by McKillop *et al.* (2013), Bond and Lipovsky (2011), and Bond and Sanborn (2006). An idealized cross section of the surficial geology in the Dawson Range is presented in Figure 6-2. Prolonged weathering of the unglaciated terrain has resulted in a landscape covered by colluvium and fluvial deposits that are derived from local bedrock. Much of the bedrock weathering is associated with mechanical processes such as frost shattering and mass wasting. Chemical weathering is less common and typically observed on more stable landscape positions such as mountain summits where surficial sediments are thin and the topography is gentle. Previous research has determined that element mobilization or partitioning within soil horizons, related to chemical weathering, is not a significant consideration when exploring Yukon's unglaciated terrain (Bond and Sanborn, 2006).

Variable accumulation of eolian sediment (particularly loess) can affect element concentrations in the soil profile (Bond and Sanborn, 2006). This is an important factor in the study area due to the close proximity of glaciated environments, and especially the large glaciofluvial plains of the Nisling, Donjek and White rivers. These floodplains were abundant sources for loess during glacial periods. Eolian deposits proximal to the glacial limits tend to have a sandier texture. Tributaries to the Nisling River on the northeast side

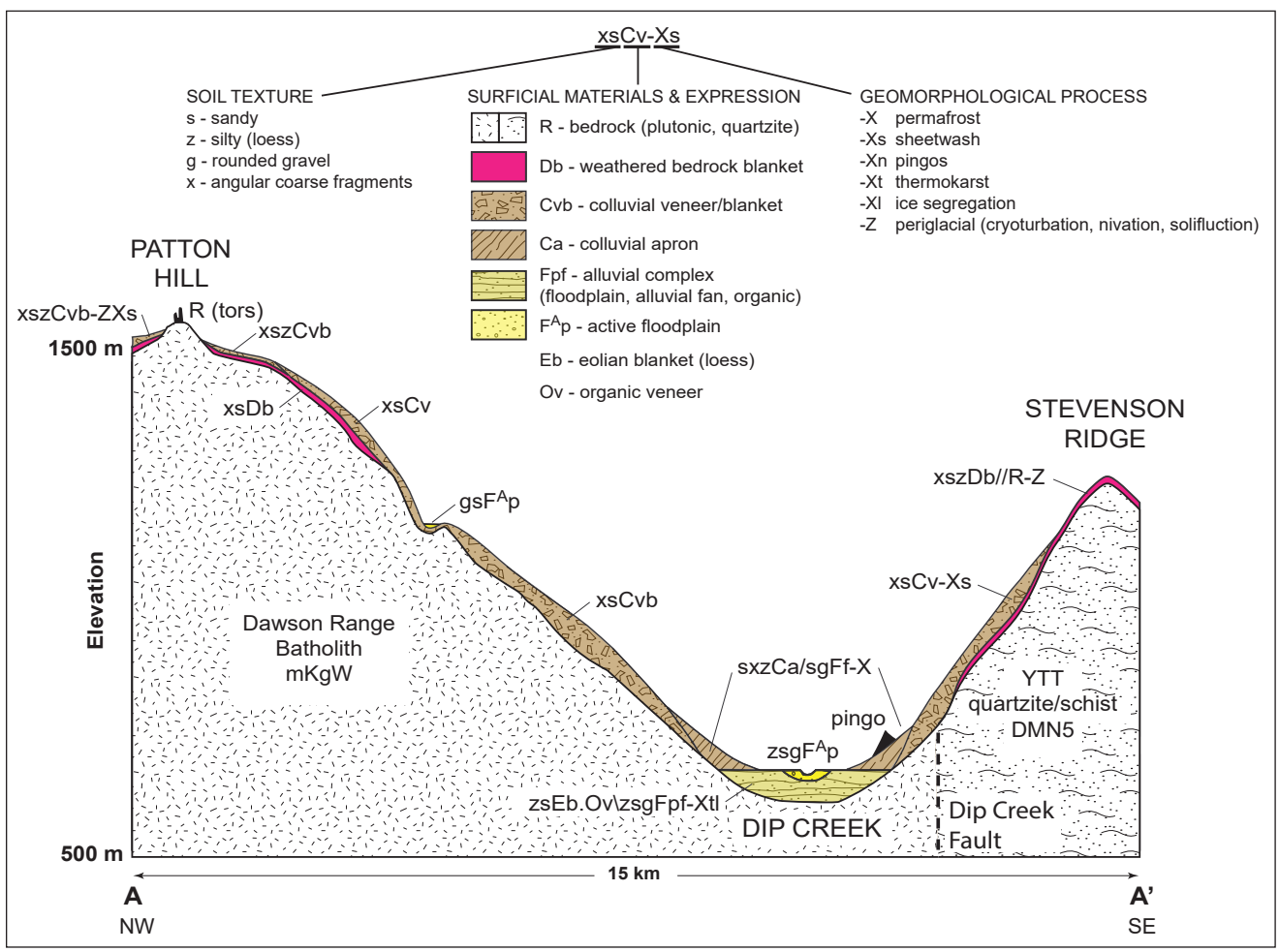

Figure 6-2. *An idealized cross section of the surficial geology in the Dawson Range (adapted from Bond and Lipovsky, 2011). The upland environments are covered with weathered-bedrock colluvium whereas the valley bottoms contain thick colluvial aprons and fluvial sediments. Permafrost is widespread on cold-aspect slopes.*

of the valley contain thick deposits of sand (Fig. 6-3), and dunes were mapped northeast of Wellesley Lake near the Donjek River. These deposits will mask or dilute local geochemical signatures in both soil and stream sediment environments. Loess accumulations up to 20 m thick were noted in tributaries to the White River, such as Home Creek, and in drainages flowing south off the Dawson Range. Incorporation of loess into underlying mineral soil material depends on the intensity of cryoturbation. On south-facing permafrost-free slopes, the loess and colluvium remain as separate layers of sediment and are easily distinguished in a soil pit. On colder aspect slopes, cryoturbation and solifluction mix loess more deeply into the soil profile. This requires soil samplers to diligently sample deeper and observe the amount of silt content within the sample. As a rule of thumb, samples should be collected from greater than 50 cm below the top of the uppermost mineral horizon. This is usually deep enough to maximize the amount of locally produced weathered bedrock fragments within the sample. Thin veneers of loess are not typically identified on the surficial geology maps, but they are very widespread through the Dawson Range. It is therefore recommended that soil pits be dug within various topographic positions on an exploration property in order to understand local loess distribution and thickness.

Loess can also affect the geochemistry of stream sediment samples. This is a particular problem in higher order streams that have a lower gradient, and resedimented loess (and organics) have accumulated into thick deposits blanketing the valley bottom. Drainages on the south side of the Dawson Range, such as Doyle and Dip creeks (Fig. 6-4), and tributaries to the Klotassin River have thick loess accumulations in their basins. A strategy to overcome this issue is to focus sampling in headwater streams, such as first or second order streams, that have a steeper gradient and more readily flush loess out of the alluvium. Creeks draining the north side of the Dawson Range into the Yukon River have undergone base level change, are more deeply incised, and have less loess accumulation, so would be better candidates for stream sediment sampling than drainages on the south side.

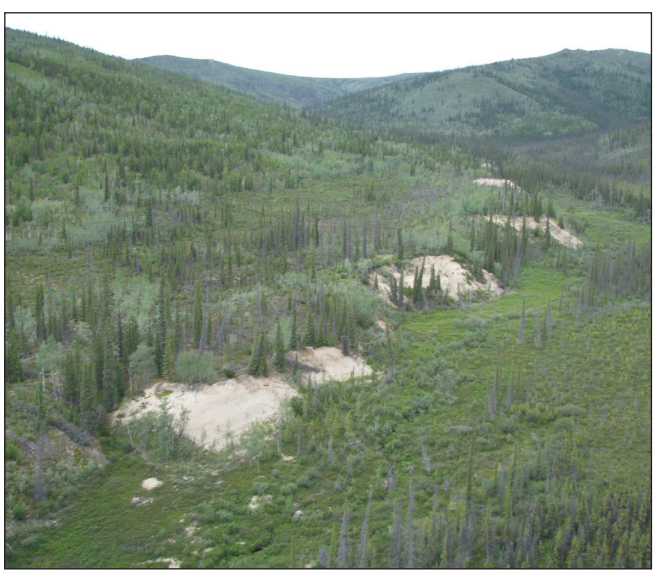

Figure 6-3. *A tributary to the Nisling River in the southeastern part of the study area (08PL049). Thick accumulations of eolian sand have blown into the drainage from the Nisling River. This sediment then gets partially reworked by stream erosion and becomes incorporated into the alluvium.*

Figure 6-4. *A view to the east of a tributary in the Dip Creek drainage. Thick accumulations of reworked loess and organic material cover the valley bottoms of most drainages on the south side of the Dawson Range. This material can mask stream sediment geochemistry and provide a thick cover over potential placer deposits.*

Placer mining and exploration

Placer exploration and mining have largely focused in tributaries to the Yukon River on the north side of the Dawson Range. Gold mineralization is relatively abundant in the Dawson Range and the area is accessible via the Casino winter trail from Freegold Mountain or from the Yukon River using a barge.

Canadian Creek, which has its headwaters in the study area, has been the most productive local placer creek, producing more than 15,000 crude ounces. The majority of that gold was mined between 1996 and 2002, although activity has recently resumed on upper Canadian Creek and Patton Gulch.

A small mining operation has focused on Sonora Gulch, a tributary to Hayes Creek, in recent years and produced relatively coarse placer gold from the first-order drainage (Fig. 6-5.). The placer gold was being mined from a gulch gravel that had eroded into a pre-Reid glaciofluvial terrace of Hayes Creek. The thin gulch gravel was buried under organic-rich colluvium (muck).

South of the Casino deposit, there has been limited placer production from Rude Creek, a tributary of Dip Creek, which is accessed southeast from the Casino mining camp road network (Fig. 6-6). Placer gold in Rude Creek was discovered in 1915 near the mouths of Ray and Trombley creeks; tributaries of Rude Creek (Yukon Geological Survey, 2010). In June of 1915, up to 25 men were prospecting and working along the creek. Since that time, it has been worked intermittently with the majority of modern production occurring in the late 1980s to early 1990s.

Abundant drilling and test pitting programs have been completed in Hayes Creek, a tributary of Selwyn River.

In the northwestern part of the study area, Carlisle and Independence creeks, and tributaries of Coffee Creek are being evaluated as part of a larger program to determine placer potential near the Coffee gold deposit. In this area, placer gold has been discovered on the Boulevard property, in basins that contain Klondike schist. However, gold particle sizes in the Coffee deposit appear to preclude placer formation.

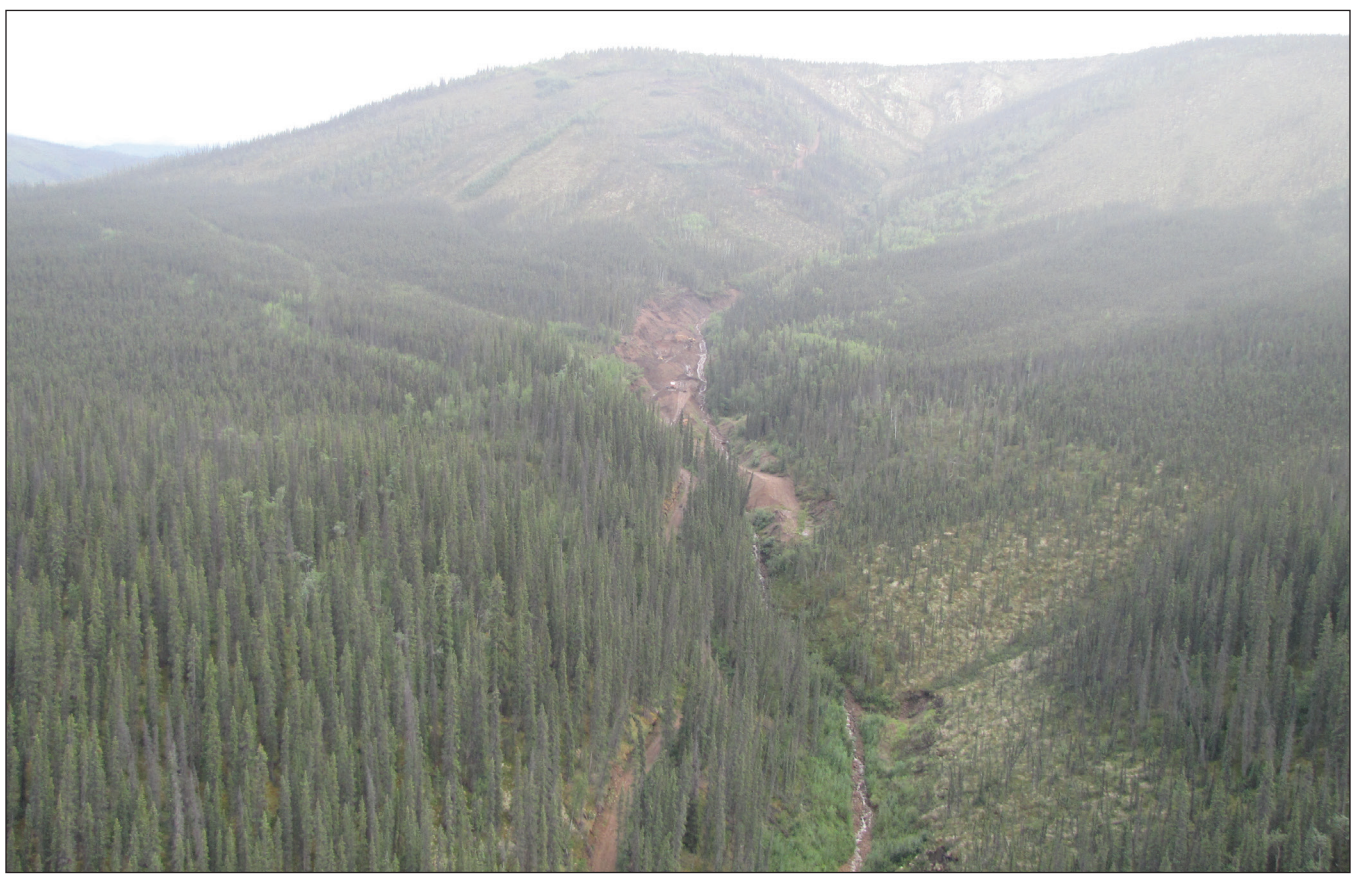

Figure 6-5. *A view of upper Sonora Gulch where most of the placer mining was occurring in 2010. Placer gold-bearing gulch gravel has incised into and accumulated on a pre-Reid glaciofluvial terrace.*

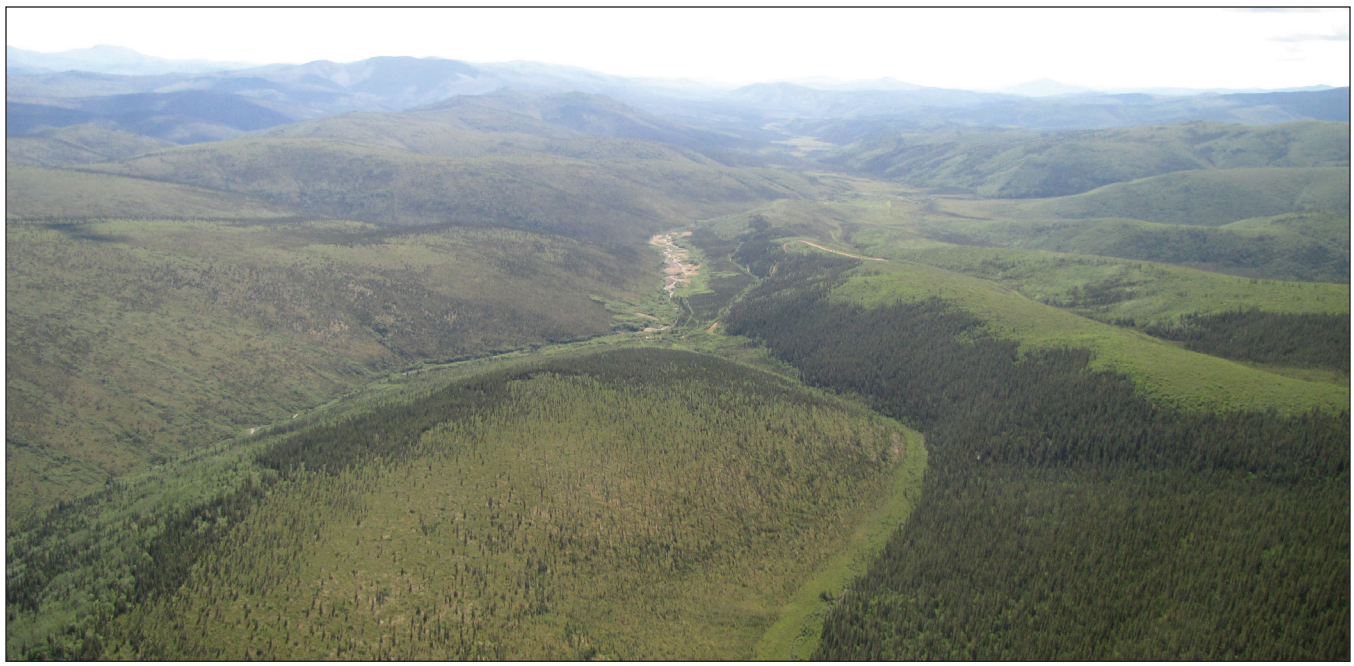

Figure 6-6. *An aerial view to the west looking down Rude Creek towards the placer workings. Upper Dip Creek is visible in the distance.*

The exploration program on Shovel Creek, a tributary to Coffee Creek, has consisted of rotary air-blast drilling, resistivity geophysics, lidar and shafting. Up to six personnel have been actively exploring the creek and have delineated a placer gold-bearing stream channel more than 3 km long.

Heavy mineral sampling

A heavy mineral sampling program was undertaken in selected drainages of the study area. This program aimed to identify valuable detrital elements or gems. The primary goal was to determine the presence or absence of visible gold, and potential for a placer deposit. Fifty-nine samples were collected and evaluated using a variety of methods and analyses (Fig. 6-7, Table 2). The sampling methods included pan samples, sluice samples and bulk (sieved) alluvium. Pan sampling was completed using a 16-inch gold pan and it was typically conducted as a quick check for gold and overall heavy mineral volume. Analyses were limited to a visual inspection of the concentrate in the field and gold grains were counted. Sluice samples utilized a portable Keene sluice box that enabled a larger sample to be processed (Fig. 6-8). A volume of sediment, ranging between 7.5 and 100 gallons, was excavated by hand, sieved with a 4 mesh screen and washed through the sluice box.

Concentrates from these samples were either visually evaluated in the field or sent to Overburden Drilling Management Ltd. (ODM) for detailed heavy mineral description. The third type of sample collected was a bulk alluvium sample that was sieved using a 12 mesh screen (2 mm) in the field. The unconcentrated -12 mesh sediment was then submitted to ODM for analysis.

Samples sent to ODM were evaluated for gold, platinum group metals, kimberlite indicators and metamorphosed or magmatic massive sulphide indicators. The samples were initially panned to separate gold and platinum group metals. The non-ferromagnetic fraction was then split to 25 or 50% (bulk samples only) before undergoing heavy liquid separation to a specific gravity of 3.2. The 0.25 to 2 mm non-ferromagnetic +3.2 specific gravity heavy mineral fraction was then hand picked for minerals. A scanning electron microscope was used to differentiate minerals with similar character.

Summary results for the heavy mineral sampling program are described in Table 2. Detailed results from samples submitted to ODM can be found in Appendix 1. Of the 59 samples collected in the study area, 31 contained gold particles and two samples contained ruby corundum.

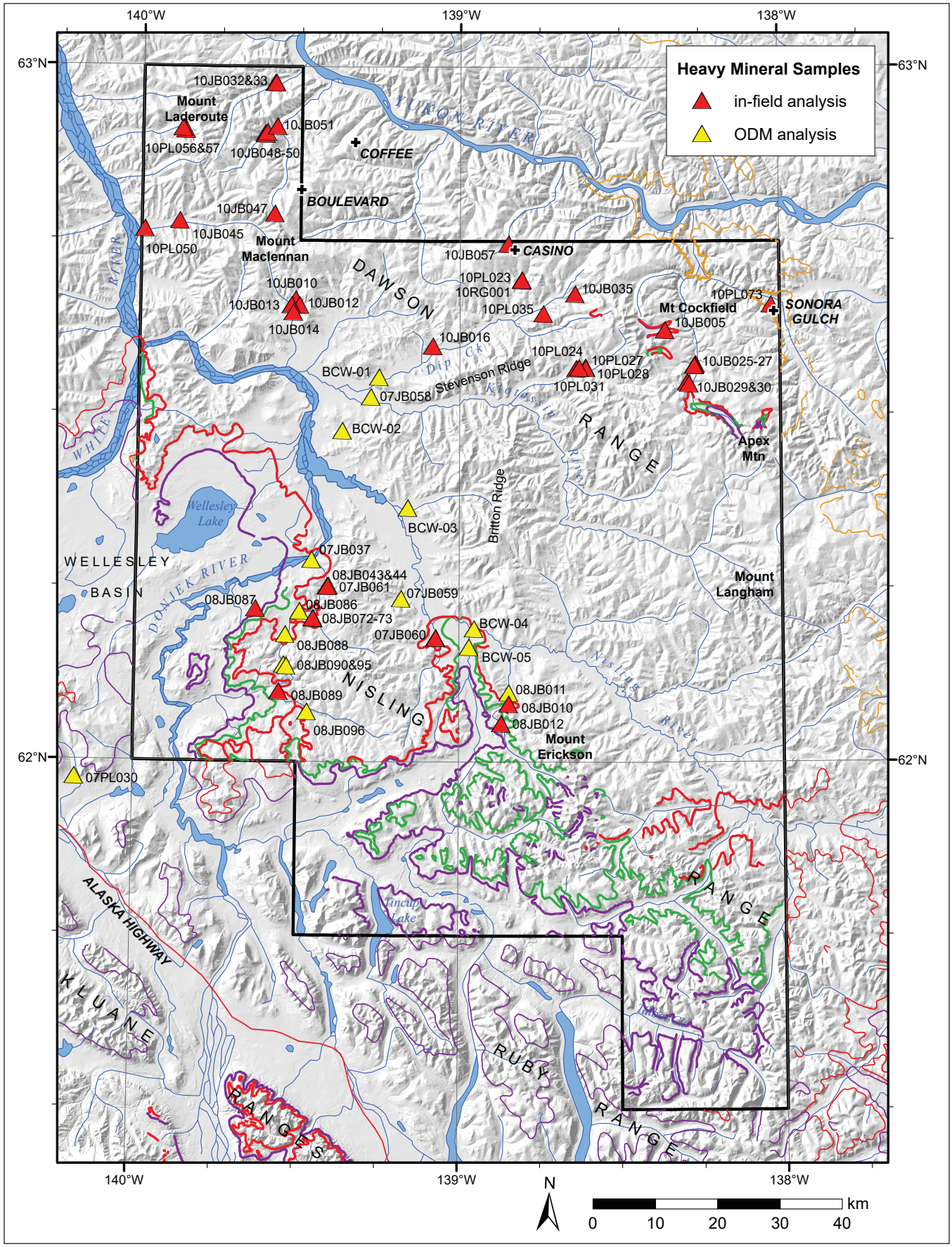

Figure 6-7. *Location map of heavy mineral samples. Glacial limits are displayed: McConnell (MIS 2; purple), Gladstone (MIS 4; green), Reid (MIS 6; red), and pre-Reid (yellow).*

Table 2. *Heavy mineral sample locations and results.*

Site Number	Easting	Northing	ODM	Visual	Type	Results
07JB037	580078	6907534	y		bulk heavy min	15 gold grains, 1 ruby corundum (0.25–0.5 mm fraction)
07JB058	588677	6933895	y		bulk heavy min	3 gold grains
07JB059	594641	6901731	y		bulk heavy min	1 gold grain
07JB060	600420	6895623	y		bulk heavy min	3 gold grains, 1 ruby corundum
07JB060	600420	6895623		y	sluice (7.5 gallons)	No gold grains
07JB061	582710	6903382	y		sluice (7.5 gallons)	4 gold grains, one 1–2 mm in size
08JB010	612519	6885475		y	sluice (7.5 gallons)	No gold
08JB011	612477	6887167	y		sluice (7.5 gallons)	1 gold grain (small)
08JB012	611406	6882280		y	sluice (7.5 gallons)	No gold
08JB043	582756	6903273		y	sluice (7.5 gallons)	no gold, but contains garnet and magnetite
08JB044	582902	6903515	y		sluice (7.5 gallons)	6–8 small gold grains; abundant magnetite and garnets
08JB072	580675	6898056	y		sluice (7.5 gallons)	3 gold grains (2 reshaped, 1 pristine)
08JB073	580612	6898138		y	pan	No gold observed
08JB086	578397	6899211	y		sluice (7.5 gallons)	6 gold grains (5 reshaped, 1 pristine)
08JB087	571328	6899418		y	sluice (7.5 gallons)	no visible gold
08JB088	576276	6895462	y		sluice (7.5 gallons)	3 small gold grains
08JB089	575472	6886297		y	sluice (7.5 gallons)	no gold observed
08JB090	576123	6890615	y		sluice (7.5 gallons)	6 gold grains
08JB095	576587	6890376	y		sluice (7.5 gallons)	no gold observed
08JB096	580116	6883164	y		sluice (7.5 gallons)	7 gold grains (7 reshaped)
10JB005	635457	6946263		y	pan (×6)	no gold
10JB010	576171	6949109		y	pan (2 kg)	no gold; magnetite-rich heavy minerals
10JB012	576794	6948242		y	pan (×2)	no gold; magnetite-rich heavy minerals
10JB013	575473	6948287		y	pan (×2)	no gold; magnetite-rich heavy minerals
10JB014	575873	6947135		y	pan (×2)	5 gold grains
10JB016	598372	6942333		y	pan	no gold; moderate heavy minerals
10JB025	640538	6940996		y	pan (×3)	4 very fine gold grains, abundant black sand
10JB026	640417	6940835		y	pan (×2)	no gold, minor magnetite
10JB027	640398	6940797		y	pan (×4)	5 very fine gold grains + 1 small gold grain
10JB029	639355	6938089		y	pan (×2)	no gold, minor black sand
10JB030	639631	6937836		y	pan (×2)	no gold, moderate black sand
10JB032	571743	6983773		y	sluice (24 gallons)	1 large gold grain ($4.69/yd @ $1000/oz); many quartz crystals, red garnets, coarse magnetite
10JB033	571834	6983749		y	sluice (48 gallons)	no gold; translucent pink mineral
10JB035	620907	6951534		y	pan (×2)	4 small gold grains
10JB045	557118	6961191		y	pan	no gold; fine magnetite-rich heavies
10JB047	572345	6962821		y	pan	3 small gold grains and lots of magnetite.
10JB048	570358	6975617		y	sluice (100 gallons)	15 fine gold grains ($0.56/yd @ $1000/oz)
10JB049	570495	6975450		y	pan (×2)	2 gold grains
10JB050	570632	6975750		y	pan (×2)	2 very fine gold grains; abundant orange garnet

Table 2. *Heavy mineral sample locations and results.*

Site Number	Easting	Northing	ODM	Visual	Type	Results
10JB051	572254	6976744		y	pan (×2)	no gold; minor magnetite
10JB057	609920	6959105		y	sluice (50 gallons)	149 fine gold grains ($1.24/yd @ $1000/oz), magnetite
07PL026	537347	6883694	y		sluice (7.5 gallons)	1 gold grain
07PL030	543168	6871683	y		sluice (7.5 gallons)	5 gold grains
10PL023	612327	6953362		y	pan (×2)	4 gold grains + 1 wire gold ($1.81/yd @ $1000/oz)
10PL024	621503	6939541		y	pan	no gold
10PL027	622945	6939751		y	pan	no gold
10PL028	623005	6939705		y	pan	no gold
10PL031	621904	6939632		y	pan	no gold
10PL035	615928	6948100		y	pan	no gold
10PL050	551583	6959804		y	pan	no gold; abundant heavy minerals
10PL056	557648	6975758		y	pan (×2)	no gold; scarce heavy minerals
10PL057	557145	6976140		y	pan	no gold; abundant heavy minerals
10PL073	652261	6950960		y	pan (×4)	2 large gold grains + 6 small gold grains
10RG001	612327	6953362		y	sluice (75 gallons)	14 gold grains ($0.49/yd @ $1000/oz)
BCW-01	589944	6937178	y		bulk heavy min	1 gold grain
BCW-02	584334	6928380	y		bulk heavy min	no visible gold
BCW-03	595207	6916339	y		bulk heavy min	1 gold grain
BCW-04	606496	6897292	y		bulk heavy min	11 gold grains
BCW-05	605782	6894240	y		bulk heavy min	4 gold grains

Figure 6-8. *Using a portable sluice box to concentrate heavy minerals on a tributary to Grayling Creek (sluice sample). Alluvium was first pre-screened with a 4 mesh screen. The -4 mesh sediment is a manageable size fraction for the small sluice, and pre-screening allows fine sediment to be decanted out-of-stream eliminating suspended effluent into the creek.*

The two samples containing ruby corundum (07JB037 and 060) in the 0.25–0.5 mm fraction were collected using the bulk heavy mineral methods described above. This sampling method involved sieving the sample but did not involve further concentration in the field. Separation was completed using heavy liquids in the lab, which preserves the light-heavy fraction normally lost during gravity separation (*e.g.*, sluicing). These two samples were collected near Mount Forrest. Sample 07JB037 was collected at the mouth of Grayling Creek, which has a drainage basin underlain by Carmacks Group basalt and Finlayson Group carbonaceous metasedimentary rocks. Sample 07JB060 was collected in an unnamed tributary to the Nisling River draining east off Mount Forrest. This drainage is almost entirely underlain by rocks of the Finlayson Group carbonaceous schist, which is likely the source for the rubies.

Of particular interest was the gold grain count in sample 07JB037 from the mouth of Grayling Creek. Eleven additional samples were collected from the drainage to trace the gold anomaly upstream (07JB061, 08JB043, 044, 072, 073, 086, 088, 089, 090, 095 and 096). With the exception of one location, samples collected from the main-stem of Grayling Creek consistently contained 6–8 gold grains in 7.5-gallon sluice samples. In 2016, field investigations were completed in the upper reaches of Grayling Creek to further understand the placer gold potential. This section of the drainage is unglaciated; however it was affected by meltwater draining off the Cordilleran Ice Sheet from the south. Deep canyons are carved at the headwaters of two tributaries to upper Grayling Creek, which highlight the glaciofluvial activity that affected the drainage (Fig. 6-9). Glaciofluvial deposits could be traced from these flows into the main stem of Grayling Creek and the placer gold appears to be associated with these coarse meltwater deposits. Economic placer gold grades were not discovered in upper Grayling Creek, and the dispersion of near surface, low grade, widespread placer gold in the modern alluvium is likely associated with the vigorous glaciofluvial flows.

Figure 6-9. *An upstream view of the canyon on a tributary to upper Grayling Creek. Erosion of the canyon was caused by meltwater draining off the Cordilleran Ice Sheet. Gravel associated with the meltwater flow was deposited for many kilometres downstream.*

The bedrock geology of upper Grayling Creek largely comprises Carmacks Group basalt, which is not regarded for its gold mineralization potential. Visible placer gold was not observed in tributaries to upper Grayling Creek that were unaffected by meltwater. A more likely source for the placer gold is located at the bedrock contact between early Cretaceous granodiorite and Finlayson Group metasedimentary rocks, on the south side of upper Grayling Creek near the meltwater canyons (Murphy *et al.*, 2007). This may also be a better location to target placer exploration in the drainage, although access to the area is difficult.

Heavy mineral sampling in the northwestern part of the study area identified a prospective target in Carlisle Creek (10JB032), a tributary of Yukon River. A left limit fluvial terrace rising 20 m above the floodplain was sampled. A shallow trench was excavated into the terrace in order to focus sampling near the bedrock/gravel contact. The estimated gravel thickness on the terrace is 2 m. Quartz clasts up to 28 cm in size were noted in the alluvium. Bedrock consists of a green-coloured schist. One relatively thick gold grain with a surface area of 1.14 mm^2 was recovered. Placer gold was also noted in Independence Creek, and in upper Independence Creek in an unnamed drainage north of Coffee Peak (10JB047).

In the northeastern part of the study area, abundant gold grains were obtained from a former placer mine site in upper Canadian Creek below Patton Hill (10JB057), and in Casino Creek a tributary to Dip Creek. An attempt was made to find gold on terraces to the Selwyn River, and a small amount was recovered (10JB027). A number of gold grains were obtained from panning at an active placer mine on Sonora Gulch (10PL073).

Farther south on the Nisling River, 11 gold grains were obtained from a bulk heavy mineral sample located at the limit of glaciation in the drainage (BCW-04).

The placer potential of the study area is highest in the Dawson Range where most gold hardrock occurrences are found; however, limited visible gold appears to be associated directly with the Coffee deposit. Exploration should focus in tributaries of Yukon River where base level changes have caused accelerated fluvial erosion of valleys and reduced their accommodation space for alluvium and overburden, thereby increasing concentrations of heavy elements and minerals. This area is also favourable given the availability of barge transportation on the Yukon River. Additional placer reserves undoubtedly remain in Canadian, Sonora and Rude creeks since placer mining in these areas has been sporadic and generally small-scale.

Natural hazards

Permafrost

Permafrost is defined as ground that remains frozen for at least two consecutive years (van Everdingen, 2005). Certain permafrost landforms can indicate areas where permafrost is locally very ice-rich. Clearing or disturbance of organic cover in these areas can produce rapid thaw settlement and ground disturbance and should therefore be avoided where possible. In southern and central Yukon, forest fires, river erosion and anthropogenic surface disturbance are common triggers for thermokarst subsidence and permafrost-related landslides (Huscroft *et al.*, 2004).

Permafrost distribution is extensive but discontinuous throughout the study area, based on both air photo interpretation and field observations. In some cases, permafrost was not directly observed in soil pits or cutbanks, but it was generally assumed present at greater depth or farther back from exposure scarps, based on the morphology of local landforms, or evidence of periglacial processes in the vicinity. Permafrost was interpreted to be absent or at great depth on well-drained south facing slopes (typically covered by aspen forest) and within recently active, coarse-grained floodplain sediments immediately adjacent to large watercourses.

In high elevation (>1000 m) alpine areas, permafrost presence is indicated by widespread periglacial landforms that are produced by ongoing frost-shatter, freeze-thaw, cryoturbation and gelifluction activity. Patterned ground landforms (*e.g.*, sorted stone polygons/nets, block fields, and frost boils) are found in stable landscape positions (*i.e.*, along alpine ridge crests and plateaus), while stone stripes, solifluction features and cryoplanation terraces (*see* Chapter 4) are commonly found on alpine slopes. In the eastern Nisling Range, rock glaciers form preferentially at the base of steep talus slopes (Fig. 6-10). Active layer detachment slides on some valley sides also served as an indicator of permafrost presence. In valley bottom settings, permafrost is almost universally present in organic-covered alluvial, eolian and glaciolacustrine sediments.

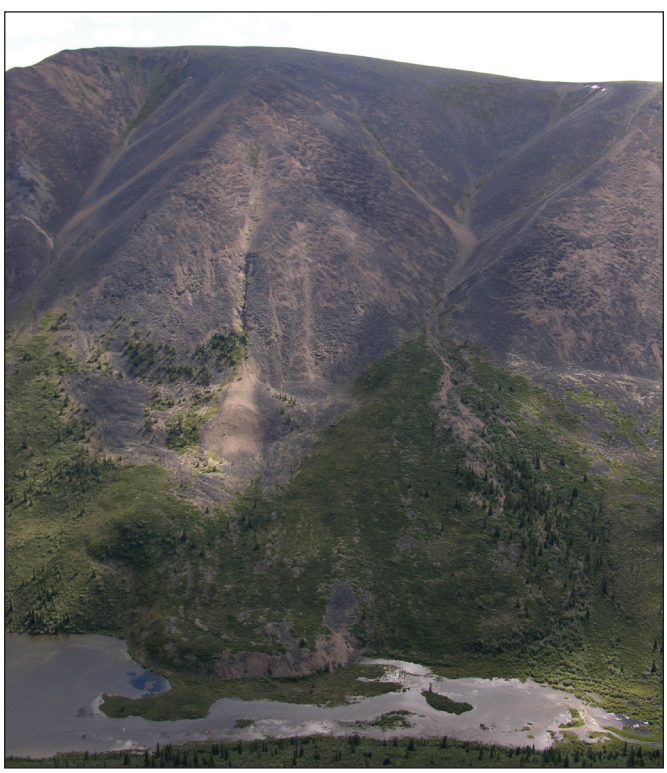

Figure 6-10. *Rock glacier developed at the base of a talus-covered slope in the Nisling Range.*

Solifluction

Solifluction is the slow downhill flow of saturated surface materials (van Everdingen, 2005; French, 2017; Price, 1973). Gelifluction is a type of solifluction specifically associated with the presence of underlying frozen ground (van Everdingen, 2005). Solifluction within the study area commonly results from restricted drainage above a shallow permafrost table. It typically gives rise to a characteristic bumpy or melting surface appearance that is readily apparent when observed from afar (*e.g.*, Fig. 6-11). Solifluction lobes were investigated 4 km north of Mount Pattison, on a small peak unofficially dubbed Pyramid Mountain (Fig. 4-12; 10JB053 to 056). At this location, rubbly stone banked-solifluction lobes have developed above 1300 m elevation on slopes of varying aspect and steepness (ranging from 13 to 34˚). They are composed of very coarse grained (cobble to boulder) diamicton on the order of 1 m thick. Deformation within the lobes appeared to occur within loose rubble near the base. In contrast, turf-banked solifluction also commonly occurs within or above frozen peaty colluvium covered by thick moss mats (Fig. 6-12).

Sheetwash

On gentle lower elevation slopes, sheetwash (also known as slopewash or thermo-erosional wash) is commonly associated with permafrost (van Everdingen, 2005; French, 2017). It typically occurs on moderately sloped valley sides that are blanketed by till or colluvium and underlain by shallow permafrost (Fig. 6-13). Sheetwash occurs when water moves at or near the surface in unconcentrated overland flow and/or percolates through soil pores, rather than being concentrated in channels. A thin active layer promotes saturated surface conditions by limiting the volume of soil available for infiltration. Seasonal thaw of ice within the active layer also supplies an additional source of soil moisture. Sheetwash gradually transports fine sediment (sand, silt and clay) down to slope toes and valley bottoms where it is commonly interstratified with organic deposits. Evidence of sheetwash is indicated by a diagnostic surface expression that is visible from the air whereby the land surface appears to be flowing.

Figure 6-11. *Solifluction lobes on a north-facing slope near Mount Maclennan (10PL052). These lobes contain a mix of coarse-rubbly colluvium and organics.*

Figure 6-12. *A solifluction lobe on a north-facing slope was excavated near Sonora Gulch. Approximately 80 cm of frozen organics overlies colluvium composed of weathered bedrock. Much of the creep within the solifluction lobe occurs within the organic material; however, weathered bedrock sediment is entrained and mixed with the organic material near the contact.*

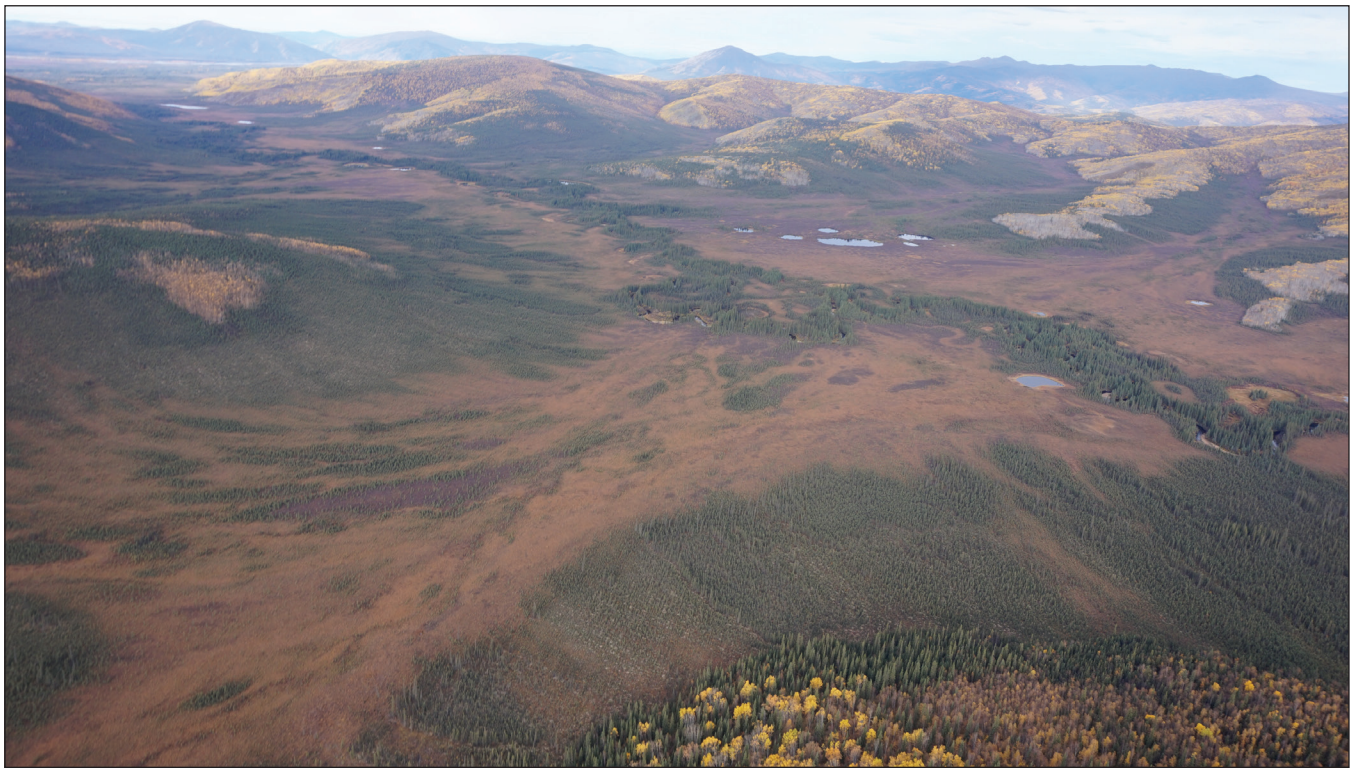

Figure 6-13. *An aerial view of the Dip Creek drainage where broad sheetwash features form on permafrost-rich deposits in the valley bottom. Much of the valley bottom fill is loess derived from nearby glaciofluvial floodplains of the Nisling and Donjek rivers.*

Thermokarst

Ice-wedge polygons are concentrated in peat-covered lowlands north and east of Wellesley Lake and west of Donjek River, and in the Doyle Creek basin (Fig. 6-14a). Thermokarst lakes occupy closed depressions formed by thaw settlement of ice-rich permafrost. They are most prevalent in many of the same areas described for ice-wedges (*e.g.*, Fig. 6-14b), as well as in lowlands adjacent to Dip Creek, Nisling River, Grace Lake and Kluane River. Many thermokarst lakes are actively expanding as their banks continue to thaw and collapse (Fig. 6-14c).

Rock glaciers

Active rock glaciers are another excellent indicator of local permafrost (Fig. 6-10). These lobate or tongue-shaped masses of angular rock fragments and finer material gradually creep downslope due to deformation of ice within (*i.e.*, a buried glacier ice core or interstitial ice that has grown in void spaces between rock fragments). They commonly have transverse furrows and ridges on their surface that provide evidence of movement. Active rock glaciers possess a very steep unvegetated front at their snouts or termini. Within the study area, rock glaciers are found primarily in the headwaters of Tyrrell Creek within the Nisling Range, where abundant talus rubble has accumulated on lower slopes.

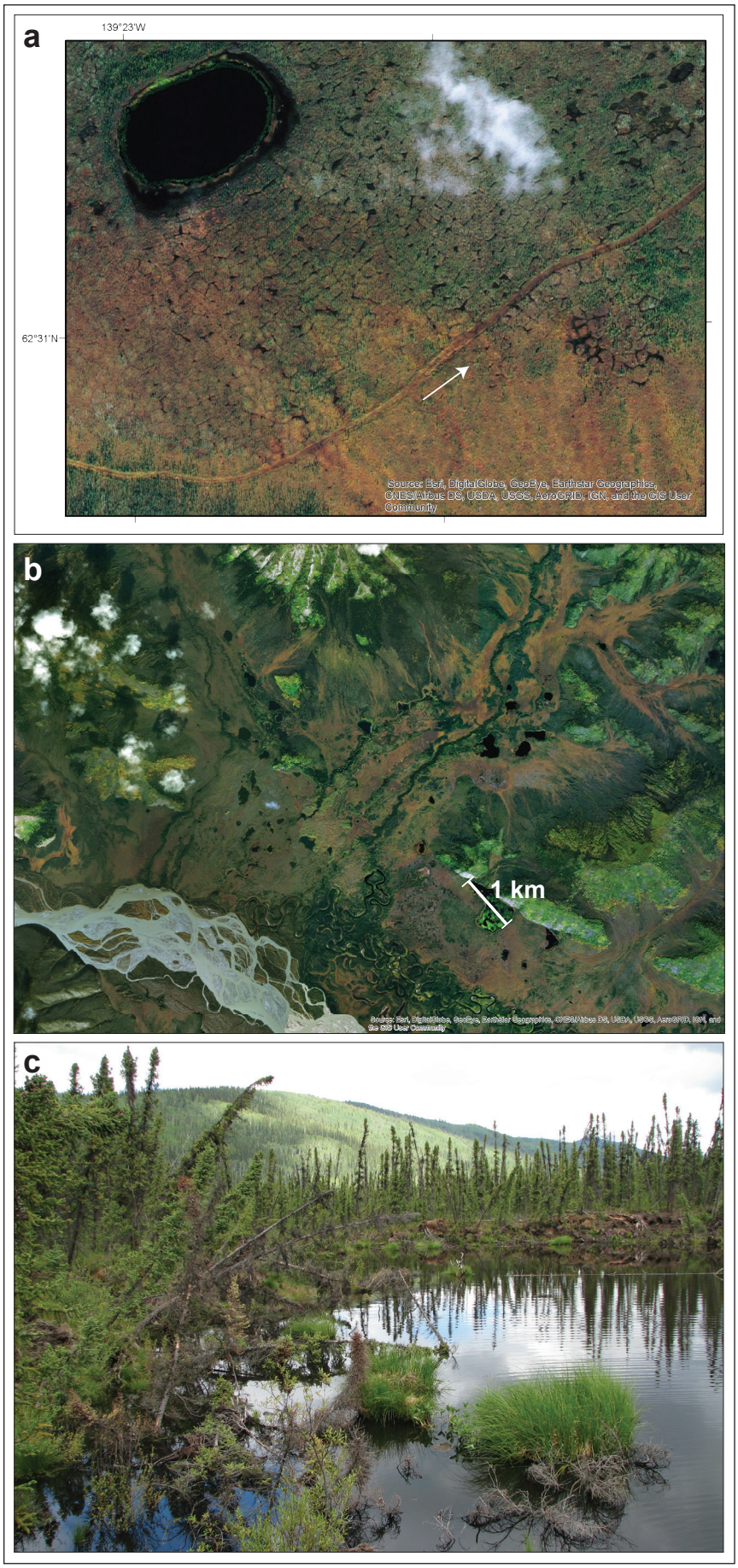

Figure 6-14. (a) *Orthogonal degrading high centred ice wedge polygons traversed by a winter road (approximately 10 m wide) near the mouth of Doyle Creek (Digital Globe/ GEO1 0.46 m resolution imagery, 6 September 2015). Polygon edges are approximately 15 to 20 m long and they are roughly oriented parallel and orthogonal to the lake edge indicating they are likely formed in drained lake sediments.* ***(b)*** *Abundant thermokarst lakes near the confluence of Doyle Creek and Donjek River indicate ice-rich permafrost conditions in the broad valley bottom (1 July 1989 ortho-image). Most of the larger lakes are on the order of 200 m in diameter, although the largest is more than 1 km long.* ***(c)*** *Thermokarst lake near Rude Creek (10PL040). Ongoing permafrost degradation along the crater rim is causing trees to topple into the lake.*

Pingos

Open-system pingos are very abundant in the region (88 pingos were identified in the map area), particularly within the unglaciated northern Dawson Range (Bond and Lipovsky, 2011; Fig. 6-15). Pingos are ice-cored conical mounds, on the order of 10–20 m high and 100–200 m wide within the study area. Most of these have collapse craters which indicates that their ice cores have largely degraded and thawed. Pingos are typically located in slope toe positions within small (low-order) drainages where artesian groundwater pressures likely develop beneath valley bottom permafrost as a result of groundwater recharge from unfrozen slopes above. Factors that control the distribution of open system pingos include topography, permafrost thickness and the appropriate configuration of discontinuous permafrost (Hughes, 1969). Surficial material cover does not seem to be relevant because pingos were documented within a variety of sediment types, including fine-grained loess and alluvium, coarser-grained grus (grit to pebble-size weathered intrusive fragments), and even bedrock (McKillop *et al.*, 2013; Bond and Lipovsky, 2010).

Figure 6-15. *Collapsed open-system pingos in a tributary to Rude Creek (10PL036 and 039).*

Icings

Icings (or aufeis) were observed in several locations in the valley bottoms of low-order drainages. Icings are thick sheets of layered ice produced by successive freezing of surface seepage water (Fig. 6-16). The seepage water may originate from a variety of sources, including groundwater springs discharging from beneath permafrost or within the active layer, and/or stream overflow throughout the winter. Underlying bedrock fractures may also provide pathways for local groundwater discharge (Wanty *et al.*, 2007). Icings are commonly referred to as “glaciers”, although this terminology is incorrect. In many cases, icings persist throughout the summer and become buried. Icings can present significant challenges for maintenance of winter transportation routes, particularly where they block culverts or where road cuts intersect a near-surface ground water table perched above permafrost.

Active layer depth

The active layer is the ground surface layer above permafrost that freezes and thaws annually. It reaches its maximum depth of thaw in late summer, at which point it may or may not reach the permafrost table (top of permafrost) in the discontinuous permafrost zone (van Everdingen, 2005).

Frost tables in soil pits and stream cutbank exposures were observed at depths between 20 and 170 cm in late June and July of each field season, although they were typically less than 1 m deep. Where surface organic cover exceeded a thickness of 10 cm, the frost table was commonly observed as shallow as 20–40 cm depth. In coarse-sand tephra dunes with no vegetation cover, the frost table was observed at 145 cm depth (08PL069). These field observations only provide a minimum estimate of active layer depth in the region because it must technically be measured in late summer or early fall, at the end of the thaw season. However, it is expected that active layer depths would be of a similar magnitude or slightly greater than the observed frost table depths. Based on field observations, active layers are interpreted to be very shallow (<50 cm) throughout much of the study area, particularly along alpine summits and ridges, within loess-rich colluvial aprons, and beneath thick (>10 cm) peat or sphagnum moss.

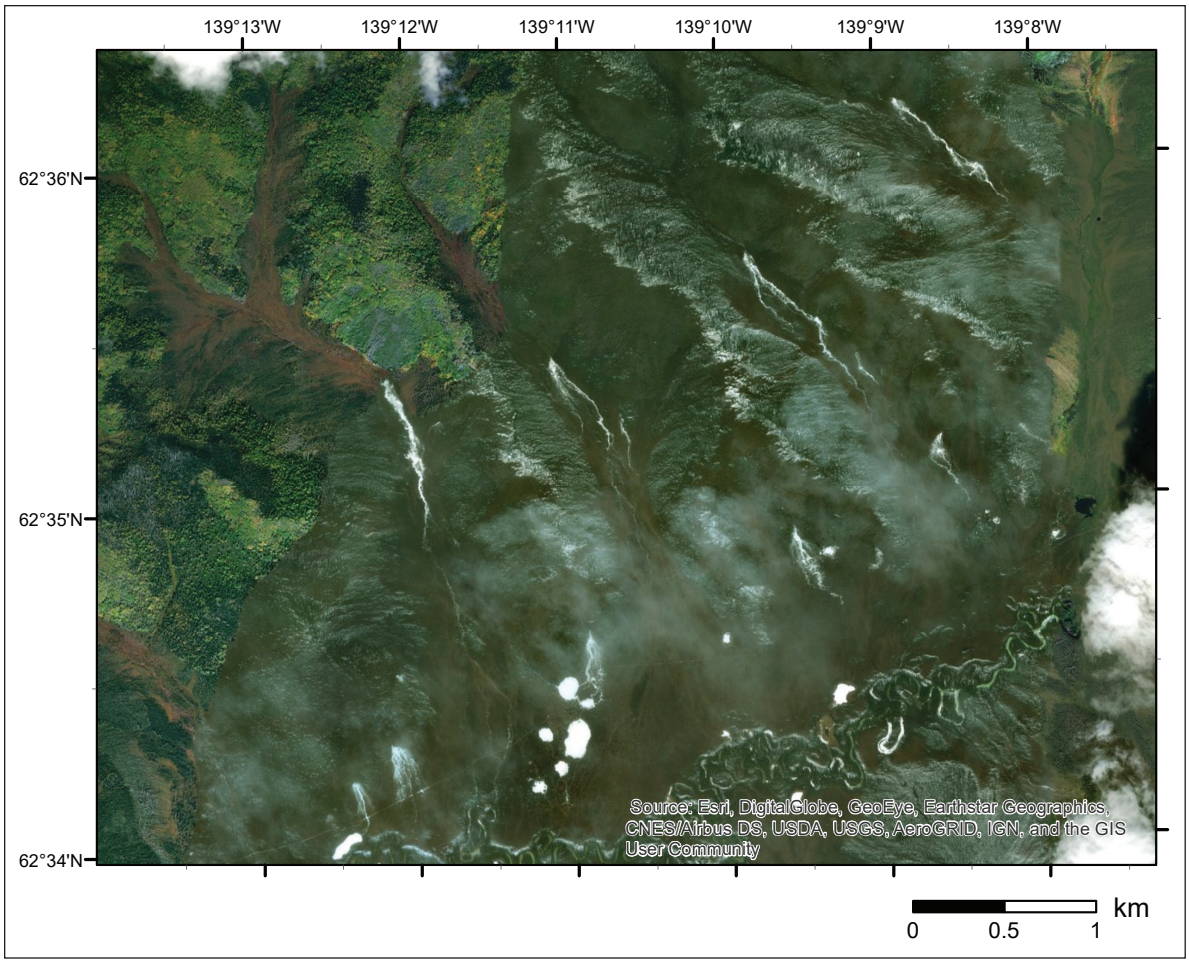

Figure 6-16. *A series of icings in the Dip Creek basin occur in very similar topographic positions suggesting that they are linked to a common regional groundwater flow regime. Digital Globe/WorldView2, 0.5 m resolution imagery, 15 April, 2015.*

Active layer depth has important implications for soil moisture and slope stability. Because the underlying permafrost table is impermeable, thinner active layers are subject to greater moisture content or saturation following rainfall, snowmelt or heating events such as forest fires or extreme high temperatures. Higher moisture content increases pore water pressure, which results in a corresponding reduction in soil strength. On slopes, saturated soils are susceptible to active layer detachment landslides and/or slow periglacial wasting through the processes of slopewash, solifluction, gelifluction and frost creep.

Permafrost thickness and ice-content

Permafrost thickness is difficult to characterize due to lack of deep exposure, and it likely varies considerably with topographic position and aspect and surficial material. The largest exposures observed revealed minimum permafrost thicknesses of approximately 10 m in valley bottoms: 12 m of permafrost was exposed in a Sonora Gulch placer excavation (10PL073); 7 m was exposed in a cutbank on a tributary to the Donjek River (10PL045); and 9 m was exposed in a Home Creek cutbank (10PL051). Permafrost was at least 11 m thick along MacKinnon Creek (07PL035; Bond *et al.*, 2008) and at least 6.5 m thick within clayey silt that was exposed in a Kluane River cutbank (07PL042) west of Toshingermann Lake. Ice-rich colluvial apron sediments at least 30 m thick were encountered during drilling completed for a proposed airstrip alignment in the Dip Creek valley (DH11-05 and DH11-06; Knight Piésold, 2012).

Ice-rich permafrost in the area is generally associated with fine-grained alluvial, glaciolacustrine and colluvial apron sediments in valley bottoms, although massive ice has been found in coarse-grained glaciofluvial materials adjacent to the study area along the Alaska Highway (Bond and Lipovsky, 2011). Permafrost within bedrock and along ridge crests is typically ice-poor and is considered thaw stable.

Volumetric ice content within the soil was visually estimated in the field and is extremely variable. Within the northern Dawson Range, less than 20% visible ice was generally observed in permafrost exposures, and consisted of thin layers or lenses, crustal particle coatings and pore ice. However, up to 50% visible ice was observed at some sites, likely where local groundwater convergence occurred. Up to 20% visible ice was exposed within slopewash sediments exposed in thermo-erosion gullies (08PL042). Ice lenses up to 57 cm thick were exposed along the Klaza River (08PL056) where the thickness of permafrost was at least 3.5 m. Massive ice in the form of ice wedges was also observed in thick loess accumulations exposed in a Home Creek cutbank (10JB046).

Farther south, within frozen glaciolacustrine sediments exposed along Mackinnon Creek (07PL035), visible ice varied between 30 and 80% by volume, and consisted of small crystals (<2 mm in diameter) and stratified veins up to 50 cm long. Along the bank of an active thermokarst lake in the Grace Lake valley (Fig. 4-14a,b; 07PL010), ice content within glaciolacustrine sediments was less (15% by volume) and consisted of thin, stratified and randomly oriented veins with an average thickness of 2 mm.

Landslides

Permafrost-related landslides and periglacial mass wasting

Shallow mass wasting activity and permafrost-related landslides commonly occur throughout the study area, as a result of widespread periglacial conditions (*i.e.*, freeze/thaw processes in cold climate regions), which promote slope instability in a variety of ways. Firstly, ongoing freeze/thaw or frost action promotes gradual downslope movement of surface sediment via frost creep, contributing to widespread solifluction. High soil moisture conditions are also very common due to seasonal melting of ground ice within the active layer and restricted drainage of rainfall and snowmelt at the permafrost table. High soil moisture conditions or saturation elevates pore water pressure thereby reducing structural strength and promoting solifluction and shallow failures. Finally, the permafrost table may also act as a slip plane in active-layer detachment slides. In many locations within the study area, the permafrost table was located near the base of a thick, coarse-sand textured layer of White River ash. This interface was documented as an active-layer detachment failure plane immediately south of the study area (Fig. 6-17a,b; Huscroft *et al.*, 2004).

Active-layer detachments are shallow translational failures that typically occur on gentle to moderate permafrost slopes and are relatively small in size (hundreds of metres long, tens of metres wide, and <1 m deep; Lipovsky *et al.*, 2006). They are commonly triggered by events that cause rapid thawing or thickening of the active layer at greater than normal rates, such as periods of extreme hot and/or wet weather, or sudden vegetation disturbances resulting from human activity or forest fires (van Everdingen, 2005; Huscroft *et al.*, 2004; Lipovsky *et al.*, 2006; Lipovsky and Huscroft, 2007; Lewkowicz and Harris, 2005). Very few active or recent failures were observed during field surveys: one was documented in a recent burn in the Grace Lake valley (07PL013) while several others were observed south of the study area, on slopes located near the Alaska Highway (Fig. 6-17a–c). Older landslide scars overgrown by early successional vegetation were, however, very widespread throughout the study area.

Retrogressive thaw slumps are slope failures that result from thaw of ice-rich permafrost, commonly in association with fine-grained glaciolacustrine or morainal sediment. They generally possess a steep headwall that retreats for extended periods of time due to ongoing thaw of massive ice. Mud and debris flows then transport the thawed saturated sediment away. They rarely occur within the study area, but can be expected if river erosion (*e.g.*, Kluane River, upstream of 07PL042) or other disturbances expose ice-rich permafrost. They may also occur on hillslopes where vegetation is suddenly disturbed.

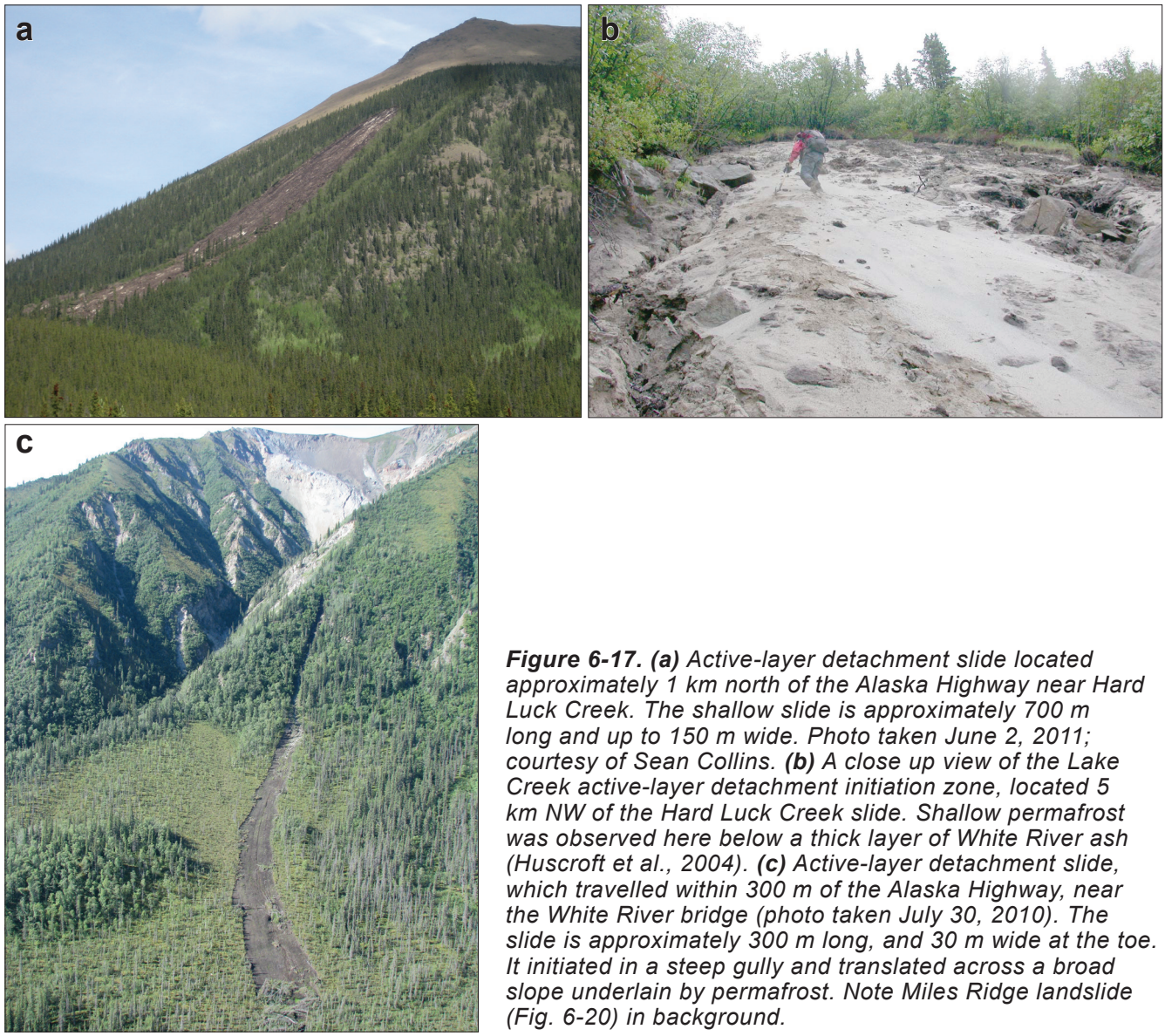

Figure 6-17. (a) *Active-layer detachment slide located approximately 1 km north of the Alaska Highway near Hard Luck Creek. The shallow slide is approximately 700 m long and up to 150 m wide. Photo taken June 2, 2011; courtesy of Sean Collins.* ***(b)*** *A close up view of the Lake Creek active-layer detachment initiation zone, located 5 km NW of the Hard Luck Creek slide. Shallow permafrost was observed here below a thick layer of White River ash (Huscroft et al., 2004).* ***(c)*** *Active-layer detachment slide, which travelled within 300 m of the Alaska Highway, near the White River bridge (photo taken July 30, 2010). The slide is approximately 300 m long, and 30 m wide at the toe. It initiated in a steep gully and translated across a broad slope underlain by permafrost. Note Miles Ridge landslide (Fig. 6-20) in background.*

These landslides are of particular concern because they can be far-reaching, occur on gentle slopes, and remain active for decades (Lipovsky *et al.*, 2006; Lipovsky and Huscroft, 2007; Ward *et al.*, 1992).

Debris flows

Debris flows are rapid flows of saturated sediment that commonly occur in steep streams and gullies where loose colluvial or morainal material accumulates and becomes mobilized during intense rainfall and/or snowmelt events. They generally travel down to valley bottoms where levees are deposited and contribute to the aggradation of colluvial cones and/or colluvial-alluvial fans. They may also cause avulsion or redirection of stream channels on alluvial fans. Abundant evidence of debris flows was observed on moderate to steep gullied slopes and colluvial fans in mountainous portions of the study area, particularly in upper Alaskite and Talbot Creek drainages, and near Mount Cockfield (Fig. 6-18), Britton Ridge, Mount Erickson and Mount Forrest. Any development near fans and stream crossings in mountainous terrain should carefully consider the risk of debris flows, as they can potentially be very destructive and have long runout distances up to 1 km.

Figure 6-18. *An alpine debris flow on the west side of Mount Cockfield traveled up to 1 km, following a narrow track up to 15 m wide.*

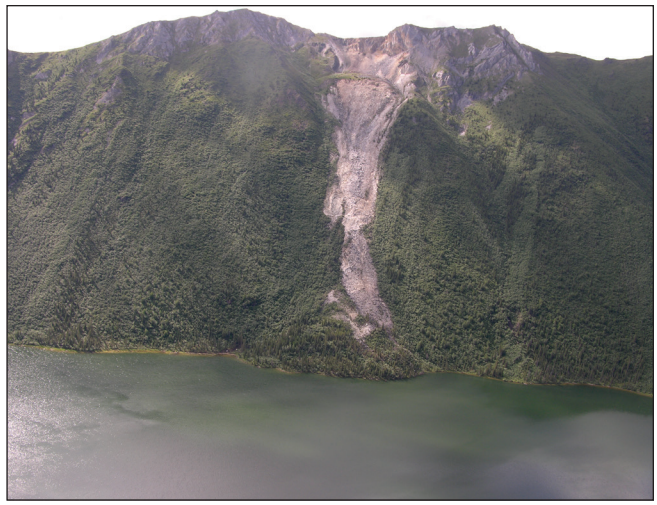

Figure 6-19. *A large rockslide extends approximately 1 km down a steep slope on the west side of Dogpack Lake.*

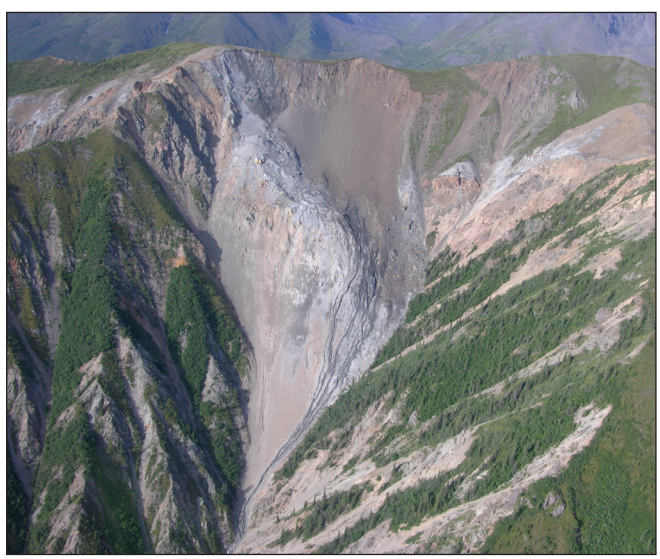

Figure 6-20. *A view of the Miles Ridge rockslide near the White River bridge just west of the study area. The slide is associated with the Denali fault system and is a hazard to the Alaska Highway transportation corridor.*

Bedrock-controlled landslides

Large, deep-seated, bedrock-controlled landslides were only observed just outside the map area in steeper areas of high relief within the Ruby and Kluane ranges.

Two rockslides are located a few kilometres southeast of Tincup Lake within Snowcap assemblage schist bedrock (Fig. 6-19; Yukon Geological Survey, 2020). Based on the presence of mature vegetation on the debris, these are both relatively old features, but it is important to consider that relict rockslides have been known to reactivate in other parts of Yukon (Brideau *et al.*, 2016), including one also within the Snowcap assemblage at Little Salmon Lake (Brideau *et al.*, 2010).

Farther west of the study area, a large rock slump is actively deforming on Miles Ridge, above the White River Bridge on the Alaska Highway (Fig. 6-20). This landslide was described in detail by Bond *et al.* (2008), and occurs within volcanic and highly altered ultramafic rocks that are bounded by strike-slip faults in the Denali fault system. If the landslide fails catastrophically in the future, it has the potential to impact the White River bridge, located less than 2 km directly downslope.

Earthquakes

The study area is located within the moderate to moderately high relative seismic hazard zone (Fig. 6-21; Natural Resources Canada, 2015). Seismic activity in the area is related to tectonic activity in the Gulf of Alaska to the southwest, and the presence of several major fault systems in southwestern Yukon and neighbouring Alaska, including the Denali and Duke River faults.

Seventy-five earthquakes were recorded within the map area itself between 1970 and 2021, with a maximum magnitude of 4.1 (Natural Resources Canada, 2022). Eighty-one magnitude 4.0 to 6.0 earthquakes have been recorded within 100 km south of the study area since 1920, while seven magnitude 6.0 to 8.0 earthquakes have been recorded within 200 km of the study area throughout the same period.

Earthquakes have the potential to trigger landslides (Everard, 1994) and rockfall, damage infrastructure and buildings, and can cause liquefaction of saturated sandy sediments such as deltaic or fluvial deposits, beach sands or poorly compacted artificial fills.

Ground shaking intensity felt at a particular location varies depending on proximity to the epicenter, local ground conditions, and topography. Intensity generally increases closer to the epicentre and is amplified in softer and thicker sediments, or on raised topographic features such as hills, ridges and cliff tops. Seismic hazard is greatest in areas underlain by thick deposits of soft clay, particularly where they are capped by peat and organic soils, and it is lowest where bedrock is at or near the surface. However, the amount of amplification due to soil conditions does diminish as the strength of ground shaking increases (Monahan *et al.*, 2000).

Avalanches

Avalanche activity was not mapped as part of this study, although avalanche hazards are generally assumed to be present on moderately steep mountainous slopes during winter months when snow depths exceed 50 cm above the top of surface features such as bushes and rocks. Most large avalanches are initiated on slope angles between 25 and 40°; however, slope shape, orientation to prevailing wind and surface roughness are also important factors that determine their distribution (Canadian Avalanche Association, 2002). The most obvious sign of avalanche activity on a slope is the presence of former avalanche paths that are highlighted by damaged or successional vegetation.

River flooding

The major rivers and their tributaries in the study area, including the White, Donjek, Kluane, Nisling, Klaza and Klotassin rivers are all susceptible to flooding hazards. The glacial-fed rivers reach peak flows during the maximum glacier melt season in July and August and therefore flood potential increases with heavy rains during this period. Non-glacially fed rivers are more likely to experience flooding during the spring freshet.

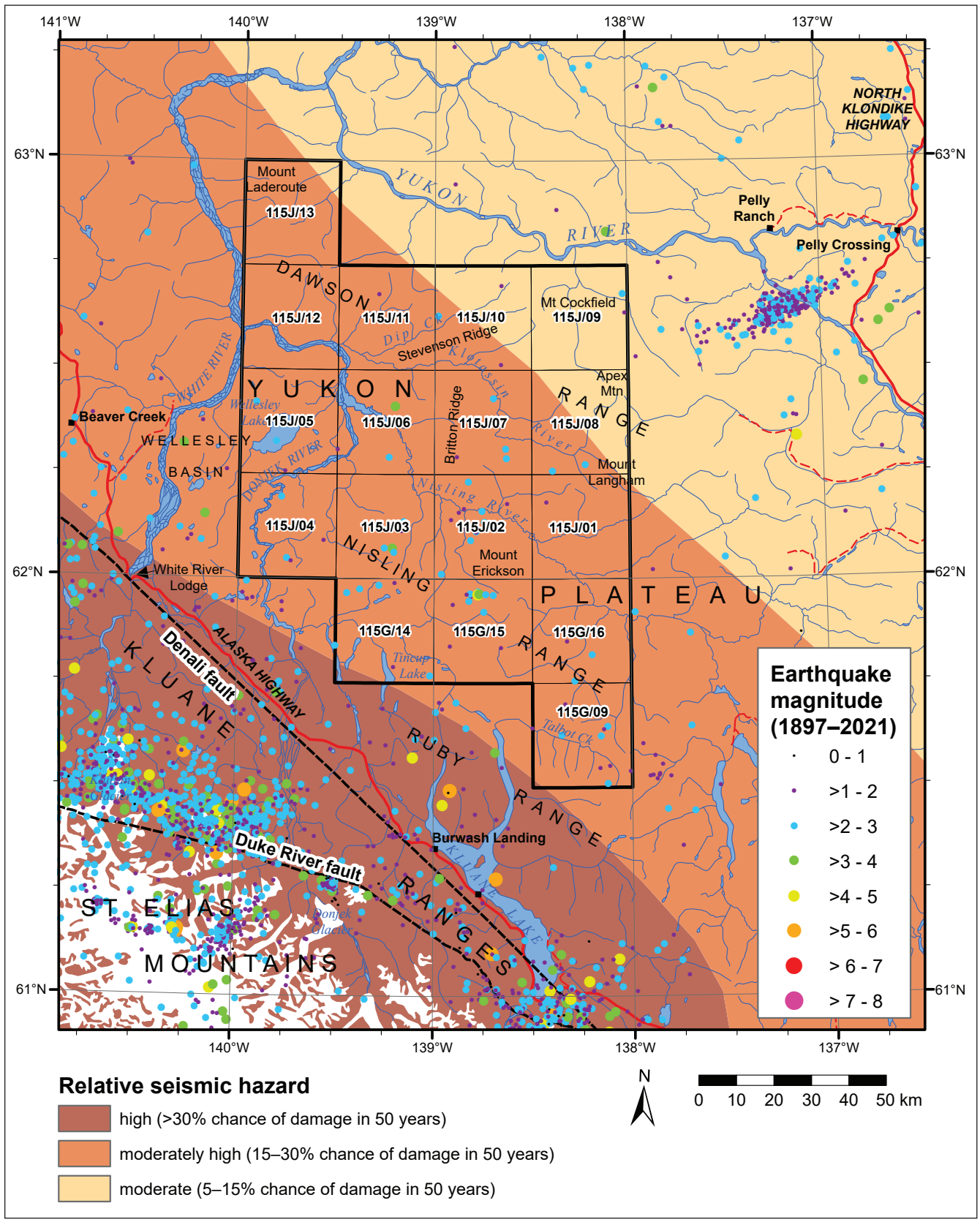

Figure 6-21. *Earthquake epicenters (Natural Resources Canada, 2022) and simplified seismic hazard map for the study area. Seismic hazard is classified according to the chance of significant damage occurring to one or two story buildings in a 50 year period (Natural Resources Canada, 2015).*

References

Barendregt, R. and Duk-Rodkin, A., 2004. Chronology and extent of late Cenozoic ice sheets in North America: A magnetostratigraphic assessment. Quaternary Science Reviews, vol. 2, p. 1–7.

Bond, J.D., Lipovsky, P.S. and von Gaza, P., 2008. Surficial geology investigations in Wellesley basin and Nisling Range, southwest Yukon. *In:* Yukon Exploration and Geology 2007, D.S. Emond, L.R. Blackburn, R.P. Hill and L.H. Weston (eds.), Yukon Geological Survey, p. 125–138.

Bond, J.D. and Lipovsky, P.S., 2009a. Surficial geology of Toshingermann Lake (NTS 115G/14), Yukon. Yukon Geological Survey, Open File 2009-45, scale 1:50 000.

Bond, J.D. and Lipovsky, P.S., 2009b. Surficial geology of Kiyera Lake (NTS 115G/15), Yukon. Yukon Geological Survey, Open File 2009-46, scale 1:50 000.

Bond, J.D. and Lipovsky, P.S., 2009c. Surficial geology of Rhyolite Creek (NTS 115G/16), Yukon. Yukon Geological Survey, Open File 2009-47, scale 1:50 000.

Bond, J.D. and Lipovsky, P.S., 2009d. Surficial geology of Talbot Creek (NTS 115G/9), Yukon. Yukon Geological Survey, Open File 2009-48, scale 1:50 000.

Bond, J. and Lipovsky, P., 2010. Pre-Reid surficial geology investigations in southwest McQuesten map area (115P). *In:* Yukon Exploration and Geology 2009, K.E. MacFarlane, L.H Weston and L.R. Blackburn (eds.), Yukon Geological Survey, p. 103–117.

Bond, J.D. and Lipovsky, P.S., 2011. Surficial geology, soils and permafrost of the northern Dawson Range. *In:* Yukon Exploration and Geology 2010, K.E. MacFarlane, L.H. Weston and C. Relf (eds.), Yukon Geological Survey, p. 19–32.

Bond, J.D. and Lipovsky, P.S., 2012a. Surficial Geology of Selwyn River (NTS 115J/9), Yukon. Yukon Geological Survey, Open File 2012-1, scale 1:50 000.

Bond, J.D. and Lipovsky, P.S., 2012b. Surficial Geology of Colorado Creek (NTS 115J/10), Yukon. Yukon Geological Survey, Open File 2012-2, scale 1:50 000.

Bond, J.D. and Lipovsky, P.S., 2015a. Surficial geology of Mackinnon Creek (NTS 115J/4), Yukon. Yukon Geological Survey, Open File 2015-4, scale 1:50 000.

Bond, J.D. and Lipovsky, P.S., 2015b. Surficial Geology of NTS 115J/3. Yukon Geological Survey, Open File 2015-5, scale 1:50 000.

Bond, J.D. and Sanborn, P.T., 2006. Morphology and geochemistry of soils formed on colluviated weathered bedrock: Case studies from unglaciated upland slopes in west-central Yukon. Yukon Geological Survey, Open File 2006-19, 70 p.

Bonnaventure, P.P., Lewkowicz, A.G., Kremer, M. and Sawada, M.C., 2012. A permafrost probability model for the southern Yukon and Northern British Columbia, Canada. Permafrost and Periglacial Processes, vol. 23, p. 52–68.

Bostock, H.S., 1966. Notes on glaciation in central Yukon. Geological Survey of Canada, Paper 65-36, 18 p.

Bostock, H.S., 1969. Kluane Lake, Yukon Territory, Its drainage and allied problems (115G, and 115 F E). Geological Survey of Canada, Paper 69-28, 19 p.

Brideau, M.-A., Stead, D., Lipovsky, P., Jaboyedoff, M., Hopkinson, C., Demuth, M., Barlow, J., Evans, S. and Delaney, K., 2010. Preliminary description and slope stability analyses of the 2008 Little Salmon Lake and 2007 Mt. Steele landslides, Yukon. *In:* Yukon Exploration and Geology 2009, K.E. MacFarlane, L.H. Weston and L.R. Blackburn (eds.), Yukon Geological Survey, p. 119–133.

Brideau, M.-A., Shugar, D.H. and Wong, C., 2016. Preliminary investigation of the 2014 Vulcan Creek landslide dam, Kluane National Park and Reserve, Yukon. *In:* GeoVancouver 2016, 69th Canadian Geotechnical Conference Proceedings, Vancouver, October 2–5, 2016.

Canadian Avalanche Association, 2002. Land Managers Guide to Snow Avalanche Hazards in Canada. Canadian Avalanche Association, J.B Jamieson, C.J. Stethem, P.A. Schaerer and D.M. McClung (eds.), Revelstoke, BC, Canada. https://cdn.ymaws.com/www.avalancheassociation.ca/resource/resmgr/standards_docs/land_managers_guide.pdf.

Clague, J.J., Evans, S.G., Rampton, V.N. and Woodsworth, G.J., 1995. Improved age estimates for the White River and Bridge River tephras, western Canada. Canadian Journal of Earth Sciences, vol. 32, p. 1172–1179.

Clague, J.J., Luckman, B.H., Van Dorp, R.D., Gilbert, R., Froese, D., Jensen, B.J.L. and Reyes, A.V., 2006. Rapid changes in the level of Kluane Lake in Yukon Territory over the last millennium. Quaternary Research, vol. 66, p. 342–355.

Cronmiller, D.C., 2019. Surficial geology, stratigraphy and placer deposits of the Ruby Ridge, Yukon Territory. Unpublished MSc thesis, Simon Fraser University, Burnaby, BC, 148 p.

Cronmiller, D., Ward, B. and Bond, J.D., 2018. Surficial geology of Gladstone Creek (NTS 115G/8 and part of 115G/7). Yukon Geological Survey, Open File 2018-20, scale 1:50 000.

Cronmiller, D.C., Ward, B.C., Bond, J.D. and Layton-Matthews, D., 2019. Constraints on the evolution of placer deposits at Gladstone Creek, Yukon (NTS 115G/7, 8). *In:* Yukon Exploration and Geology 2018, K.E. MacFarlane (ed.), Yukon Geological Survey, p. 61–74.

Dampier, L., Sanborn, P., Bond, J., Clague, J.J. and Smith, S., 2009. Soil genesis in relation to glacial history in central Yukon. *In:* Yukon Exploration and Geology 2008, L.H. Weston, L.R. Blackburn and L.L. Lewis (eds.), Yukon Geological Survey, p. 113–123.

Duk-Rodkin, A., 1999. Glacial limits map of Yukon Territory. Exploration and Geological Services Division, Yukon Region, Indian and Northern Affairs Canada, Geoscience Map 1999-2; *also* Geological Survey of Canada, Open File 3694, scale 1:1 000 000.

Duk-Rodkin, A., 2001a. Glacial limits of Stevenson Ridge, Yukon Territory (115 J&K). Geological Survey of Canada, Open File 3804, scale 1:250 000.

Duk-Rodkin, A., 2001b. Glacial limits of Kluane Lake, Yukon Territory (115 G&F). Geological Survey of Canada, Open File 3806, scale 1:250 000.

Duk-Rodkin, A., Barendregt, R.W., White, J.M. and Singhroy, V.H., 2001. Geologic evolution of the Yukon River: implications for placer gold. Quaternary International, vol. 82, p. 5–31.

Everard, K.A., 1994. Regional characterization of large landslides in southwest Yukon, with emphasis on the role of neotectonics. Unpublished MSc thesis, University of British Columbia, Vancouver, BC, 178 p.

French, H.M., 2017. The Periglacial Environment, Fourth Edition. Wiley-Blackwell, 544 p.

French, H.M. and Heginbottom, J.A., 1983. Guidebook to permafrost and related features of the Northern Yukon Territory and Mackenzie Delta, Canada. Fourth International Conference on Permafrost, Fairbanks, Alaska, July 18–22, 1983, 186 p.

Froese, D.G., Barendregt, R.W., Enkin, R.J. and Baker, J., 2000. Paleomagnetic evidence for multiple Late Pliocene—Early Pleistocene glaciations in the Klondike area, Yukon Territory. Canadian Journal of Earth Sciences, vol. 37, p. 863–877.

Heginbottom, J.A., 1995. Canada Permafrost, Plate 2.1, (MCR 4177). National Atlas of Canada (5th edition), Canada Permafrost, Plate 2.1, (MCR 4177), scale 1:7 500 000.

Heginbottom, J.A. and Radburn, L.K., 1992. Permafrost and ground ice conditions of northwestern Canada; Geological Survey of Canada, Map 1691A, scale 1:1 000 000.

Howes, D.E. and Kenk, E., 1997. Terrain Classification System for British Columbia, version 2. Resource Inventory Branch, Ministry of Environment, Lands and Parks, 112 p.

Hughes, O.L., 1969. Distribution of open-system pingos in central Yukon Territory with respect to glacial limits. Geological Survey of Canada, Paper 69, 34 p.

Hughes, O.L., 1989a. West Aishihik River (NTS 115H SW). Geological Survey of Canada. Preliminary Map 21-1987, scale 1:100 000.

Hughes, O.L., 1989b. Stevens Lake (NTS 115H NW). Geological Survey of Canada. Preliminary Map 22-1987, scale 1:100 000.

Hughes, O.L., 1990. Surficial geology and geomorphology, Aishihik Lake, Yukon Territory. Geological Survey of Canada. Paper 87-29.

Huscroft, 2002a. Coffee Creek (NTS115J/14). Geological Survey of Canada, Open File 4344, scale 1:50 000.

Huscroft, 2002b. Britannia Creek (115J/15). Geological Survey of Canada, Open File 4345, scale 1:50 000.

Huscroft, 2002c. Cripple Creek (115J/16). Geological Survey of Canada, Open File 4346, scale 1:50 000.

Huscroft, C.A., Lipovsky, P.S. and Bond, J.D., 2004. A regional characterization of landslides in the Alaska Highway corridor, Yukon. Yukon Geological Survey, Open File 2004-18, 65 p., report and CD-ROM.

Israel, S., Cobbett, R., Westberg, E., Stanley, B. and Hayward, N., 2011. Preliminary bedrock geology of the Ruby Ranges, southwest Yukon (parts of NTS 115G, 115H, 115A and 115B). Yukon Geological Survey, Open File 2011-2, scale 1:150 000.

Jackson, L.E. Jr., 1997a. Victoria Creek (NTS 115I SW). Geological Survey of Canada, Map 1876A, scale 1:100 000.

Jackson, L.E. Jr., 1997b. Victoria Rock (NTS 115I NW). Geological Survey of Canada, Map 1877A, scale 1:100 000.

Jackson, L.E. Jr., 2000. Quaternary geology of the Carmacks map area, Yukon Territory. Geological Survey of Canada, Bulletin 539.

Jackson, L.E. Jr., 2005. Los Angeles Creek (NTS 115O/4). Geological Survey of Canada, Open File 4581, scale 1:50 000.

Jackson, L.E. Jr., Barendregt, R.W., Baker, J. and Irving, E., 1996. Early Pleistocene volcanism and glaciation in central Yukon: a new chronology from field studies and paleomagnetism. Canadian Journal of Earth Sciences, vol. 33, p. 904–916.

Jackson, L.E., Jr., Froese, D.G., Huscroft, C.A., Nelson, F.E., Westgate, J.A., Telka, A.M., Shimamura, K. and Rotheisler, P.N., 2009. Surficial geology and Late Cenozoic history of the Stewart River and northern Stevenson Ridge map areas, west-central Yukon Territory. Geological Survey of Canada, Open File 6059, 414 p.

Jackson, L.E. Jr., Shimamura, K. and Huscroft, C.A., 2001. Late Cenozoic geology, Ancient Pacific Margin NATMAP Project, Report 3: A re-evaluation of glacial limits in the Stewart River basin of Stewart River map area, Yukon Territory. Geological Survey of Canada, Current Research 2001-A3, 8 p.

Jackson, L.E. Jr., Tarnocai, C. and Mott, R.J., 1999. A middle Pleistocene paleosol sequence from Dawson Range, central Yukon Territory. Geographie physique et Quaternaire, vol. 53, p. 313–322.

Jensen, B.J.L., Pyne-O'Donnell, S., Plunkett, G., Froese, D.G., Hughes, P.D.M., Sigl, M., McConnell, J.R., Amesbury, M.J., Blackwell, P.G., van den Bogaard, C., Buck, C.E., Charman, D.J., Clague, J.J., Hall, V.A., Koch, J., Mackay, H., Mallon, G., McColl, Pilcher J.R., 2014. Transatlantic distribution of the Alaskan White River Ash. Geology 42, vol. 10, p. 875–878.

Kennedy, K.E., 2018. Evidence for limited glaciation in northern Kluane Ranges, southwestern Yukon, with implications for surficial geochemical exploration. *In:* Yukon Exploration and Geology 2017, K.E. MacFarlane (ed.), Yukon Geological Survey, p. 89–102.

Kennedy, K.E. and Ellis, S.E., 2020. Surficial geology of the northern Kluane Ranges (parts of NTS 115G/5, 6, 11, 12). Yukon Geological Survey, Open File 2020-5, 4 sheets, scale 1:50 000.

Knight Piésold, 2012. Terrain hazard assessment for proposed access roads and air strip. Prepared for Casino Mining Corporation, 140 p. https://casinomining.com/_resources/YESAA_Project_Proposal/additional/Terrain_Hazards.pdf.

Lerbekmo, J.F., 2008. The White River Ash: Largest Holocene Plinian tephra. Canadian Journal of Earth Sciences, vol. 45, p. 693–700.

Lerbekmo, J.F. and Campbell, F.A., 1969. Distribution, composition and source of the White River Ash, Yukon Territory. Canadian Journal of Earth Sciences, vol. 6, p. 109–116.

Lerbekmo, J.F., Westgate, J.A., Smith, D.G.W. and Denton, G.H., 1975. New data on the character and history of the White River volcanic eruption, Alaska. *In:* Quaternary Studies, R.P. Suggate and M.M. Cresswell (eds.). Royal Society of New Zealand, Bulletin 13, p. 203–209.

Lewkowicz, A.G. and Harris, C., 2005. Frequency and magnitude of active-layer detachment failures in discontinuous and continuous permafrost, northern Canada. Permafrost and Periglacial Processes, vol. 16, p. 115–130.

Lipovsky, P.S. and Bond, J.D., 2012a. Surficial Geology of Doyle Creek (NTS 115J/11). Yukon Geological Survey, Open File 2012-3, scale 1:50 000.

Lipovsky, P.S. and Bond, J.D., 2012b. Surficial Geology of Tom Creek (NTS 115J/12). Yukon Geological Survey, Open File 2012-4, scale 1:50 000.

Lipovsky, P.S. and Bond, J.D., 2012c. Surficial Geology of Home Creek (NTS 115J/13). Yukon Geological Survey, Open File 2012-5, scale 1:50 000.

Lipovsky, P.S. and Bond, J.D., 2013a. Surficial Geology of Klaza River (NTS 115J/1). Yukon Geological Survey, Open File 2013-7, scale 1:50 000.

Lipovsky, P.S. and Bond, J.D., 2013b. Surficial Geology of Onion Creek (NTS 115J/2). Yukon Geological Survey, Open File 2013-8, scale 1:50 000.

Lipovsky, P.S. and Bond, J.D., 2013c. Surficial Geology of Wellesley Lake (NTS 115J/5). Yukon Geological Survey, Open File 2013-9, scale 1:50 000.

Lipovsky, P.S. and Bond, J.D., 2013d. Surficial Geology of NTS 115J/6. Yukon Geological Survey, Open File 2013-10, scale 1:50 000.

Lipovsky, P.S. and Bond, J.D., 2013e. Surficial Geology of Mount Pattison (NTS 115J/7). Yukon Geological Survey, Open File 2013-11, scale 1:50 000.

Lipovsky, P.S. and Bond, J.D., 2013f. Surficial Geology of Apex Mountain (NTS 115J/8). Yukon Geological Survey, Open File 2013-12, scale 1:50 000.

Lipovsky, P.S., Coates, J., Lewkowicz, A.G. and Trochim, E., 2006. Active-layer detachments following the summer 2004 forest fires near Dawson City, Yukon. *In:* Yukon Exploration and Geology 2005, D.S. Emond, G.D. Bradshaw, L.L. Lewis and L.H. Weston (eds.), Yukon Geological Survey, p. 175–194.

Lipovsky, P. and Huscroft, C., 2007. A reconnaissance inventory of permafrost-related landslides in the Pelly River watershed, central Yukon. *In:* Yukon Exploration and Geology 2006, D.S. Emond, L.L. Lewis and L.H. Weston (eds.), Yukon Geological Survey, p. 181–195.

McKillop, R., Turner, D., Johnston, K. and Bond, J., 2013. Property-scale classification of surficial geology for soil geochemical sampling in the unglaciated Klondike Plateau, west-central Yukon. Yukon Geological Survey, Open File 2013-15, 85 p., including appendices.

Menounos, B., Goehring, B.M., Osborn, G., Margold, M., Ward, B., Bond, J., Clarke, G.K.C., Clague, J.J., Lakeman, T., Koch, J., Caffee, M.W., Gosse, J., Stroeven, A.P., Seguinot, J., and Heyman, J., 2017. Cordilleran Ice Sheet mass loss preceded climate reversals near the Pleistocene Termination. Science, vol. 358, p. 781–784.

Monahan, P.A., Levson, V.M., Henderson, P. and Sy, A., 2000. Relative liquefaction and amplification of ground motion hazard maps of Greater Victoria. British Columbia Geological Survey, Geoscience Map 2000-3.

Muller, J.E., 1967. Kluane Lake Map-area, Yukon Territory (115G, 115F, E half). Geological Survey of Canada, Memoir 340, 137 p.

Murphy, D.C., 2007. The three 'Windy McKinley' terranes of Stevenson Ridge (115JK), western Yukon. *In:* Yukon Exploration and Geology 2006, D.S. Emond, L.L. Lewis and L.H. Weston (eds.), Yukon Geological Survey, p. 223–236.

Murphy, D.C., Van Staal, C. and Mortensen, J.K., 2007. Preliminary bedrock geology of part of Stevenson Ridge area (NTS 115J/3, 4, 5, 6, 7, 8, parts of 11 and 12; 115K/1, 2, 7, 8, 9, 10, parts of 15 and 16). Yukon Geological Survey, Open File 2007-9, scale 1:125 000.

Murphy, D.C., van Staal, C. and Mortensen, J.K., 2008. Windy McKinley terrane, Stevenson Ridge area (115JK), western Yukon: composition and proposed correlations, with implications for mineral potential. *In:* Yukon Exploration and Geology 2007, Emond, D.S., L.R. Blackburn, R.P. Hill and L.H. Weston (eds.), Yukon Geological Survey, p. 225–235.

Murphy, D.C., Mortensen, J.K. and van Staal, C., 2009. 'Windy-McKinley' terrane, western Yukon: new data bearing on its composition, age, correlation and paleotectonic settings. *In:* Yukon Exploration and Geology 2008, L.H. Weston, L.R. Blackburn and L.L. Lewis (eds.), Yukon Geological Survey, p. 195–209.

Natural Resources Canada, 2015. Simplified seismic hazard map for Canada, the provinces and territories. https://earthquakescanada.nrcan.gc.ca/hazard-alea/simphaz-en.php#YT [accessed Oct. 25, 2021].

Natural Resources Canada, 2022. National earthquake database. https://earthquakescanada.nrcan.gc.ca/stndon/NEDB-BNDS/index-en.php, [accessed 2022/04/08].

Nelson, F.E.N. and Jackson, L.E., Jr., 2003. Cirque forms and alpine glaciation during the Pleistocene, west-central Yukon. *In:* Yukon Exploration and Geology 2002, D.S. Emond and L.L. Lewis (eds.), Exploration and Geological Services Division, Yukon Region, Indian and Northern Affairs Canada, p. 183–198.

Nelson, F.E. and Nyland, K.E., 2017. Periglacial cirque analogs: elevation trends of cryoplanation terraces in eastern Beringia. Geomorphology, vol. 293, p. 305–317.

Preece, S.J., McGimsey, R.G., Westgate, J.A., Pearce, N.J.G., Hart, W.K. and Perkins, W.T., 2014. Chemical complexity and source of the White River Ash, Alaska and Yukon. Geosphere, vol. 10, p. 1020–1042.

Price, L.W., 1973. Rates of mass wasting in the Ruby Range, Yukon Territory. *In:* Permafrost: North American Contributions to the Second International Conference, Yakutsk, USSR, July 13–28, 1973, p. 235–245.

Rampton, V.N., 1979a. Surficial geology and geomorphology Mirror Creek, Yukon Territory. Geological Survey of Canada, Preliminary Map 4-1978, scale 1:100 000.

Rampton, V.N., 1979b. Surficial geology and geomorphology Koidern Mountain, Yukon Territory. Geological Survey of Canada, Preliminary Map 5-1978, scale 1:100 000.

Rampton, V.N., 1979c. Surficial geology and geomorphology Burwash Creek, Yukon Territory. Geological Survey of Canada, Preliminary Map 6-1978, scale 1:100 000.

Rampton, V.N., 1979d. Surficial geology and geomorphology Generc River, Yukon Territory. Geological Survey of Canada, Preliminary Map 7-1978, scale 1:100 000.

Rampton, V.N., 1979e. Surficial geology and geomorphology Congdon Creek, Yukon Territory. Geological Survey of Canada, Preliminary Map 8-1978, scale 1:100 000.

Rampton, V.N., Ellwood, J.R. and Thomas, R.D., 1983. Distribution and geology of ground ice along the Yukon portion of the Alaska Highway gas pipeline. Permafrost, Fourth international conference Proceedings, Washington, DC, 1983, p. 1030–1035.

Reger, R.D. and Péwé, T.L., 1976. Cryoplanation terraces: indicators of a permafrost environment. Quaternary Research, vol. 6, p. 99–109.

Reuther, J., Potter, B., Coffman, S., Smith, H. and Bigelow, N., 2020. Revisiting the timing of the northern lobe of the White River Ash volcanic event in eastern Alaska and western Yukon. Radiocarbon, vol. 62, p. 169–188.

Richter, D.H., Preece, S.J., McGimsey, R.G. and Westgate, J.A., 1995. Mount Churchill, Alaska: Source of the late Holocene White River Ash. Canadian Journal of Earth Sciences, vol. 32, p. 741–748.

Robinson, S.D., 2001. Extending the late Holocene White River Ash distribution, northwestern Canada. Arctic, vol. 54, p. 157–161.

Ryan, J.J., Hayward, N., Jackson, L.E., 2014a. Landscape antiquity and Cenozoic drainage development of southern Yukon, through restoration modeling of the Tintina Fault. Canadian Journal of Earth Science, vol. 54, p. 1085–1100.

Ryan, J.J., Zagorevski, A., Roots, C.F. and Joyce, N., 2014b. Paleozoic tectonostratigraphy of the northern Stevenson Ridge area, Yukon. Geological Survey of Canada, Current Research 2014-4, 13 p.

Ryan, J.J., Hayward, N. and Jackson, L.E. Jr., 2017. Landscape antiquity and Cenozoic drainage development of southern Yukon, through restoration modeling of the Tintina Fault. Canadian Journal of Earth Science, vol. 54, p. 1085–1100.

Smith, C.A.S., Meikle, J.C. and Roots, C.F., 2004. Ecoregions of the Yukon Territory: Biophysical properties of Yukon landscapes. Agriculture and Agri-Food Canada, PARC Technical Bulletin No. 04-01, 313 p.

Smith, C.A.S., Sanborn, P.T., Bond, J.D. and Frank, G., 2009. Genesis of Turbic Cryosols on north-facing slopes in a dissected, unglaciated landscape, west-central Yukon Territory. Canadian Journal of Soil Science, vol. 89, p. 611–622.

Tempelman-Kluit, D., 1980. Evolution of physiography and drainage in southern Yukon. Canadian Journal of Earth Sciences, vol. 17, p. 1189–1203.

Turner, D.G., 2014. Pleistocene stratigraphy, glacial limits and paleoenvironments of the White River and Silver Creek, southwest Yukon. Unpublished PhD thesis, Simon Fraser University, Burnaby, BC, 138 p.

Turner, D.G., Ward, B.C., Bond, J.D., Jensen, B.J.L., Froese, D.G., Telka, A.M., Zazula, G.D. and Bigelow, N.H., 2013. Middle to Late Pleistocene ice extents, tephrochronology and paleoenvironments of the White River area, southwest Yukon. Quaternary Science Reviews, vol. 75, p. 59–77.

van Everdingen, R.O., 2005. Multi-language glossary of permafrost and related ground-ice terms (revised edition). International Permafrost Association, 159 p.

Wanty, R.B., Wang, B., Vohden, J., Day, W.C. and Gough, L.C., 2007. Aufeis Accumulations in Stream Bottoms in Arctic and Subarctic Environments as an Indicator of Geologic Structure. *In:* Recent U.S. Geological Survey Studies in the Tintina Gold Province, Alaska, United States, and Yukon, Canada — Results of a 5-Year Project; Chapter F, L.P. Gough and W.C. Day (eds.), U.S. Geological Survey, Scientific Investigations Report 2007–5289–F.

Ward, B.C., Bond, J.D., Froese, D.G. and Jensen, B.J.L., 2008. Old Crow tephra (140 ± 10 ka) constrains penultimate Reid glaciation in central Yukon Territory. Quaternary Science Reviews, vol. 27, p. 1909–1915.

Ward, B.C., Gosse, J.C., Bond, J.D. and Froese, D., 2007a. Evidence for a 55–50 ka (early Wisconsin) glaciation of the Cordilleran Ice Sheet, Yukon Territory, Canada. Geological Society of America, poster session T23 - Using Geochronology to Build Better Records and Solve Geomorphic and Paleoclimate Questions—Recent Advances and Findings, Denver, Colorado, October 28–31, 2007.

Ward, B.C., Bond, J.D. and Gosse, J.C., 2007b. Evidence for a 55–50 ka (early Wisconsin) glaciation of the Cordilleran Ice Sheet, Yukon Territory, Canada. Quaternary Research, vol. 68, p. 141–150.

Ward, B.C., Jackson, L.E. Jr. and Savigny, K.W., 1992. Evolution of Surprise Rapids Landslide, Yukon Territory. Geological Survey of Canada, Paper 90-18, 25 p.

Westgate, J.A., Preece, S.J., Froese, D.G., Walter, R.C., Sandhu, A.S. and Schweger, C.E., 2001. Dating early and middle (Reid) Pleistocene glaciations in central Yukon by tephrochronology. Quaternary Research, vol. 56, p. 335–348.

West, K.D. and Donaldson, J.A., 2002. Resedimentation of the late Holocene White River tephra, Yukon Territory and Alaska. *In:* Yukon Exploration and Geology 2002, D.S. Emond, L.H. Weston and L.L. Lewis (eds.), Exploration and Geological Services Division, Yukon Region, Indian and Northern Affairs Canada, p. 239–247.

Yukon Geological Survey, 2010. Yukon placer database – geology and mining activity of placer occurrences. Yukon Geological Survey, CD-ROM.

Yukon Geological Survey, 2022. Yukon digital bedrock geology. Yukon Geological Survey, https://data.geology.gov.yk.ca/Compilation/3, [accessed May 10, 2022].

Zazula, G.D., Turner, D., Ward, B.C. and Bond, J., 2011. Last interglaciation western camel (*Camelops hesternus*) from eastern Beringia. Quaternary Science Reviews, vol. 30, p. 2355–2360.